CSDL-T-1002

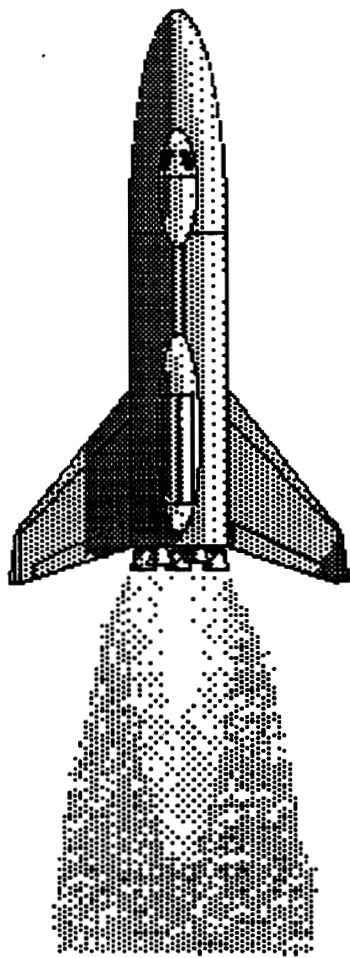## ASCENT GUIDANCE FOR
A WINGED BOOST VEHICLE

by

Michael A. Corvin

August 1988

The Charles Stark Draper Laboratory,

555 Technology Square
Cambridge, Massachusetts 02139

Advanced Ascent Guidance Study

Ascent Guidance for a Winged Boost Vehicle

CSDL - T - 1002

by

Michael A. Corvin

August, 1988

The Charles Stark Draper Laboratory

555 Technology Square, Cambridge, Massachusetts 02139

Ascent Guidance for a Winged Boost Vehicle

by

Michael Alexander Corvin

B.Eng. (M.E.), Technical University of Nova Scotia (1986)
Dipl.Eng., Dalhousie University (1983)

Submitted in Partial Fulfillment
of the Requirements for the
Degree of

Master of Science
in
Aeronautics and Astronautics

at the

Massachusetts Institute of Technology

August, 1988

© Michael Alexander Corvin, 1988

Signature of Author _____
Department of Aeronautics and Astronautics
August, 1988

Certified by _____
Prof. Richard H. Battin, Thesis Advisor

Approved by _____
Gilbert S. Stubbs, CSDL Project Supervisor

Accepted by _____
Prof. Harold Y. Wachman, Chairman, Departmental Graduate Committee

1

Ascent Guidance for a Winged Boost Vehicle

by

Michael Alexander Corvin

submitted to the
Department of Aeronautics and Astronautics on August 12, 1988
in partial fulfillment of the requirements for the degree of
Master of Science in Aeronautics and Astronautics

Abstract

The objective of the advanced ascent guidance study was to investigate guidance concepts which could contribute to increased autonomy during ascent operations in a winged boost vehicle such as the proposed Shuttle II. The guidance scheme was required to yield near a fuel-optimal ascent in the presence of vehicle system and environmental dispersions. The study included consideration of trajectory shaping issues, trajectory design, closed loop and predictive-adaptive guidance techniques and control of dynamic pressure by throttling. An extensive ascent vehicle simulation capability was developed for use in the study.

Study of trajectory shaping led to a simple design approach that yielded near optimal ascent trajectories. The design technique was employed in the study to generate reference trajectories for use during investigation of the steering system. It was not considered suitable for an operational system, however.

A closed-loop steering technique for the endoatmospheric phase of the ascent trajectory, employing control of the velocity vector direction (flight path angle), was studied. This technique was implemented in combination with a flight control system that controlled angle of attack, enabling inherent load relief. This steering approach was demonstrated to be robust in the presence of wind and trajectory dispersions. It would therefore be suitable for use in systems in which increased autonomy is desired.

Predictive-adaptive guidance schemes for use in conjunction with the flight path angle steering were investigated. In one case, the objective was to adjust the trajectory to improve the final

mass at orbit. This was achieved in the presence of one type of trajectory dispersion (an off-optimal reference trajectory) but not in other situations. The second predictive-adaptive scheme was intended to reduce the loading experienced by the vehicle by making use of excess performance capability. The preliminary implementation of this scheme successfully demonstrated load reduction but requires further development. Predictive-adaptive load reduction is felt to be a potentially valuable concept for a reusable vehicle such as Shuttle II.

The control of dynamic pressure by throttling the engines to control thrust was demonstrated to be very effective. A closed loop implementation of the control scheme was demonstrated. The maximum dynamic pressure experienced during ascent was prevented from exceeding the vehicle limit by the control system with a negligible loss in vehicle performance.

Thesis Supervisor: Dr. Richard H. Battin
Title: Adjunct Professor of Aeronautics and Astronautics

Acknowledgments

Table of Contents

Table of Contents (continued)

Table of Contents (continued)

List of Figures

List of Tables

1. Introduction

1.1 Background

This study investigated ascent guidance for a winged boost vehicle. The proposed single-stage-to-orbit (SSTO) Shuttle II was used in the study as the vehicle model. The work was based on previous efforts at CSDL in Air Force boost vehicle studies. Input and background information were received from NASA and the McDonnell Douglas Astronautics Company - Engineering Services who were engaged in concurrent Shuttle II studies. NASA Langley Research Center oversaw the study.

1.2 Objective : Towards Autonomous Ascent

The objective for Shuttle II vertical launch system ascent guidance is a guidance scheme capable of yielding near fuel-optimal ascent in the presence of vehicle system and environmental dispersions. A guidance system is desired which enables high launch rate frequency in a wide range of weather conditions. The amount of long term planning and day of launch (DOL) ground support should be minimized. These requirements point towards a highly autonomous on-board guidance approach which can accommodate dispersions or employs adaptive techniques to minimize the impact of dispersions[1]. The guidance system will have available to it aerodynamic and inertial information derived from on-board sensors, and a measurement of the ascent wind profile obtained immediately before launch by a ground-based doppler radar wind profiler.

The objective of vehicle autonomy and flexibility is driven by the experience gained in the current Shuttle I Space Transportation System (STS). The STS is a primarily non-autonomous system requiring extensive, long lead time mission planning which is very costly. The endoatmospheric ascent guidance, employed from launch up to separation of the Solid Rocket Boosters (SRBs), is an open loop system which follows an attitude and thrust schedule designed during the mission planning phase. During ascent the vehicle flight control system (FCS) provides load relief adjustments to vehicle attitude, reacting to the vehicle response to

---

[1] Condon, J., "Autonomous Ascent", Mission Planning and Analysis Division presentation, NASA Johnson Spaceflight Center, Autonomous Ascent - Quarterly Meeting, May 27, 1987.

variations in the winds from the design environment. These adjustments can cause trajectory dispersions. The trajectory design performed during mission planning is based on monthly mean winds and is primarily driven by operational constraints (vehicle and crew limitations and abort considerations). To date, most of the missions flown have each required completely new mission designs. Thus, a closed loop guidance approach which can accommodate or adapt to environmental dispersions during ascent and which simplifies the trajectory design required during the mission planning phase would provide an increase in overall system flexibility and a reduction in cost.

The ideal launch system would be a fully autonomous one which would enable "light the fires and go" operation. Such a system would require no mission planning for ascent apart from verification that the mission falls within the vehicle's performance capabilities. The on-board guidance system would design and follow the ascent trajectory based on the environmental data received immediately prior to launch and would handle abort situations. Such a fully autonomous system may not be required, however. It may prove to be the case that a cost-effective, flexible system can be attained by a more easily achieved mix of increased vehicle autonomy and reduced mission planning and ground support. In any case, an improvement in guidance robustness to dispersions would be advantageous.

1.3   Overview

The main focus of the CSDL study was the endoatmospheric phase of the ascent trajectory. Factors affecting trajectory shape and their application to the design and following of the ascent profile were studied. A closed loop steering technique and related flight control system were demonstrated. They showed good performance in the presence of wind dispersions. Predictive-adaptive techniques for adjustment of the trajectory for use in conjunction with the closed-loop steering system were investigated. A simple trajectory design technique was developed based on the trajectory shaping studies and was implemented in an automated form.

This thesis summarizes these activities. Chapter 2 describes the proposed Shuttle II vehicle that was used as the model for the study. Chapter 3 briefly outlines the simple flight control system used in the study and discusses the throttling scheme that was developed for the vehicle. The throttling scheme included closed-loop control of dynamic pressure. Chapter 4 covers the primary area of the study, the in-flight guidance of the vehicle. The topics in this

chapter include flight path angle steering with angle of attack control, predictive-adaptive guidance for maximization of final mass and predictive-adaptive guidance for load reduction. Chapter 5 describes the trajectory design procedures that were developed to generate the reference ascent trajectories employed by the in-flight guidance system. Chapter 6 provides a summary of the results and conclusions of the ascent guidance study.

A major part of the effort in the CSDL study was devoted to the creation of an ascent vehicle simulation for use in testing guidance and control concepts for ascent vehicles. The form and capabilities of this vehicle simulation are outlined in the Appendix.

2. Vehicle Description and Modelling

2.1   Physical Arrangement of Single-Stage-to-Orbit (SSTO) Vehicle

The vehicle model employed in the ascent guidance study was based on a proposed single-stage-to-orbit (SSTO) Shuttle II launch system[2,3]. The general arrangement of this vehicle is illustrated in Figure 2.1.

The SSTO Shuttle II is a fully reusable manned vertical launch system in which the entire single vehicle system goes into orbit. The vehicle is recovered by means of a gliding return to a runway landing and has a swept delta wing with winglets. The fuselage consists primarily of an integral tank structure with the propulsion group mounted at the rear. During launch, the crew is accommodated in a flight deck module located on the forward upper fuselage. This module can be jettisoned for crew escape in the event of an emergency during launch. Additional crew facilities are provided in a section behind the flight deck module. A pressurized connecting tunnel runs aft along the upper fuselage to the payload canister which is carried on the rear upper fuselage. Various interchangeable payload canisters can be carried, some equipped with cabin space to which the tunnel provides access.

The vehicle uses dual-fuel propulsion. It is equipped with four hydrocarbon / liquid oxygen (RP) engines and three liquid hydrogen / liquid oxygen (LH) engines. All engines are employed at take-off. The RP engines are shut down upon RP fuel depletion approximately halfway to orbit. The LH engines, which are used for the entire boost phase, operate in two modes with the change between modes occurring at RP engine shut down. The LH engines are equipped with extendible skirts which are deployed to increase performance following the RP engine shutdown. All of the engines are gimballed to provide thrust vector control (TVC) during ascent. The engines all may be throttled up or down from their nominal operating points, subject to minimum and maximum limits. This thrust control is used to meet vehicle and crew constraints and in the event of engine failure to minimize the performance lost.

---

2   Talay, T.A., "Shuttle II." SAE Paper 871335, Aerospace Vehicle Conference, Washington, D.C., June 8–10, 1987.

3   Talay, T.A., "Shuttle II - A Progress Report." Space Systems Division, NASA Langley Research Center, May 6, 1986.

The proposed Shuttle II is equipped with aerodynamic sensors which can be used during ascent as well as during the return glide to provide dynamic pressure (q), angle of attack (α), and sideslip angle (β) data. Inertial measurements are provided by inertial measurement units (IMUs).

Flight Deck Module

Work / Sleep Cabin

Connecting Tunnel

Payload Canister
(with Payload Bay)

LH

Integral
Propellant
Tanks

RP

LOX

Length:
164 ft
Wing Area:
4935 sq.ft
Gross Lift-Off Weight:
2,654 Klb
Dry Weight:
276 Klb

3 LH / LOX engines
4 RP / LOX engines
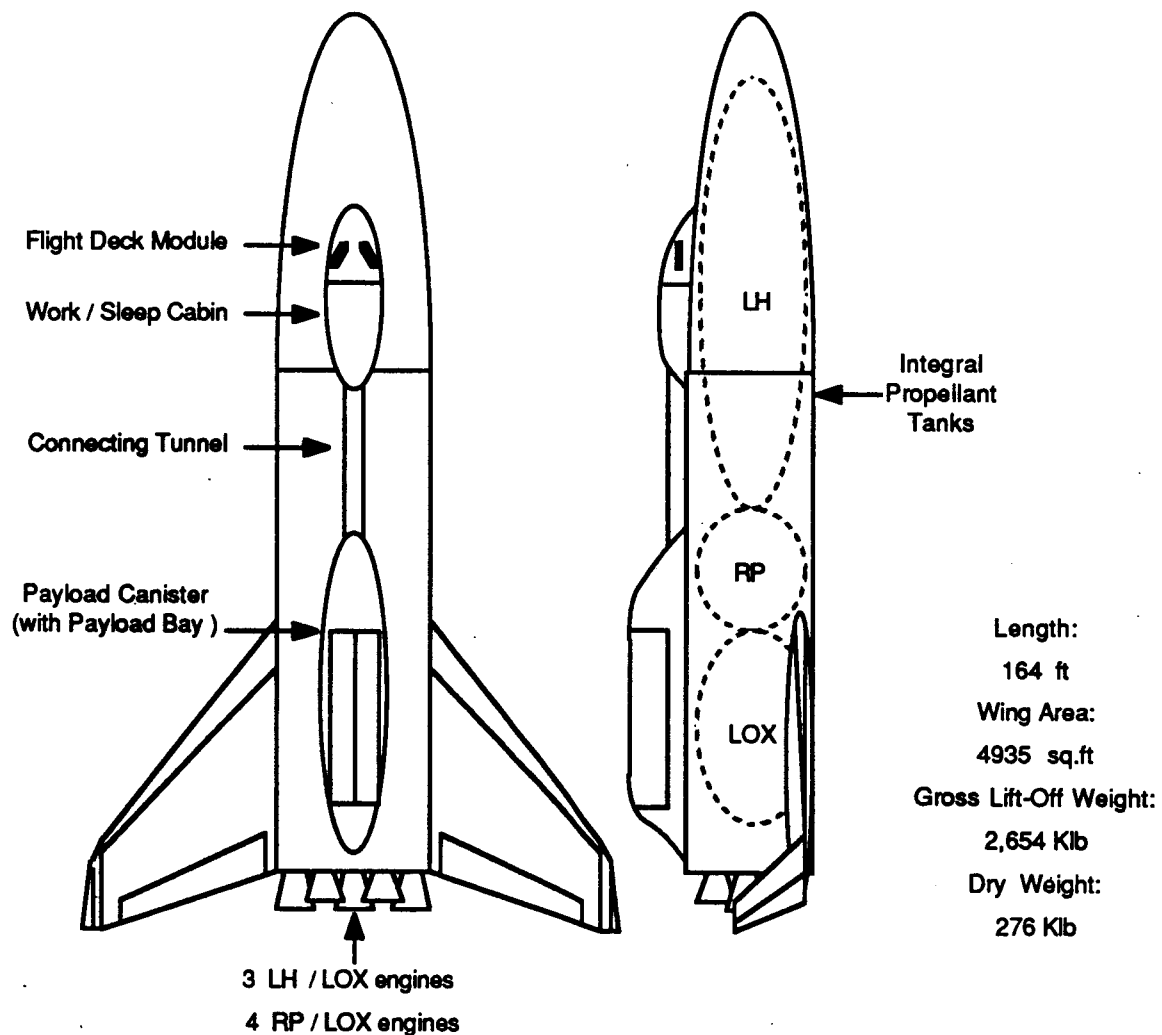
Figure 2.1   General arrangement of the proposed SSTO Shuttle II.

2.2　The Vehicle Model

The design of the SSTO Shuttle II was preliminary at the time of the study and few physical parameters were fully defined. Thus, the model used in this study was quite simple. The overall size and configuration of the vehicle shown in Figure 2.1, the vehicle weight and propellant load, the engine characteristics, and tabular lift and drag data were supplied to CSDL by NASA Langley Research Center. Where data was not available an approximate model was assumed.

2.2.1　Aerodynamic Characteristics

Data were available for the vehicle normal and axial aerodynamic force coefficients over the Mach number (M) range 0 to 40 and the angle of attack (α) range -2° to 15°. The tables of data, functionalized in terms of M and α, were employed by the vehicle simulation which interpolated between the data points (see Appendix A) to obtain the coefficients for the current vehicle state. These were used with the current dynamic pressure to calculate the aerodynamic normal and axial forces at each step in the simulation. Approximate linear fits to the vehicle lift characteristics at each Mach number in the data table were calculated for use by the steering algorithms.

Lateral aerodynamic characteristics were unknown. Lateral forces were neglected in the vehicle model used in the study. Thus, any sideslip angles which were developed had no effect on the trajectory and the effect of crosswinds on the trajectory could not be studied.

No aerodynamic moment or center of pressure data was available, nor was any control surface force or moment data available. It was therefore assumed for the study that the vehicle would employ its aerodynamic longitudinal control surfaces to completely trim-out the aerodynamic pitching moment. Additionally, it was assumed that this control surface action was accounted for in the lift and drag data. Thus, thrust vectoring was not required to control the aerodynamic moment. The control surfaces were assumed not to be used in the control of the vehicle attitude during ascent. The assumption of zero steady-state thrust vector trim angle was believed to be significant. Some of the results discussed in following sections, particularly those dealing with the trajectory shaping effects of α, may need to be modified in cases in which there is a steady-state thrust vector deflection due to trim requirements.

16

2.2.2 Mass Properties

The vehicle mass was continuously evaluated in the vehicle simulation based on the initial propellant load, the vehicle dry mass, and the fuel flows calculated from the engine characteristics and commanded thrust levels. For the RP engines the fuel flow included fuel used by the turbopump gas generators, which did not contribute to the thrust.

In order to include pitch plane dynamics in the vehicle simulation a preliminary model of the vehicle's variable pitch inertia was developed. A simple model was formulated approximating the layout of the vehicle, including the payload, with basic geometric elements and with an assumed distribution of the structural mass among the elements. This provided an estimate of the vehicle's dry pitch inertia (30×10^2 slug-ft^2) and center of gravity (60 ft forward of the aft datum). The fuel tanks were modelled as a pair of side-by-side cylinders running lengthwise along the vehicle. These were divided into appropriate sections, in order going forwards, for LOX, RP and LH. The total tank volumes were calculated from the takeoff propellant loads. As each fuel was consumed the remaining quantities were assumed to form cylindrical masses at the aft end of each tank. Using this model the total vehicle pitch inertia and center of gravity location were calculated as a function of total RP and LH fuel quantities. (Total RP and LH fuel quantities included the respective portions of the LOX.) Time histories of the center of gravity location obtained with this model on typical ascent profiles approximated a center of gravity time history provided with the vehicle data by NASA Langley Research Center, giving some confidence in the model.

No lateral dynamics were modelled in the vehicle simulation. Yaw and roll were uncontrolled. The yaw and roll rates were simply left at the small values, due to the earth's rotation, with which they were initialized on the launch pad.

2.2.3 Engines

The characteristics of the two engine types, RP and LH, the local atmospheric pressure, the number of engines firing, and the throttle settings were all used in the vehicle simulation to calculate a single equivalent engine thrust value. The throttle levels for the RP and LH engine groups each could be set separately. In the altitude range 0 ft to 10,000 ft the LH engines could be throttled to between 90% and 65% of nominal thrust, the limit decreasing as a linear

function of altitude. Above 10,000 ft they could be throttled down to 65%. The RP engines could be throttled down to 65% at all times. The number of each type of engine firing could be changed during ascent to allow simulation of the normal RP engine shutdown and of a failure in either group of engines. In the event of engine failure a maximum throttle-up limit greater than 100% of nominal thrust could be specified. The arrangement of the individual engines, which was unknown, was assumed to be such that the equivalent thrust vector acted through the vehicle center of gravity when the thrust vector angle was zero. It was further assumed that the individual engines would be vectored as necessary to achieve the equivalent thrust vector pitch deflection (δ) commanded by the flight control system. This thrust vectoring provided pitch attitude control actuation by developing a moment about the center of gravity. A maximum thrust vector deflection limit of $\delta = \pm\, 6°$ was assumed.

2.2.4   Sensors

For the present study all sensed information required by the guidance and flight control systems was assumed to be perfectly known. No sensor dynamics, deterministic errors or noise were modelled, although the vehicle simulation contained provisions for their inclusion.

2.2.5   Summary of Vehicle Model

In summary, while the simulation was in a full six degree of freedom environment, the model of the SSTO vehicle which was used was essentially a four degree of freedom model since only the pitch dynamics were modelled and controlled. The forces acting on the vehicle were modelled as an aerodynamic axial force, an aerodynamic normal force and the weight, all acting through the center of gravity, and a net thrust. The thrust acted a distance (l_{cg}) behind the center of gravity. Deflection of the thrust vector (δ) was used for vehicle pitch control. The model is shown in Figure 2.2.

V_e - earth-relative velocity

γ_e - earth-relative flight path angle

V_a - air-relative velocity

V_w - wind velocity

θ - earth-relative pitch attitude

α - angle of attack

Normal Aerodynamic Force

Axial Aerodynamic Force

Net Thrust (T)

mass properties — mass (m) / Pitch Inertia (J)

■ - Inertial Measurement Unit (IMU)   ◉ - Air Data System (ADS)
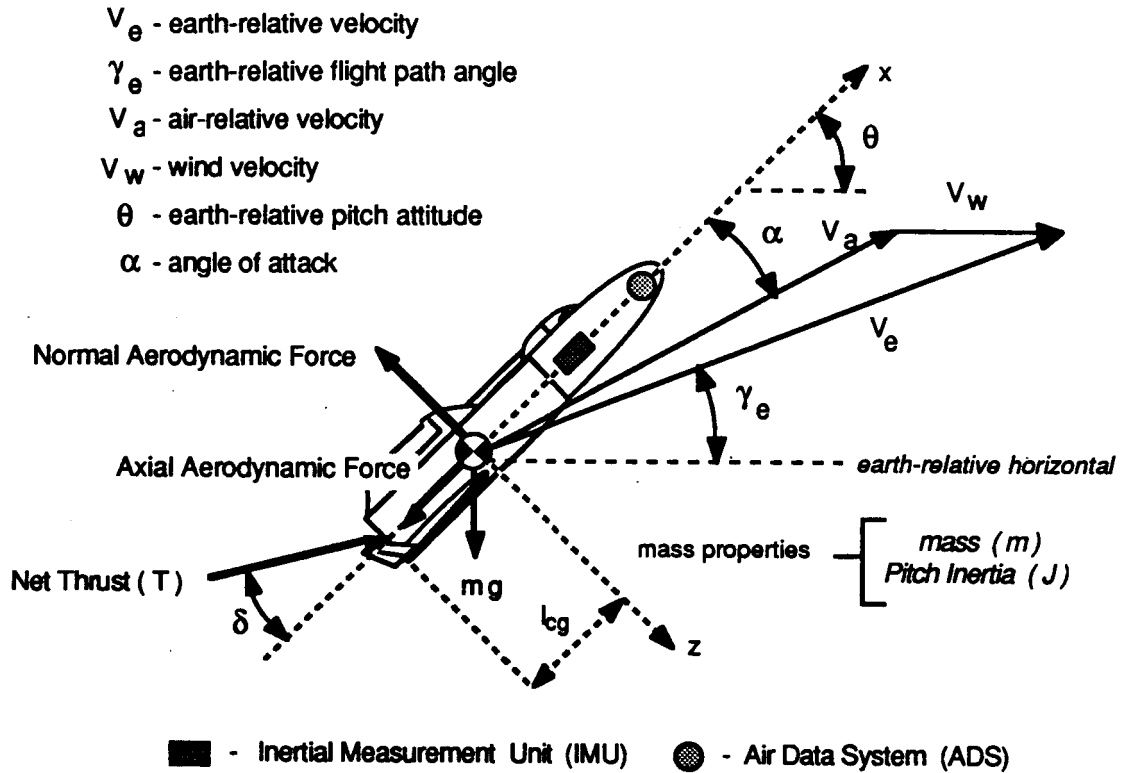
note : velocities may have components outside of the illustrated pitch plane

Figure 2.2 Definition of SSTO vehicle model used in the study.

3. Flight Control and Throttling

3.1 Flight Control System

3.1.1 Description

The vehicle model flight control system (FCS) was provided with four modes of flight control. The mode of control used during each trajectory phase depended on the type of command generated by the steering system during that phase and on selections made by the user. Flags set by the user and by the steering system determined which flight control mode was employed at any given time.

Two of the flight control modes assumed perfect control. In one of these, the pitch rate commanded by the guidance system was perfectly achieved by the vehicle. (Roll and yaw were uncontrolled.) In the other mode the body axial unit vector commanded by the guidance system was exactly followed. The perfect flight control modes were used for validation of the CSDL ascent vehicle simulation during its development. The CSDL runs were compared to runs made with other vehicle simulations. These reference simulations used three degree of freedom models and did not include control dynamics. (Reference runs using POST[4] were provided by the NASA Langley Research Center and POST runs were performed at CSDL.)

For the majority of the simulations performed for the study two modes implementing closed loop longitudinal flight control were used. The first of these employed pitch attitude (θ) as the primary feedback variable and the second one employed angle of attack (α) feedback. Either θ or α was commanded by the steering system during the different ascent phases and it set the FCS mode flags accordingly.

A model of the vehicle rotational dynamics in pitch was developed in order to design the closed loop flight control. Given the assumption that the center of pressure of the aerodynamically trimmed vehicle is coincident with the center of gravity (c.g.), the pitch plane model of the vehicle attitude response to a thrust vector deflection is given by

---

[4] Bauer, G.L., Cornick, D.E. , Harper, A.R., Peterson, F.M., Stevenson, R., "Program to Optimize Simulated Trajectories (POST)." Vol. II, *Utilization Manual*, NASA CR-132690, April 1975.

$$\frac{\theta}{\delta}(s) = \frac{K_v}{s^2} \qquad\qquad (3.1)$$

where

$$K_v = \frac{T \, l_{cg}}{J}$$

It should be noted that for the more typical case in which the vehicle is aerodynamically unstable, having the aerodynamic center of pressure a distance (l_{cp}) ahead of the c.g., the model is

$$\frac{\theta}{\delta}(s) = \frac{K_v}{s^2 - \omega_v} \qquad\qquad (3.2)$$

where, with the reference wing area (S), the dynamic pressure (q), and the derivative of the normal aerodynamic force with respect to α ($Cn\alpha$)

$$\omega_v = \sqrt{\frac{Sq \, l_{cp} \, Cn_\alpha}{J}} \, .$$

This transfer function, Equation (3.2), has an unstable pole and thus is harder to control than the case represented by Equation (3.1). However, analysis with reasonable values for l_{cp} showed that the flight control gains selected based on (3.1) would still result in adequate performance. The assumed values for l_{cp} were in the magnitude range which would be expected in a Shuttle II configuration vehicle having no active aerodynamic longitudinal control.

The basic α-control system is shown in Figure 3.1. The θ-control loop differed only in its use of θ as the outer loop feedback variable and θ_{cmd} as the input command. In both the α- and the θ-control systems a pitchrate feedback inner loop with unity feedback gain ($K_{fb} = 1$) was used. Proportional plus integral compensation was employed for the FCS compensator in each case. Since the performance of the flight control systems was not critical, the FCS compensators were designed in the continuous s-domain without analytical consideration of the effects of sampling present in the simulation. The loops were simply designed with ample phase margins to allow for the effective lag introduced by discrete sampling in the control implementation. The FCS compensator gains were trimmed based on the time-domain simulation results where necessary.

The engine deflection gain, K_δ, was a variable parameter. It was computed as the quotient of a specified constant total inner loop forward gain (KDKV) divided by the calculated vehicle gain (K_v). This held the inner loop forward gain constant as the vehicle gain varied with time, keeping the flight control loop dynamics constant. This prevented the need for scheduled gains in the flight control compensator or in the compensation used in the steering loop which was closed around the combined FCS plus vehicle system.
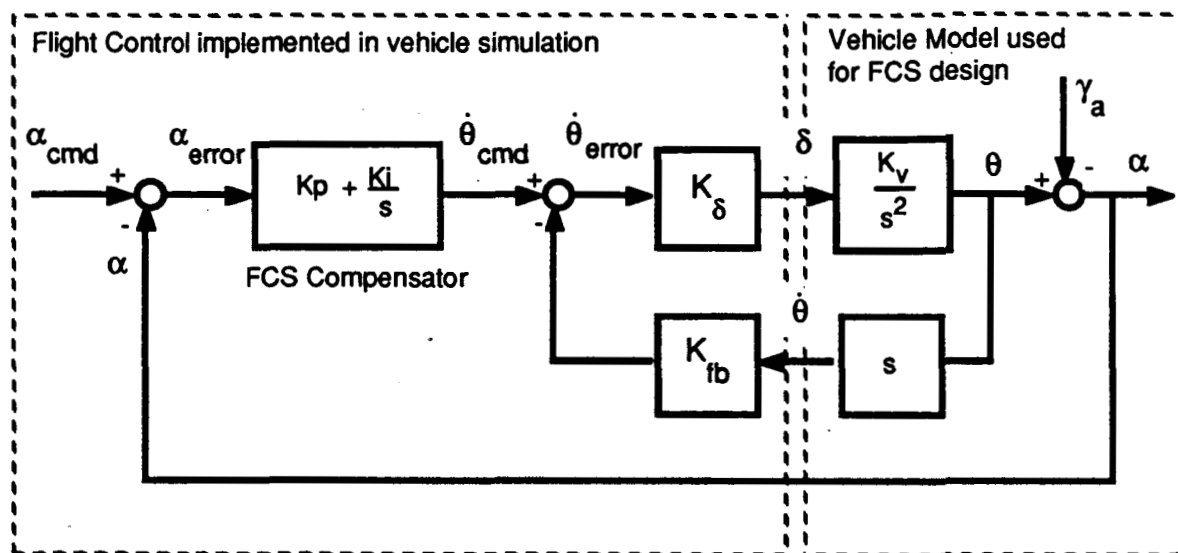
Figure 3.1   Basic α-control system block diagram.
(γ_a is the air-relative flight path angle; $\alpha = \theta - \gamma_a$)

The θ-control mode was provided with the option to feed forward a commanded pitchrate signal if one was generated by the guidance system. This feature is shown in Figure 3.2. Command feed forward was used only when a smooth rate command signal was available, such as during the launch maneuver. The speed of response and tracking accuracy were, predictably, improved when feed forward was employed.
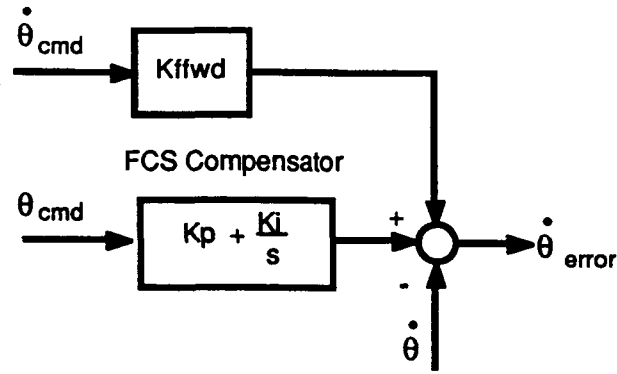
Figure 3.2   Feed forward of a pitchrate command.

In both the α- and the θ-control modes, time-varying gains were employed in the implemented algorithms to accomplish a smooth transition when switching between modes. Such mode switching occurred when going from the launch maneuver, which employed θ-control, to γ-steering, which used α-control and again when steering changed to PEG, which returned the FCS to θ-control. (See Chapter 4.1 for a description of the mission phases.) The values commanded to the outer and inner flight control loops were flared from the vehicle state at mode switching to the command signal received from the guidance system over a period of specified length (T_{flare}). The transition flare algorithm structure is illustrated by Figure 3.3. Linearly and exponentially time-varying flare parameters (K_{flare}) were tested. The best smoothing was obtained with an exponential flare parameter of the form

$$K_{flare} = 1 - e^{-5(t - t_{transfer}) / T_{flare}} \qquad (3.3)$$

A T_{flare} value of four seconds typically was used. Both of the closed loop control modes also implemented a limiter on the maximum magnitude of δ. A limit of six degrees was used throughout the study.
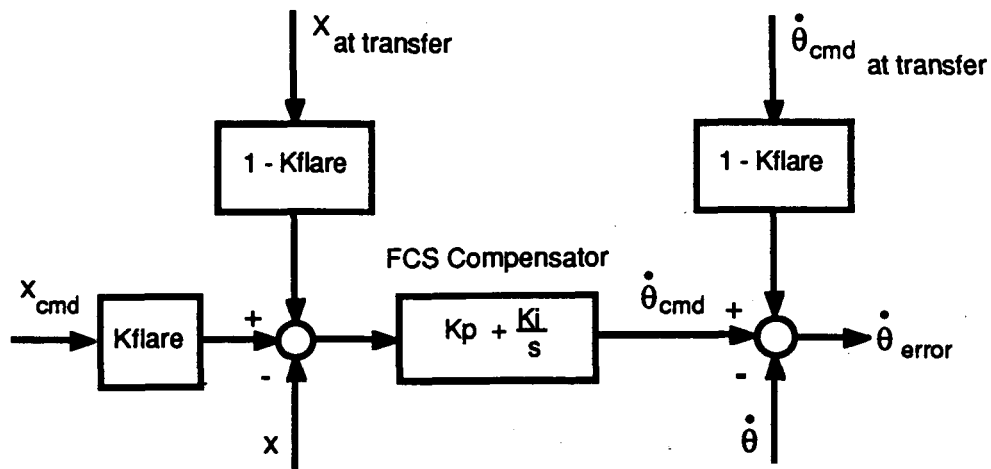
Figure 3.3 Structure of flight control mode transition algorithm.
(X represents α or θ.)

3.1.2 Representative Loop Design and Performance

The frequency response of a representative s-domain design for the α-control loop is given in Figure 3.4. A phase margin of 64° was obtained and crossover occurred at 2.7 radians/s.

Note that this is not necessarily the best possible design but that it gave good performance in the time domain when implemented in the vehicle simulation. A typical time history of the α error (α_e) in the α-control loop operating during ascent with γ-steering guidance is given Figure 3.5.
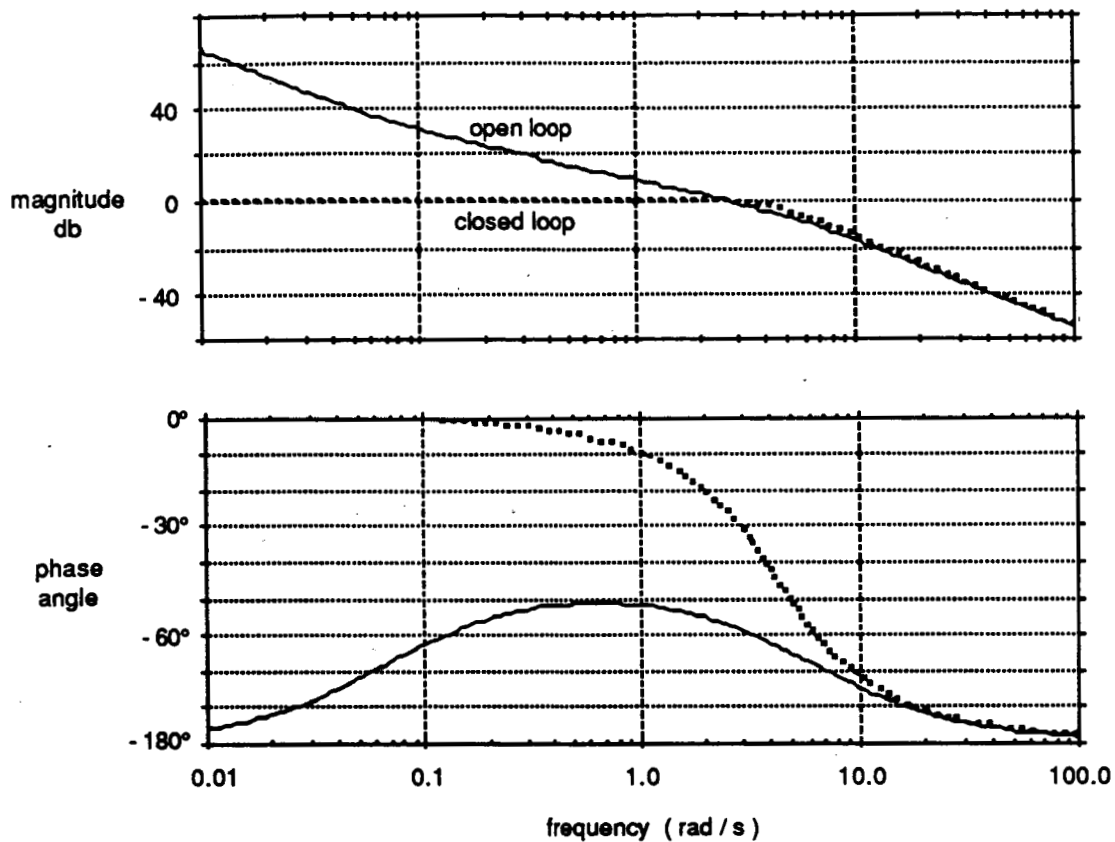
Figure 3.4   Frequency response of representative s-domain design for the α-control loop.
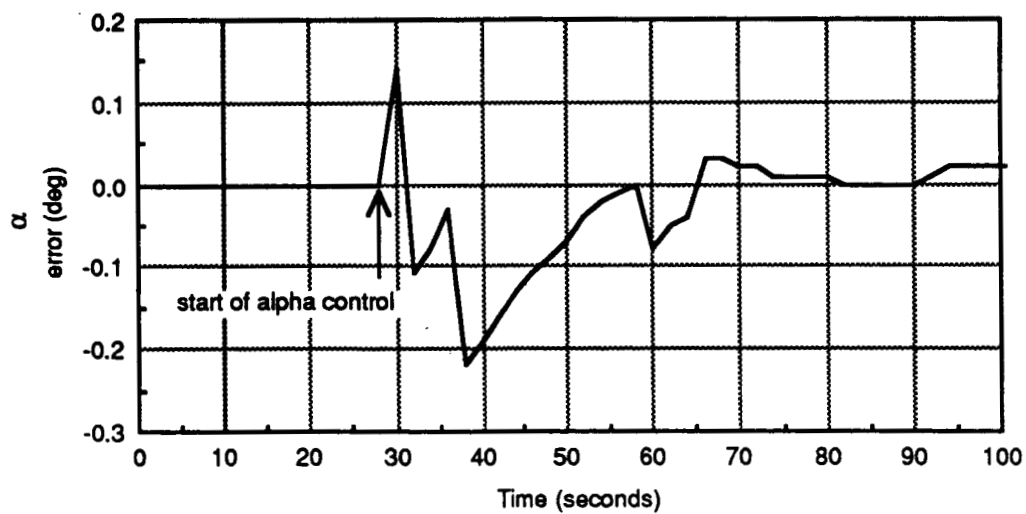
Figure 3.5   Typical time history of α error during γ-steering.

3.2   Dynamic Pressure Control using Throttling

3.2.1   Introduction

This section describes a relationship derived between thrust, drag and the rate of change of dynamic pressure (q-rate). This relationship was applied in a scheme using thrust to control dynamic pressure (q) with the objective of limiting the maximum dynamic pressure (q_{max}). The implementation of this scheme, given data which would be available from sensors in the proposed Shuttle II vehicle, is discussed. Some of the results obtained in the CSDL simulation of the SSTO Shuttle II with and without q-control are compared.

The limit on q_{max} is a primary constraint on the ascent trajectory. Under no wind or tailwind conditions it was found that the 'optimized' trajectory obtained with the α-shaping design technique usually did not exceed the vehicle q-limit (850psf). However, under headwind conditions q frequently exceeded the limit. Thus, it was considered desirable to have q explicitly controlled in flight. Even if the employed trajectory design technique accounts for q, controlling q directly ensures that dispersions do not cause the limit to be exceeded.

The control of q is included under the general heading of flight control and throttling since it is essentially independent of the vehicle guidance. While, in general, throttling would be expected to affect the trajectory, it was found that the throttling to control q actually had only a minor effect on the overall trajectory for the flight conditions investigated.

3.2.2   Derivation of the q-rate : Drag : Thrust Relationship

The basic expression for dynamic pressure is

$$q = \frac{1}{2} \rho V_a^2 \qquad (3.4)$$

where ρ is density and V_a is the air relative speed. Taking the derivative,

$$\frac{dq}{dt} = \frac{d\rho}{dt} \frac{V_a^2}{2} + \rho V_a \frac{dV_a}{dt}$$

(3.5)

Rearranging (3.4) and substituting into (3.5) gives

$$\frac{dq}{dt} = \frac{d\rho}{dt} \frac{q}{\rho} + \sqrt{2 q \rho} \frac{dV_a}{dt}$$

(3.6)

The rate of change of the air relative speed, dV_a/dt, is caused by the vehicle acceleration along $\underline{V}_a$ and by changes in wind speed. The wind speed variations are in general unknown and their effect is neglected for control purposes; dV_a/dt is taken to be equal to the acceleration along $\underline{V}_a$. It is obtained by considering the forces acting on a basic point mass model of the vehicle. The forces and other required elements of the model are defined in Figure 3.6.
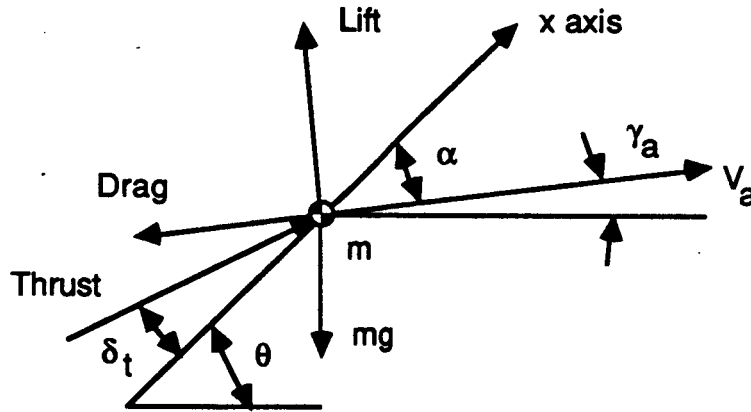
Figure 3.6   Model for derivation of q-control relationships.

In this model,

δ_t = thrust vector trim deflection

θ = vehicle attitude

α = angle of attack

γ_a = air-relative velocity angle

m = mass of the vehicle

g = acceleration due to gravity.

Also defining

$$T = \text{thrust}$$

$$a_d = \text{acceleration due to drag } (- \text{Drag/m})$$

The acceleration along $\underline{V}_a$ is then given by

$$\frac{dV_a}{dt} = a_d + \frac{T}{m} \cos(\alpha - \delta_t) - g \sin(\theta - \alpha) \qquad (3.7)$$

Combining (3.6) and (3.7) yields:

$$\frac{dq}{dt} = A + B\, a_d + C\, T \qquad (3.8)$$

where

$$A = \frac{d\rho}{dt} \frac{q}{\rho} - B\, g \sin(\theta - \alpha) \qquad (3.9)$$

$$B = \sqrt{2\, q\, \rho} \qquad (3.10)$$

$$C = B \frac{1}{m} \cos(\alpha - \delta_t) \qquad (3.11)$$

The expressions (3.8), (3.9), (3.10), (3.11) provide the basic relationships for the q-control scheme.

3.2.3 Available Data

The data required to evaluate the parameters expressed by (3.9), (3.10), (3.11) was assumed to be available from various sources of flight condition data in the Shuttle II vehicle. The angles of attack and sideslip, α and β, and the dynamic pressure, q, were measured quantities available from the air data system (ADS). Density (ρ) and density rate (dρ/dt) were generated by an atmosphere model which used as input current altitude and altitude rate provided by the navigation system. (The atmosphere model was based on the 1976 US Standard Atmosphere.) The acceleration along $\underline{V}_a$ was evaluated from inertial measurements of acceleration and the direction of $\underline{V}_a$ (calculated from α, β and the vehicle attitude).

3.2.4   Drag Estimation

In the implementation of the q-control scheme it was assumed that the thrust level was known – i.e., that it was equal to the commanded thrust – and that the drag-produced acceleration was not known and had to be estimated. First, the q-rate was estimated. Expression (3.6) was used to calculate a q-rate estimate based on the current flight condition data. The parameters A, B, and C were calculated and a_d was obtained by rearranging (3.8) to give

$$(a_d)_{estimated} = \frac{(\frac{dq}{dt})_{estimated} - A - CT}{B} \qquad (3.12)$$

3.2.5   Thrust Calculation

The q-control loop compensator generated the commanded q-rate required to track a commanded q (the q-limit). The thrust level needed to achieve this rate was calculated by another rearrangement of (3.8) employing the estimated a_d and the commanded q-rate:

$$(T)_{q\text{-limit}} = \frac{(\frac{dq}{dt})_{commanded} - A - B (a_d)_{estimated}}{C} \qquad (3.13)$$

This thrust value was provided to the throttling logic. It was assumed that the achieved thrust was equal to this commanded value.

3.2.6   The q-Control Loop

The q-control loop is shown in Figure 3.7. The sensed q was fed back and compared to the q-limit. The resulting error signal was passed through a proportional compensator which generated a q-rate command. A q-rate-command-to-thrust algorithm implementing the sequence of steps described above used this q-rate command to generate the thrust command. With the assumptions that the achieved thrust equalled the commanded thrust and that the thrust calculation was the exact inverse of the actual q-rate response to the thrust, the controlled plant,

including the q-rate command to thrust algorithm, was simply a unity gain integrator.
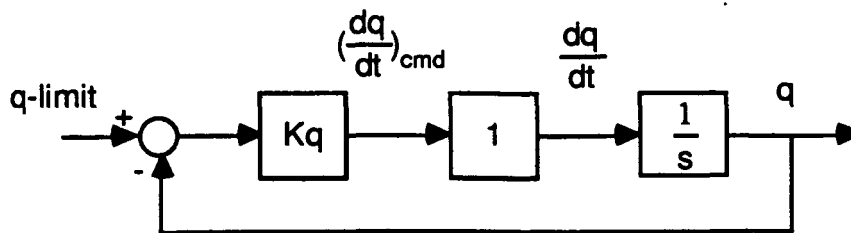
Figure 3.7   The q-control loop.

This simple loop is stable for all positive gains (K_q) so selection of the gain was based on achieving a 'realistic' throttle rate balanced against the attained steady-state error. Values in the range 0.1 to 10 were tried; $K_q = 1$ was selected.

3.2.7   Implementation of q-Control

The thrust value calculated by the q-rate to thrust algorithm was one of three alternative commanded thrust levels which were determined each steering cycle by the throttling system. A nominal thrust, corresponding to all normally operating engines running at 100% throttle, and the thrust level required to attain the 3g acceleration limit were also calculated. The minimum of these three was selected and was supplied to the throttling logic. Thus, the q-limit and the g-limit constraints were met with a continuous variation in thrust.

The throttling logic provided for equal throttling of all the engines or for LH engine-preferred throttling. With LH engine-preferred throttling the RP engines were throttled (from 100%) only when the LH engine throttle setting reached its lower limit. The LH engine-preferred throttling was employed for the majority of the simulations in this study.

3.2.8   Illustrative Results

Throttling for q-control arose mostly under headwind conditions. The following case illustrates the effectivenss of the throttling in limiting maximum q during a trajectory design simulation in which the vehicle followed a specified α-profile under a very severe headwind

condition. The α-profile used was α1=8°, α2=4°, qα = 2800 psf deg, as defined in Chapter 5. The wind profile was Vandenberg Jimsphere Profile #70, described in the Appendix. This was a very large wind which would not actually be expected as a headwind at either the Kennedy Spaceflight Center (KSC) or Vandenberg AFB, but clearly demonstrated the effectiveness of the q-control. Table 3.1 summarizes the maximum attained values of the critical load parameters. The vehicle q-limit was 850 psf and the qα-limit was 3000 psf deg.

q-control	q_{max} (psf)	qα@q_{max} (psf)	$(qα)_{max}$ (psf deg)	$F_{normal\ max}$ (lbs)	Final Mass (slugs)
no	911.2	2727.6	2878.7	585953	9506.4
yes	852.5	2790.1	2878.4	585902	9497.3

Table 3.1   Comparison of cases with and without q-control.
(For a vehicle q-limit of 850psf.)
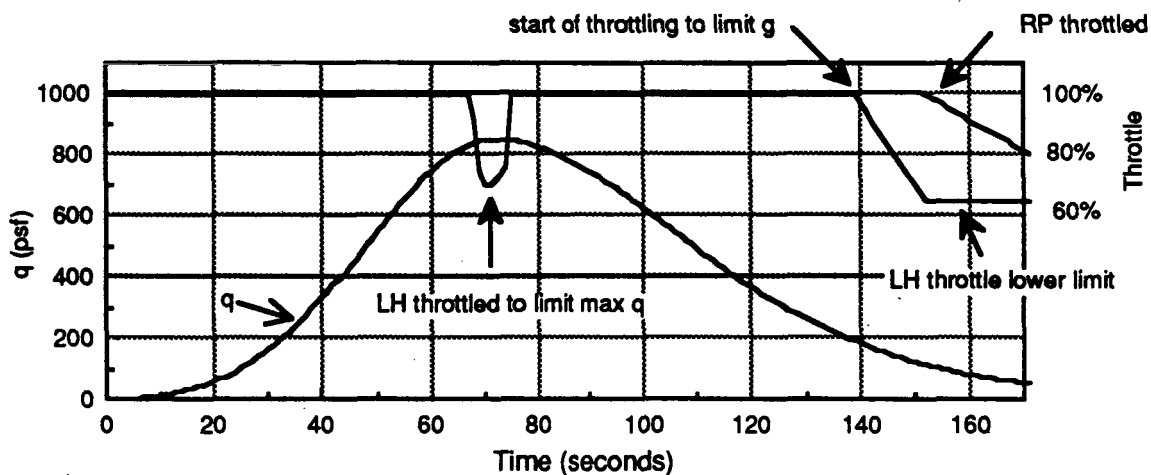
Figure 3.8   Example throttle and q time history.

Figure 3.8 shows a typical time history of engine throttling and q. In this example, with LH-preferred throttling, only the LH throttle level was reduced to limit maximum q. The throttling to limit the net acceleration to 3g commenced at 140 seconds, with the LH engines being

throttled back first. The RP engines started throttling back when the LH engines reached the 65% throttle limit. At RP engine shut down, typically at approximately 176 seconds, the LH engines were throttled back up to 100%. This setting was maintained until throttling to limit acceleration occured again near the end of the ascent trajectory.

3.2.9   Summary of Results

The following points summarize the results obtained with q-control:

1. The q-control effectively prevented q from exceeding the desired q-limit under wind conditions which caused an excessive q in the uncontrolled case. Under conditions in which the q-limit was not reached the q-control throttling mode was never entered.

2. The steady state error in tracking the q-limit was normally positive, as expected for the simple control loop implemented. However, with a high q-rate onset q was occasionally bumped over the limit and the loop subsequently tracked the q-limit from the high side. This overshoot was acceptably small. (An example of this is shown in the case given in Table 3.1.)

3. Throttling to limit q occurred over a comparatively short time, 5 to 10 seconds, even under severe headwind conditions.

4. Limiting q by this scheme caused a small loss of performance. Final mass on orbit was reduced by less than 0.1% (9 slugs) under extremely severe headwind conditions (Vandenburg Jimsphere profile #70). A more typical case resulted in a loss of 0.03% (2.5 slugs).

5. Compared to the case without q-control the trajectory is only slightly perturbed. Velocity at RP engine shut-down was decreased in the order of 0.5%.

6. Throttling to control q had no effect on the stability and response behavior of the steering and flight control loops. This was expected since the flight control loop adapted to varying thrust levels.

7. Under a very large headwind-increase perturbation, which caused the steering to be limited by the $q\alpha$-limit, the q-control did not improve or degrade the trajectory-following. The vehicle was still driven off the designed trajectory (see section 4.3.3).

In conclusion, q-control by throttling was effective in ensuring that the vehicle q-limit was not exceeded. It generally was required only under headwind conditions; under many conditions the q-control throttling mode was never entered. When it was required it was in effect for only a short time. Under all except the most extreme conditions it resulted in a small, acceptable loss of final mass on orbit.

The implementation of q-control used in this study is only one possible approach. Alternative mechanizations based on the same basic relationships might be more suitable when applied to a real system. For example, an outer control loop employing q as the feedback variable could be used in conjunction with an inner loop utilizing acceleration as the feedback variable by directly applying the q-rate-to-acceleration relationship, Equation (3.6). Such an approach would allow the 3 g acceleration limit to be met by applying a limiter directly in the inner loop. The inner loop would also indirectly accommodate thrust errors.

4. Guidance and Steering

4.1   Introduction : Mission Description

In this study, the ascent trajectory of the Shuttle II vehicle was composed of four guidance/steering phases. These phases are illustrated in Figure 4.1. The first two phases were described as the vehicle launch phases. Following a vertical rise to clear the launch pad a launch maneuver pitched the vehicle over, nose down. (A heads-up ascent trajectory was flown.) The launch maneuver placed the vehicle into the attitude required for transition to closed loop endoatmospheric steering. The endoatmospheric phase which followed the launch maneuver was the main focus of this study. The final, primarily exoatmospheric phase employed powered explicit guidance (PEG). PEG is currently used on the Shuttle I for stage two and on-orbit guidance[5].

The ascent trajectory was limited by several flight constraints. Vehicle structural limits required that corresponding limits on maximum dynamic pressure (q), maximum $q\alpha$ product and maximum aerodynamic load not be exceeded. Crew physiological requirements limited the maximum net acceleration to 3 g.

The $q\alpha$ product limit and the load limit were essentially equivalent since aerodynamic force is proportional to $q\alpha$. The $q\alpha$ product is also proportional to the thrust vector deflection required to balance the aerodynamic moment if it were included in the model. Thus, in this study only the $q\alpha$ product was monitored and limited by the guidance and control system. Also, in this study a single $q\alpha$ limit (3000 psf•deg) was applied over the whole ascent trajectory and the effect of sideslip (β) was neglected. In a detailed investigation with a more defined vehicle configuration, the load constraints would be expressed in a more extensive manner in terms of both $q\alpha$ and $q\beta$ products. In Shuttle I, a series of critical flight conditions are defined in terms of $q\beta$ vs $q\alpha$ envelopes, specified at varying Mach numbers and known as "squatcheloids", are employed[6].

---

[5]   McHenry, R.L., Brand, T.J., Long, A.D., Cockrell, B.F., Thibodeau, J.R., "Space Shuttle Ascent Guidance, Navigation and Control". *The Journal of the Astronautical Sciences*, Vol. XXVII, No. 1, pp 1-38, January-March, 1979.

[6]   Schleich, W.T., "The Space Shuttle Ascent Guidance and Control". AIAA Guidance and Control Conference, August 9-11, 1982. San Diego, California. AIAA 82-1497.

The acceleration and dynamic pressure limits were met by throttling the engines, as was discussed in section 3.2. The qα limit was met by limiting the angle of attack commanded by the guidance system during the endoatmospheric steering phase. A qα limiter was also provided during PEG steering, until q dropped below a minimum value (10 psf), but under normal conditions was not required.

The ascent trajectory objective was insertion into low earth orbit. For this study, all mission simulations were flown from launch at KSC to a 28.5°, 50 by 100 mile orbit. Trajectory designs were based on maximizing the final mass achieved on orbit.
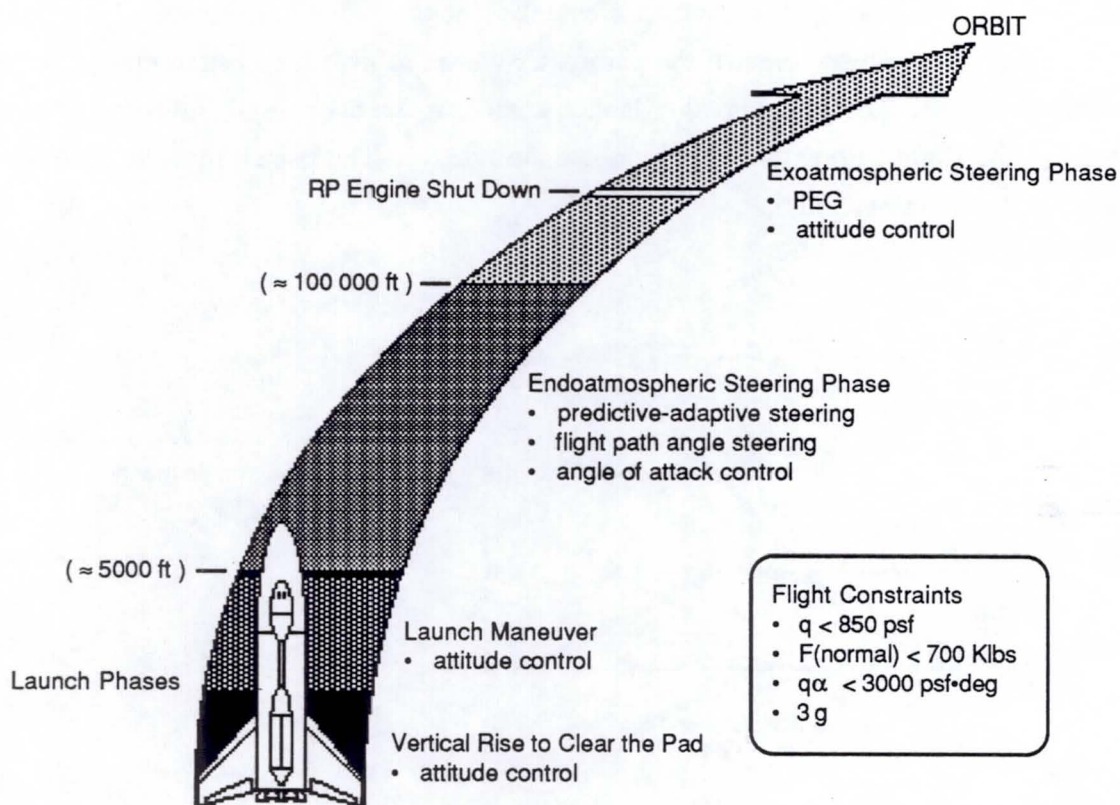
Figure 4.1 Overview of ascent steering phases.

4.2   Vehicle Launch

The vehicle launch phases involved an initial vertical rise to get the vehicle clear of the pad and a subsequent pitchover maneuver which placed the vehicle and its velocity vector into the correct attitude for the initiation of closed-loop steering. In the vertical rise phase the vehicle was commanded to maintain a 90° pitch attitude. In the pitchover maneuver, known as the launch maneuver, the vehicle attitude was commanded according to a time-based schedule. Initially, a simple constant pitchrate maneuver, or "kick maneuver", was used. However, the initiation and termination of such a kick maneuver involved large transients. It was replaced by a "smooth" launch maneuver utilizing a sinusoidally varying pitchrate schedule. The form of this maneuver is shown in Figure 4.2. The maneuver was specified in terms of its duration (t_{kick}) and one half of the maximum pitchrate magnitude (Ω_{kick}). These parameters were generated by the launch designer routine, an element of the prelaunch trajectory design process. The launch designer routine selected the parameter values to give the desired end of launch maneuver conditions. The desired end of launch conditions were expressed in terms of angle of attack (α) and flight path angle (γ) or by α and attitude (θ). The launch maneuver designer routine is discussed in Section 5.2.
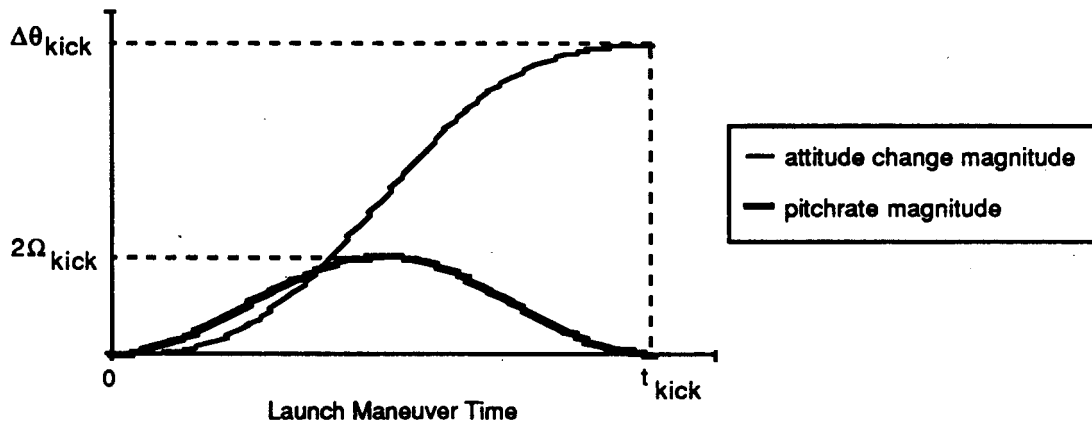
$$\text{pitchrate} = \Omega_{kick}\left(1 - \cos\left(\frac{2\pi}{t_{kick}}t\right)\right)$$

Figure 4.2   Form of the "smooth" launch maneuver.

36

4.3   γ-Steering with α-Control

4.3.1   Description

Flight path angle (γ) steering with angle of attack (α) control was the technique employed during the endoatmospheric phase of ascent for following an ascent trajectory defined in terms of a γ-profile. The γ-profile that was followed was generated by the trajectory design elements of the guidance system, which could have both prelaunch and in-flight (predictive-adaptive) elements.

The basis of the γ-steering with α-control concept is the observation that angle of attack can be used to control the net force acting on the vehicle normal to the velocity vector. The net normal force, neglecting gravity, is made up of aerodynamic and thrust forces. The magnitude of this aerodynamic force is dependent on α (as well as Mach number and dynamic pressure). The directions of the aerodynamic force and of the thrust force are also related to α since the vehicle attitude with respect to the velocity vector depends on α. (The thrust force trim angle relative to the vehicle body attitude, if one is required to control the aerodynamic moment, will also be a function of α.) Therefore, the rate of rotation of the velocity vector due to the net normal force, seen as the flight path angle rate, can be functionally related to α. This relationship can be applied in a closed-loop steering scheme employing feedback of γ. In such a γ-steering loop, the steering compensator determines a γ-rate command to null the γ error, the difference between the desired γ and the actual γ. The α required to generate this γ-rate is then calculated by an algorithm using the functional relationship between γ-rate and α. This required α is commanded to an α flight control system.

Employing γ-steering with α-control to guide the vehicle along an ascent trajectory has a variety of advantages over simply following an attitude schedule in an open loop manner, as is done during first stage in the current Shuttle I. Since α control is being used with the γ-steering, load relief can be directly included in the system by simply limiting the maximum α that the steering can command. (In an attitude control system, load relief must be achieved through an additional feedback term that modifies the attitude error.) It also turns out, as is subsequently shown, that γ-steering is quite robust in the face of environmental and other dispersions. It is also well suited for use in conjunction with predictive adaptive schemes which may be used to adjust the trajectory during flight in order to improve performance.

37

The γ-steering with α-control concept, originally developed and implemented at CSDL for the steering of conventional boost vehicles, was first reported by Bonnice[7]. The development and implementation of the concept in the present study were somewhat different than that described by Bonnice, however, since the vehicle requirements and the trajectory objectives were different in the case of Shuttle II than in the case studied by Bonnice.

4.3.2   Derivation of the Relationship Between γ-Rate and α

The relationship relating α to γ-rate was obtained from a simplified two degree of freedom pitch plane model of the vehicle. In this model the vehicle was assumed to be unbanked. All forces, velocities and accelerations were assumed to lie in the pitch plane. The earth-relative reference frame was assumed to be inertial. The model is illustrated by Figure 4.3.

V_e - earth-relative velocity
γ_e - earth-relative flight path angle
V_a - air-relative velocity
γ_a - air-relative flight path angle
V_w - wind velocity
θ - earth-relative pitch atttitude
α - angle of attack
δ - thrust vector trim deflection
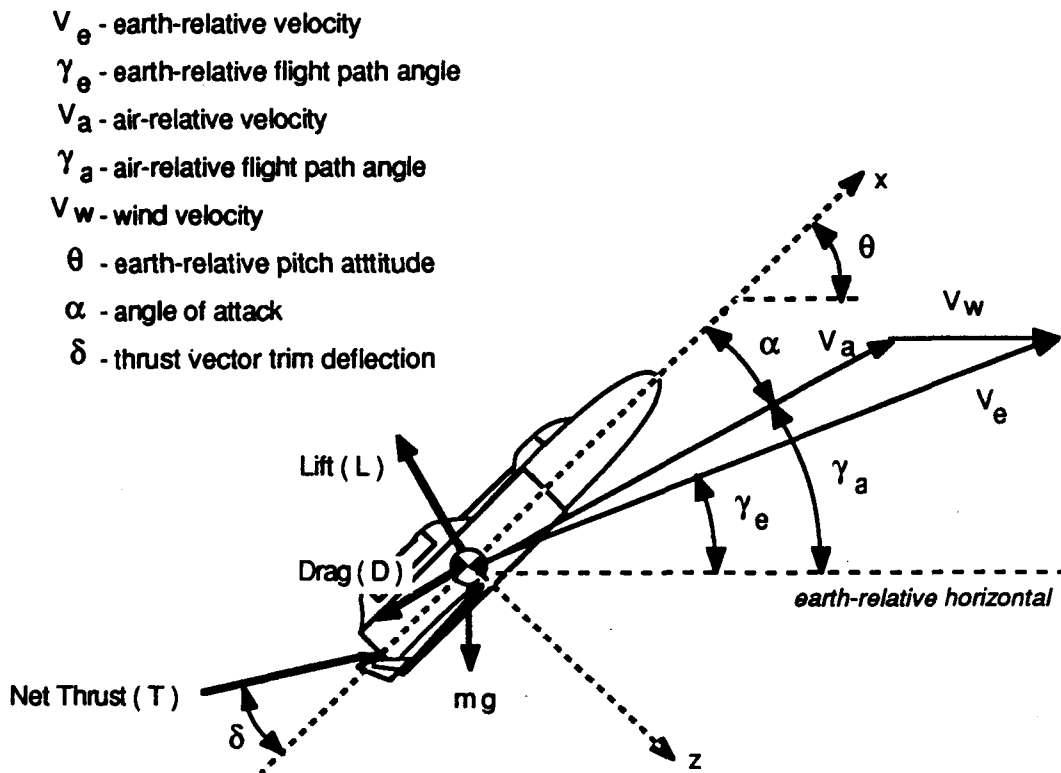
Figure 4.3.   Model for development of the α to γ-rate relationship.

7   Bonnice, W.F., "Steering of a Boost Vehicle to a Desired Flight Path Angle Trajectory using Angle of Attack Control". 1983. Massachusetts Institute of Technology Masters of Science Thesis, CSDL Report T-802.

Consideration of this model led to the basic expression

$$m \dot{\gamma}_e V_e = L \cos(\gamma_a - \gamma_e) - D \sin(\gamma_a - \gamma_e) + T \sin((\gamma_a - \gamma_e + \alpha) - \delta) - mg \cos(\gamma_e)$$

$$(4.1)$$

where the γ-rate was

$$\dot{\gamma}_e = \frac{d\gamma_e}{dt}$$

It was further assumed that the all of the angle differences in (4.1) were small values, x, so that the approximations $\cos(x) \approx 1$ and $\sin(x) \approx x$ could be used. The drag (D) was found to be at most 15% of the thrust (T) for the Shuttle II SSTO configuration considered and was assumed to be negligible. The lift (L) was assumed to be expressed as

$$L = Sq(Cl_0 + Cl_\alpha \alpha)$$

where Cl_0 and Cl_α are parameters which were varied with Mach number (M) only and S was the reference area. With these assumptions, equation (4.1) was simplified to give

$$m \dot{\gamma}_e V_e = [Sq\, Cl_0 + T(\gamma_a - \gamma_e - \delta) - mg \cos(\gamma_e)] + [Sq\, Cl_\alpha + T]\alpha \quad (4.2)$$

This expression may be rearranged into the form

$$\alpha = K1 \dot{\gamma}_e + K2 \quad\quad (4.3)$$

where the two parameters, K1 and K2, are given by:

$$K1 = \frac{m V_e}{T + Sq\, Cl_\alpha} \quad\quad (4.4)$$

$$K2 = \frac{mg \cos(\gamma_e) + T(\delta + \gamma_e - \gamma_a) - Sq\, Cl_0}{T + Sq\, Cl_\alpha} \quad\quad (4.5)$$

The parameter K2 can be thought of as the "trim" value of α at which the net thrust and

39

aerodynamic forces balance the component of gravity normal to the velocity vector and thus at which the γ-rate is zero. The parameter K1 is the actual γ-rate to α "gain". In a γ-steering system which includes integral compensation it is not necessary to include the parameter K2 in the algorithm which calculates the α command since the integrator will 'load up' and bias the γ-rate command to yield an equivalent result. However, including this parameter does ease the demand on the compensation because it effectively allows the integrator to act as a vernier, accommodating the error in K2 itself rather than accounting for the whole "trim" α. The full expression (4.3), including K2, was implemented in the γ-steering algorithm used in this study.

4.3.3   Implementation

The general form of the γ-steering loop implemented in this study is shown in Figure 4.4. Proportional plus integral compensation was used. In the event of α-limiting occurring in the FCS the steering compensator integration of γ_e was suspended to prevent integrator wind-up. The option was provided to feed forward a γ-rate signal, if one was available, in order to improve the system response. In this study the γ-profile was stored in a manner which allowed generation of a smooth commanded γ-rate signal and this feed forward feature was usually employed.

The parameters K1 and K2 used in the γ-rate to α algorithm were evaluated each steering cycle. (The steering cycle was the same as the simulation integration cycle in this study.) The data required to evaluate them was assumed to be available from vehicle sensors, state estimators and stored data. The mass (m) was assumed to be available from a mass estimator and the thrust (T) was assumed equal to that commanded by the throttling logic. V_e and the angles, γ_e and γ_a, were obtained from IMU and ADS information. Values for q and M were also obtained from the ADS. The aerodynamic coefficients, Cl_0 and Cl_α, were interpolated from data stored with respect to M in tables. For this study the thrust vector trim deflection, δ, was zero; in the more general case a value would be provided by a trim algorithm. S and g were constants.

Similar to the flight control system, the steering loop was designed in the continuous s-domain without analytical consideration of the effects of sampling present in the simulation. It was designed with an adequate phase margin to allow for the effective lag introduced by the digital

implementation. This lag was actually quite small in the frequency range of concern since the steering loop 0 db crossover was at a fairly low frequency. The gains were trimmed based on the time domain simulation results. In designing the loop it was assumed that the combined dynamics of the γ-rate to α algorithm and the FCS plus vehicle elements had the dynamics of the FCS plus vehicle system. The open- and closed-loop (γ / γ_{ref}) frequency responses of a representative s-domain design for the steering loop are shown in Figure 4.5. Crossover was at 0.3 rad/s and the phase margin was 51°.
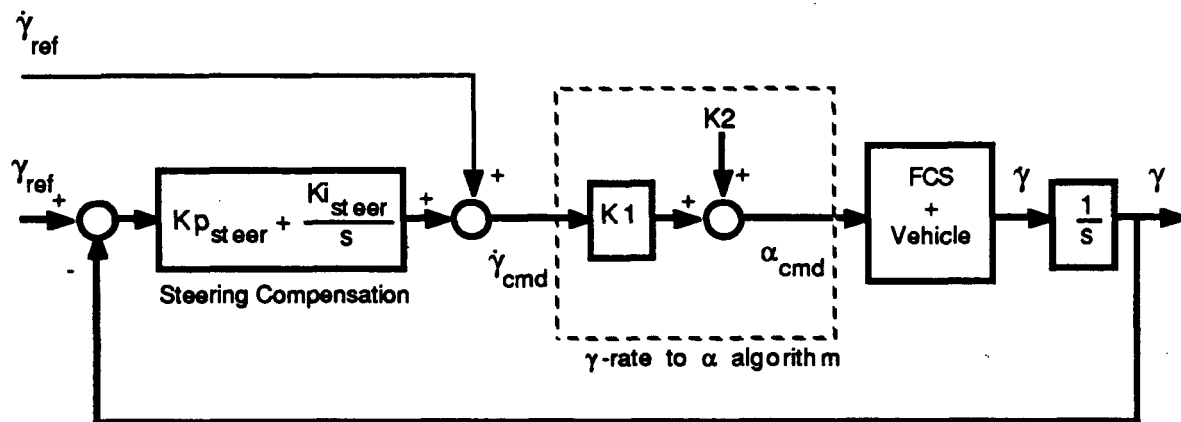
Figure 4.4   General form of the steering system.

4.3.4   Performance

The performance of the γ-steering with α-control was investigated under nominal conditions, with dispersions in the vehicle state at the end of the launch maneuver, and with dispersions in the wind environment. The trajectory tracking was very accurate in all situations except one. The one condition that was found to cause poor performance and even failure of the steering was a severe headwind increase.

Under nominal conditions the trajectory was virtually identical to the reference trajectory. The achieved final mass was usually within approximately 2 slugs of that achieved by the reference trajectory. Figure 4.6 shows a typical time history of the error in γ. After the initial transient at the start of the steering phase the error was small, less than 0.1°.
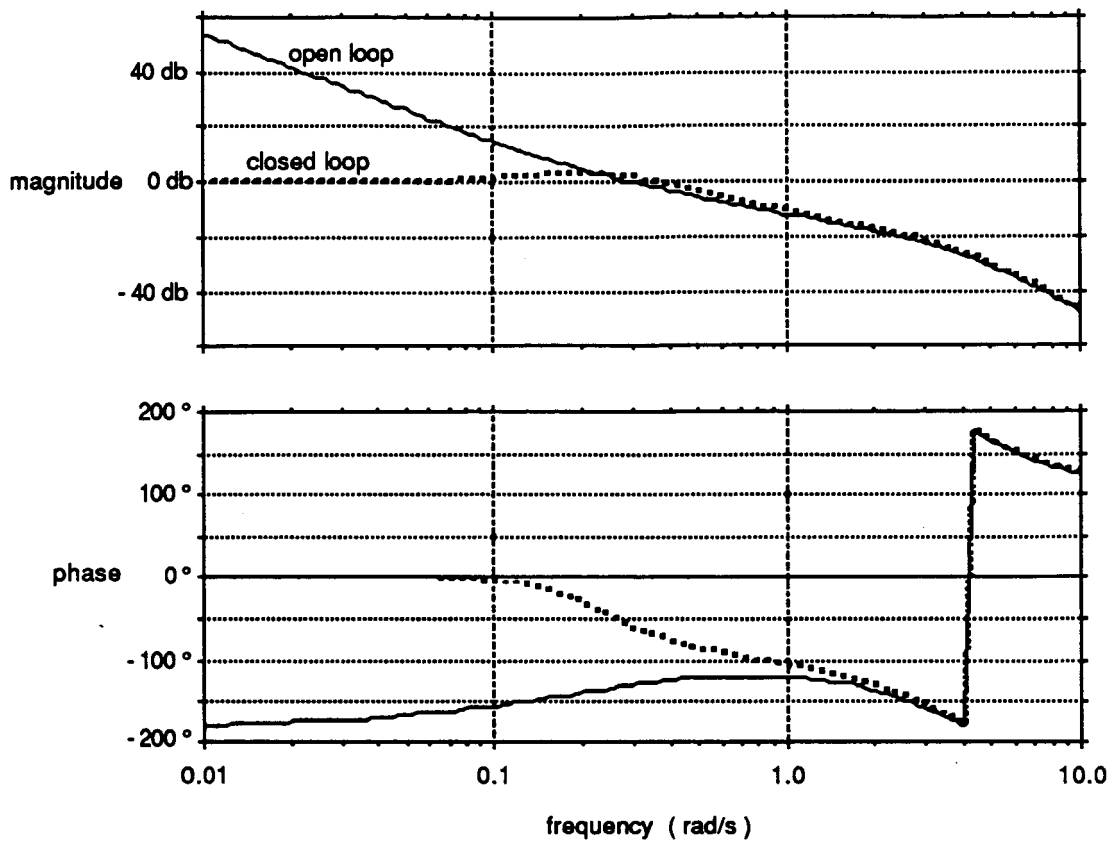
Figure 4.5   Frequency response of representative s-domain design of the steering loop.
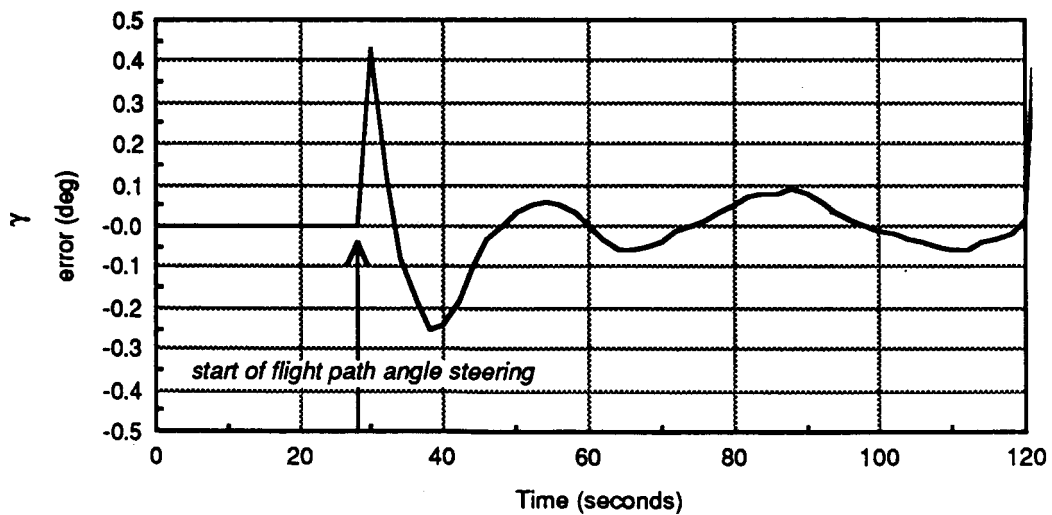
Figure 4.6   Typical γ error with γ-steering under nominal conditions.

42

The steering performance was studied with launch dispersions in order to determine the system's ability to handle a significant initial error. An optimal reference trajectory was followed after launch maneuvers in which the launch maneuver pitchrate parameter was varied ±10%, giving ±3% attitude errors at the start of steering. All of the trajectories were under no wind conditions. The γ-steering was found to be able to handle such errors. The γ error resulting from the launch dispersion was removed within approximately 25 seconds after the start of γ-steering in both cases. The launch dispersions caused only a 1 slug loss in final mass. The time histories of γ and altitude (H) are shown in Figure 4.7 for the nominal and dispersed cases. The altitude profile was not visibly effected by the launch dispersions. The effect of the γ errors on altitude in the dispersed cases was small because the errors were quickly nulled by the steering.
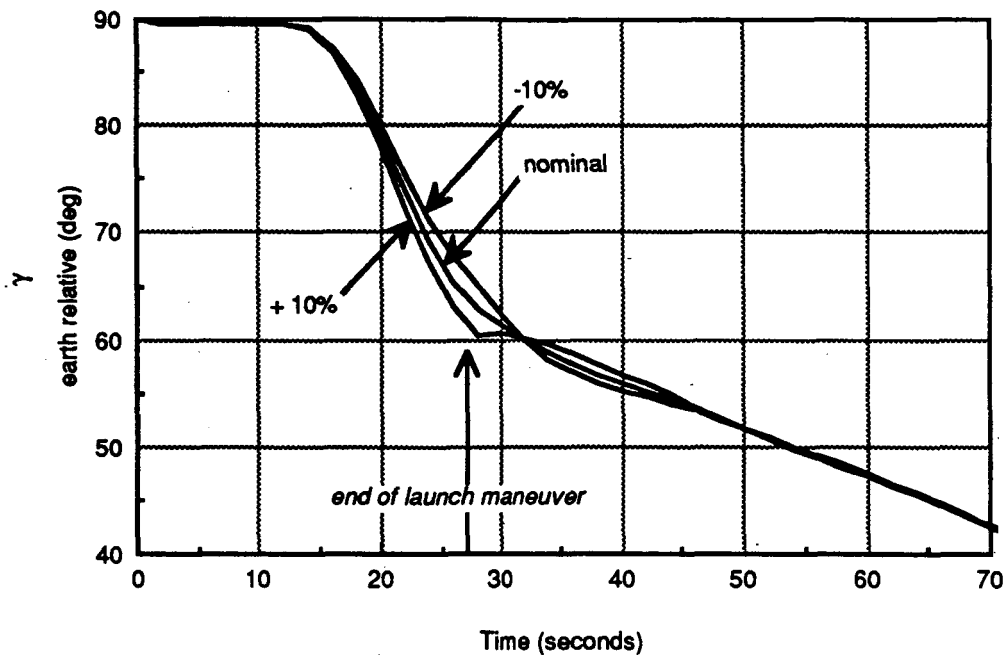
Figure 4.7 Effect of launch dispersions.

a) Flight path angle.
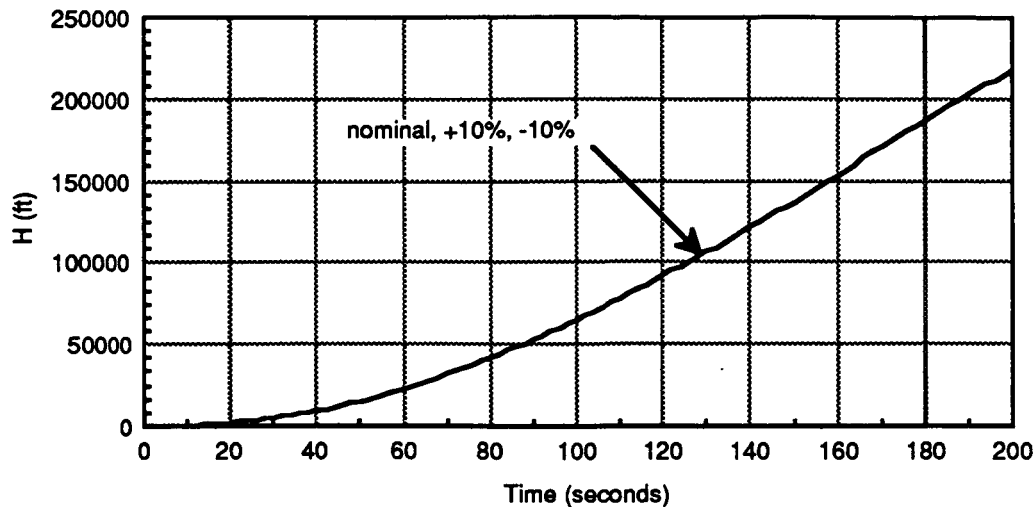
Figure 4.7   Effect of launch dispersions.

b) Altitude

The most significant dispersions which the vehicle would encounter during ascent, apart from massive vehicle dispersions such as engine failure, would be wind dispersions. Thus, the performance of the γ-steering in a wind profile perturbed from that for which the reference trajectory was designed was an important area of investigation. The perturbations that were considered were changes in the wind profile equivalent to tailwind increases and to headwind increases. (A headwind decrease is equivalent to a tailwind increase and vice versa.)

It was found that tailwind increases did not degrade the tracking performance of the γ-steering system. In fact, tailwind increases normally produced a performance benefit. In one example, when following a trajectory designed under no wind conditions in a tailwind having the shape of Vandenberg Profile #69 (described in the Appendix), the final mass was increased by 7 slugs compared to the nominal case.

Headwind increases also presented no difficulty for the γ-steering unless they were large. In the case of large headwinds the vehicle encountered what was termed "qα-limiting". This was found to degrade performance and in severe cases make it impossible for the trajectory to be successfully flown. The effect of the headwind was to increase α, resulting in an elevated qα. With a sufficient headwind increase the qα reached the vehicle limit. When this occurred the α commanded by the steering system was limited in order to prevent the qα-limit from being

exceeded. In essence, the vehicle was weathervaned into the wind for load relief. In this situation the vehicle was unable to track the reference trajectory. Thus, such limiting drove the vehicle off of the desired trajectory and a γ error was developed. The limiting tended to depress the trajectory which compounded the effect by increasing the dynamic pressure. In the most severe cases this depression of the trajectory was divergent and the vehicle went into a dive. In less severe cases the steering could fully or partly correct the error after the region of $q\alpha$-limiting was passed but performance was lost and the final mass was reduced.

The magnitude of the headwind which caused $q\alpha$-limiting, the resulting tracking error and performance loss was dependent on the $q\alpha$ margin between the maximum $q\alpha$ in the reference trajectory and the vehicle limit. This impacted the shaping of the reference trajectory, as discussed in Section 5.2.3. If the reference trajectory was designed with a reduced maximum $q\alpha$, giving an increased margin, a larger headwind increase could be accommodated by the steering system before limiting was encountered.

A comparison between a nominal trajectory and two trajectories in which limiting occurred is given in Figure 4.8. The nominal case was in a no wind environment. The other cases were simulated in headwinds having the shape of the Vandenberg Profile #69 (see the Appendix) and with their magnitudes scaled to 40% and 60% of the full magnitude of this profile.

In Figure 4.8 (a) the $q\alpha$ limiting can be seen in the cases experiencing the headwinds. Figure 4.8 (b),(c) and (d) shows the resulting error in γ and the consequent depression of the trajectory. The $q\alpha$-limiting had only a small, indirect effect on the velocity, as seen in Figure 4.8 (e). Velocity was slightly reduced in the $q\alpha$-limited cases because the depression of the trajectories caused the degree of throttling required for control of maximum q to be greater and to last longer. The q profiles are given in Figure 4.8 (f). The behavior of the FCS was not affected by the $q\alpha$-limiting, as evidenced by the similarity of the α error in the three cases given in Figure 4.8 (h).
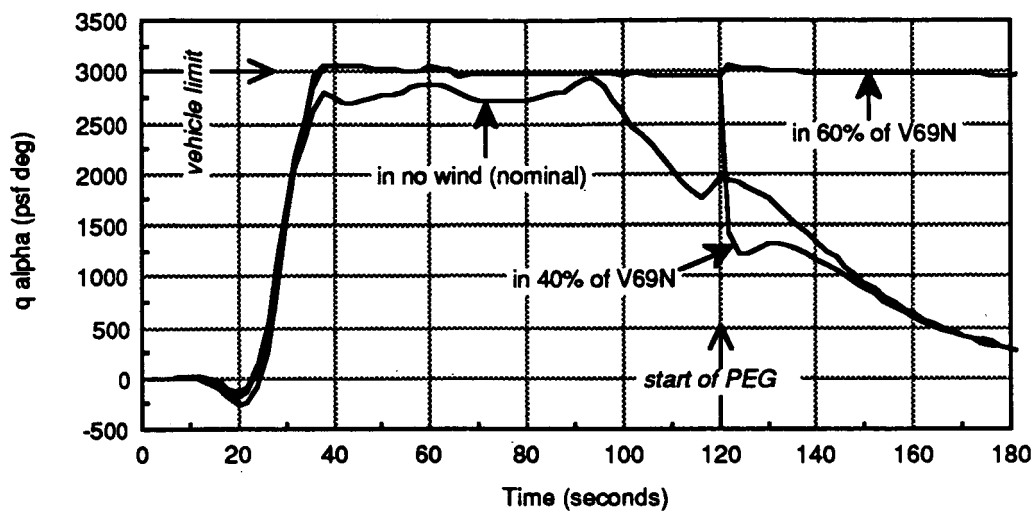
Figure 4.8   Steering performance under nominal and qα-limited conditions.

a) qα product.
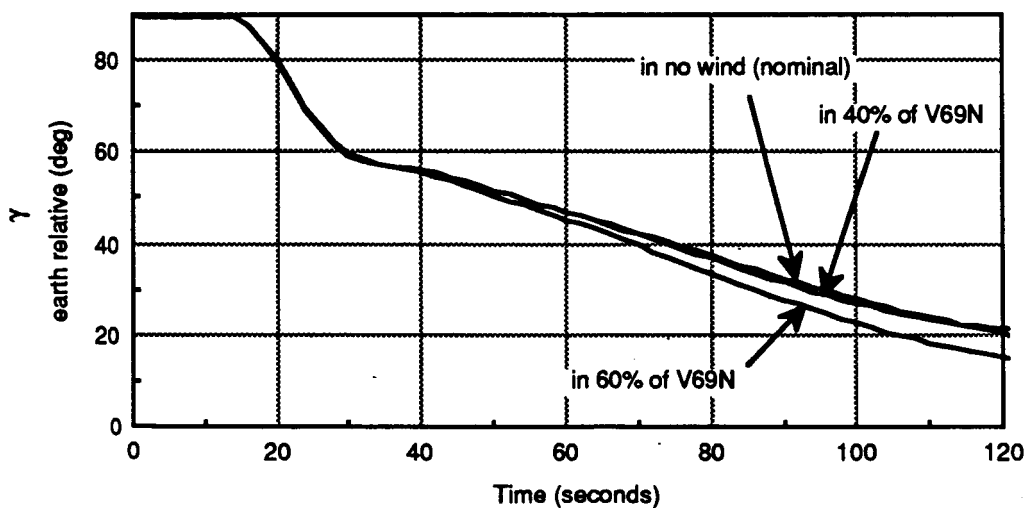
Figure 4.8   Steering performance under nominal and qα-limited conditions.

b) Flight path angle.
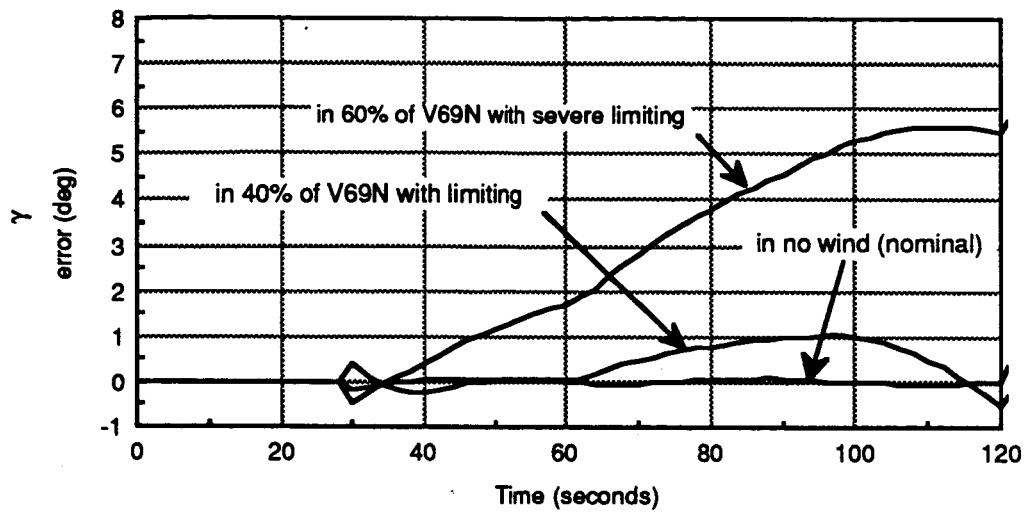
Figure 4.8 Steering performance under nominal and qα-limited conditions.
c) Flight path angle error.
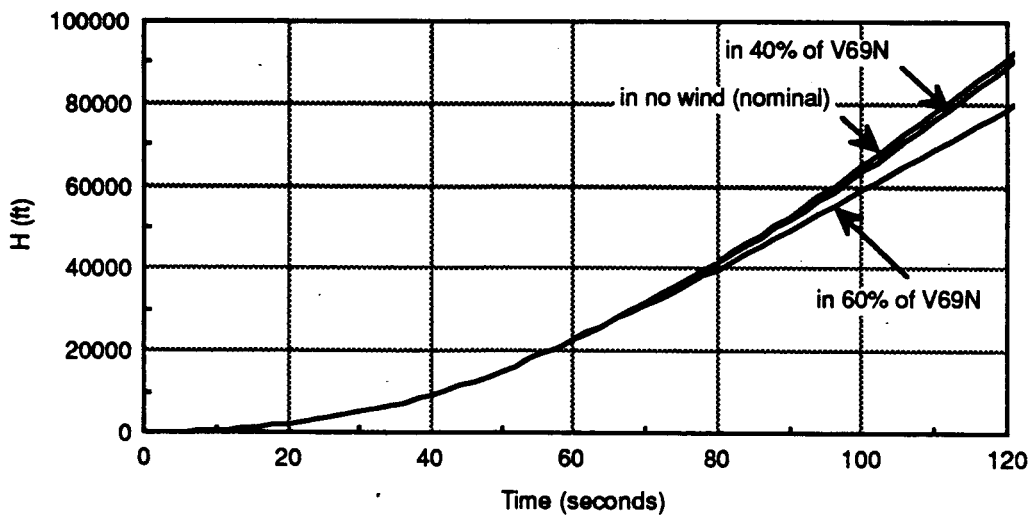
Figure 4.8 Steering performance under nominal and qα-limited conditions.
d) Altitude.
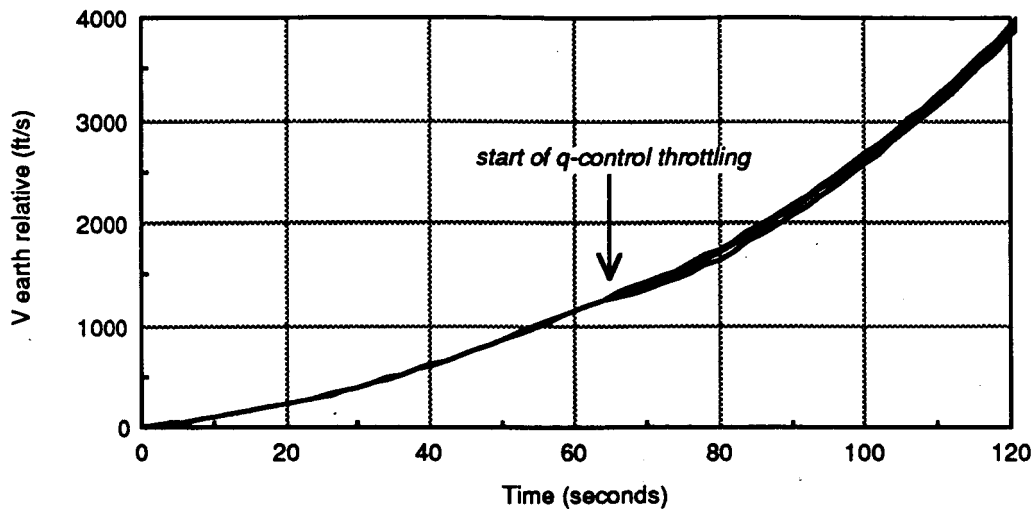
Figure 4.8   Steering performance under nominal and qα-limited conditions.
e) Earth relative velocity.
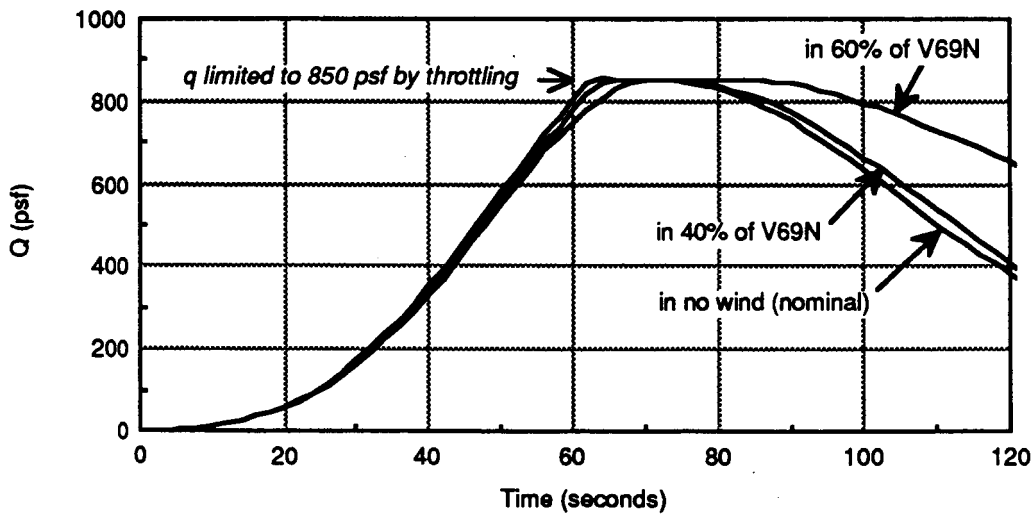
Figure 4.8   Steering performance under nominal and qα-limited conditions.
f) Dynamic pressure.

48
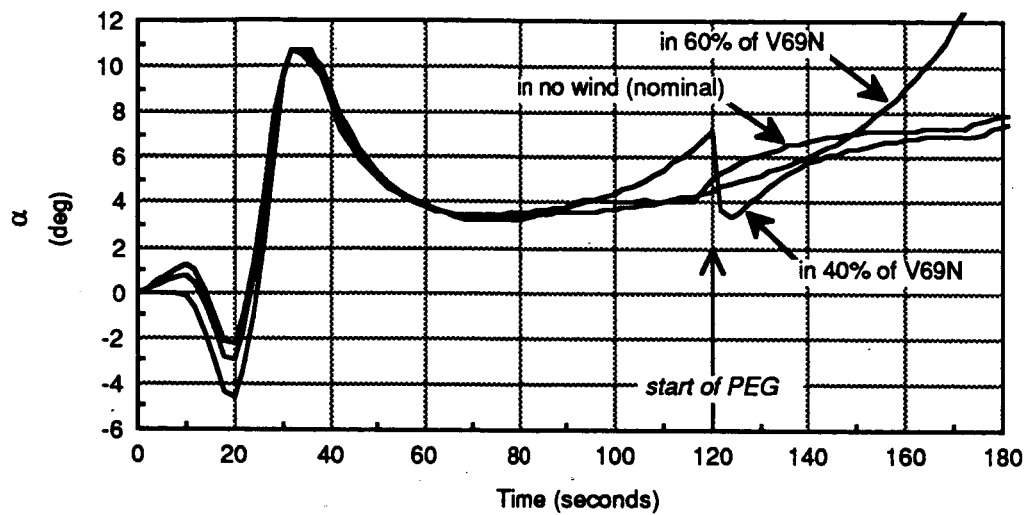
Figure 4.8   Steering performance under nominal and qα-limited conditions.

g) Angle of attack.
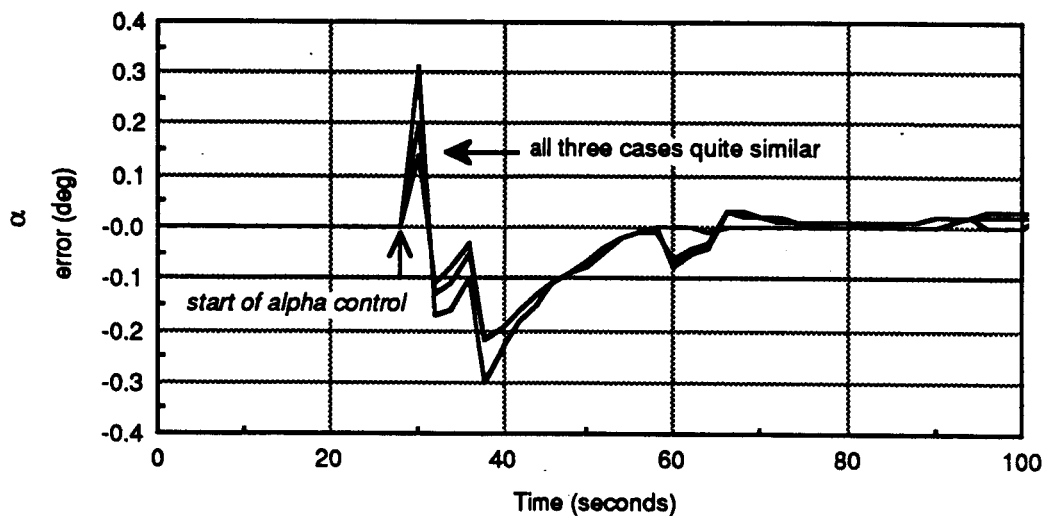
Figure 4.8   Steering performance under nominal and qα-limited conditions.

h) Angle of attack error in the FCS.

4.4 Predictive-Adaptive Guidance for Maximum Final Mass

4.4.1 Description

The γ-steering method described in the previous section provided a robust technique with which to follow a designed trajectory stored as a γ-profile. Normally, this reference trajectory would be designed before launch to give mass-optimal performance under the environment and vehicle design conditions. However, the stored reference trajectory might, for some reason, not be optimal for the conditions actually encountered during flight. For such situations, a technique which could adjust the trajectory during flight to improve performance was desired. A predictive-adaptive guidance technique was developed to accomplish this.

The predictive-adaptive technique that was developed used a γ-rate bias term (RATEBIAS) to generate an adjustment to the stored γ-profile. The adjusted γ-profile was followed using the regular γ-steering. The γ-rate bias term was updated incrementally. This was done by performing predictive simulations periodically during flight. The simulations, started at the current vehicle state, provided predictions of the final mass. They were used to determine the effect of adjustments to the γ-rate bias, which was initially zero, on the final mass. The most favorable adjustments – those increasing the final mass – were selected. The γ-rate bias term was the accumulated sum of these adjustments. Thus, throughout the ascent phase in which this technique was employed, the γ-rate bias term was incrementally varied to improve performance. If improvement was not possible, the bias term remained zero and the nominal, reference trajectory was flown.

4.4.2 Implementation

The adjustment which was applied to the γ-profile was the integral of the γ-rate bias. It was added to the nominal γ, obtained from the reference γ-profile, to yield the flight path angle command (γ_{ref}) which was supplied to the steering algorithm. The γ-rate bias itself was added to the nominal γ-rate to obtain the rate command (γ-rate$_{ref}$) which was fed forward. (See Figure 4.4). The γ-rate bias was initially set to zero when γ-steering was commenced. At selected intervals, a set of two or three predictive simulations of the trajectory from its current state up to RP burnout were performed. The first of these simulations used the current γ-rate bias. In the second run a small decrement was applied to the γ-rate bias, adjusting the

trajectory downwards. If this decrement improved the final mass on orbit, as predicted by the PEG routine at RP shutdown, it was applied to the γ-bias rate used by the actual steering equations. Otherwise, an increment was tried. The increment to the γ-bias rate adjusted the trajectory upwards. If it improved the final mass, the increment was applied to the γ-rate bias. If neither adjustment increased the final mass on orbit the γ-rate bias used by the actual steering equations was left unchanged until the next predictive-adaptive cycle. Thus, if an adjustment to the trajectory improved performance, it was gradually built-up and trimmed with each predictive-adaptive simulation cycle. Figure 4.9 illustrates the trajectory adjustments which were tried each cycle.
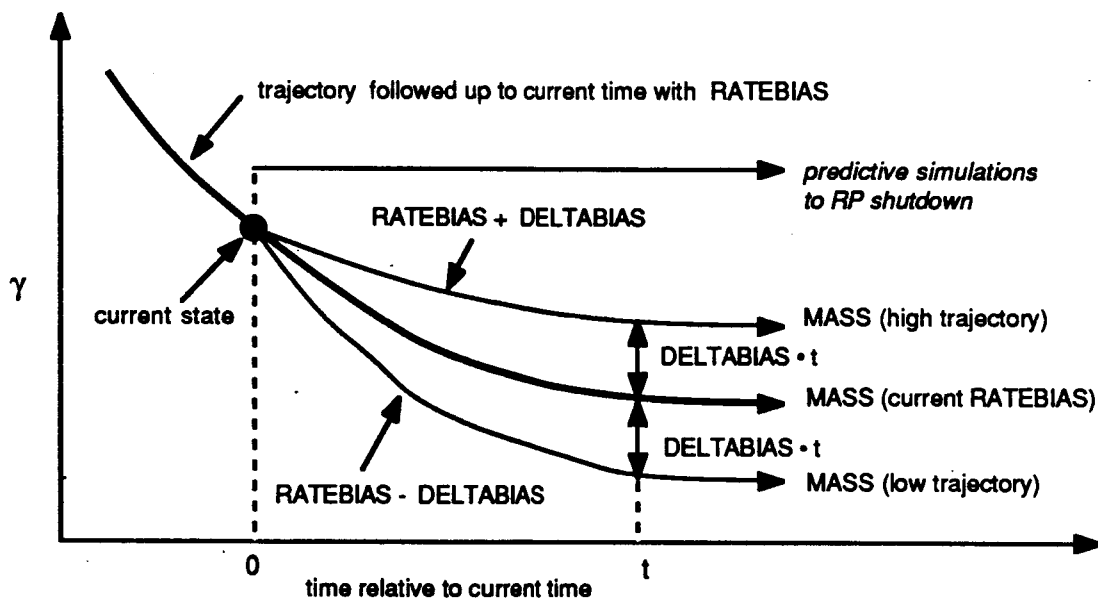
Figure 4.9 Trajectory adjustments which were tried each predictive-adaptive cycle.
(The trajectory was simulated first with the current RATEBIAS, then the low trajectory was tried. If the low trajectory resulted in improved final mass it was used immediately and the high trajectory was not simulated.)

Provisions for handling undesirable lofting or diving trajectories which could arise in extreme conditions were included in the predictive-adaptive logic. A simplified schematic is given in Figure 4.10 of the predictive-adaptive logic which was implemented.
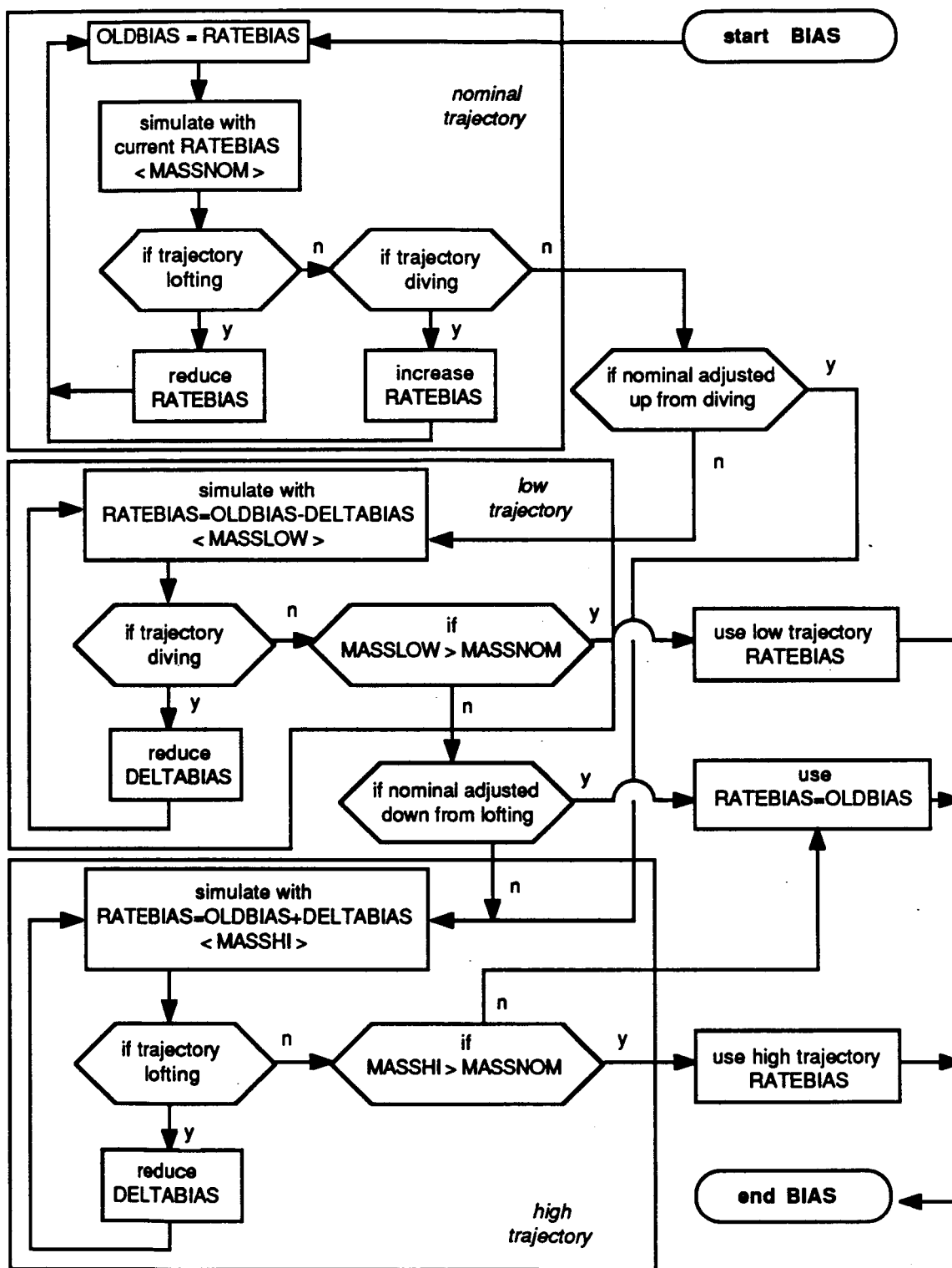
Figure 4.10 Simplified schematic of γ-rate bias selection logic.

The issues critical in determining the effectiveness of this predictive-adaptive scheme were the frequency at which the adaptive adjustments were made and the selection of the magnitude of the increment that was tried each cycle. A high adaptive cycle frequency imposed a larger computational load on the guidance system. The advantage of high frequency was that it allowed smoother and more timely adjustments to the trajectory. The selection of the increment value was related to the adaptive cycle frequency. It had to be large enough to cause meaningful adjustment of the trajectory given the length of the cycle but not so large as to risk degrading performance whenever it was applied. It was found that a cycle period of 10 seconds gave good results when a DELTABIAS adjustment of approximately $0.06°/s$ was used. The system capability to respond to commanded γ-rate changes was also a factor in determining the predictive-adaptive cycle frequency and adjustment magnitude. It was noted that this adjustment magnitude caused fairly large thrust vector deflections when it was applied during the last few cycles of predictive-adaptive guidance. Increasing the cycle frequency and decreasing the adjustment magnitude in equal proportion was found to result in the same performance but with smaller thrust vector deflections. Alternatively, since the last few adjustments produced little change in the trajectory, the bias updates could simply have been terminated sooner than one predictive simulation cycle before transfer to PEG.

A further issue in the implementation of the predictive-adaptive guidance scheme was the type of simulation used to perform the in-flight predictive simulations. Initial demonstration of the approach employed an adapted version of the full 6 degree of freedom vehicle simulation. This was expensive in terms of computer time and the accuracy which it provided was not really needed. In order for the predictive-adaptive logic to make the correct biasing decisions it was required only that the predictive simulations results compared to each other the same way as would accurate simulations. The relative magnitudes of final mass, not the absolute magnitudes, was the important issue.

A simplified three degree of freedom (3 DOF) vehicle simulation was condensed out of the full simulation to serve as the predictive simulation used by the predictive-adaptive algorithm. It had the same structure as the main simulation but the vehicle rotational and control dynamics were deleted. The vehicle was positioned to produce the attitude or angle of attack commanded by the steering each control cycle. This reduced the number of calculations performed each integration cycle and, with the elimination of the fast dynamics, allowed the use of a larger integration time step. Also, the γ-steering loop was simplified by removing the integral component of the compensator. (This also simplified changing the integration time step which

otherwise required varying the discrete integration gain.) Thus, the computational load could be significantly reduced. It was found that the 3 DOF simulation could be run with an integration time step of up to 1 second, ten times the time step size of the full simulation. With the 3 DOF predictive simulation running with this time step the predictive-adaptive guidance achieved almost the same performance as when using the full vehicle simulation for prediction.

A further reduction of the computational load was investigated using a simplification in the biasing algorithm. The logic was modified to reduce the number of calls made to the predictive simulation for each predictive-adaptive cycle. The "nominal" simulation was eliminated in all except the first cycle so that only one or two simulations were performed each cycle rather than two or three. The estimate of final mass corresponding to the selected bias adjustment was retained as the "nominal" one from one cycle to the next. The performance of the modified logic with the 3 DOF simulation using integration time steps ranging in size from 0.1 second, the value used in the main simulation, up to 1.0 second was verified. The overall performance of the predictive-adaptive guidance employing the reduced number of simulations, running with 1.0 second integration step size, in most cases matched that of the previously used logic using the simulation running with a 0.1 second step size. The simplified scheme required significantly less CPU time than the original scheme. The trajectory adjustments were slightly different in various cases tested using the two schemes, especially in the last few predictive-adaptive cycles, but these differences were generally inconsequential. Unfortunately, under some conditions involving large wind dispersions the simplified scheme had difficulties and the predictive-adaptive guidance failed to operate properly. It was decided, therefore, to use the original scheme in which the "nominal" predictive simulation was performed each cycle. However, the 3 DOF predictive simulation was normally run at the larger time step of 1 second.

4.4.3   Performance

The performance of the predictive-adaptive guidance for maximum final mass was investigated under nominal conditions, with environmental dispersions, with an engine failure, and with off-optimal reference trajectories. In all cases except the last one the scheme did not provide any performance benefits. When the reference trajectory used by the steering was off-optimal the scheme worked effectively, correcting the trajectory to yield close to the optimal performance.

Under nominal conditions, when following an optimal reference trajectory the predictive-adaptive scheme generated only minimal adjustments to the γ-profile and caused no significant change in the final mass. In the presence of wind changes, the system again did not produce any significant adjustments to the trajectory. Performance was virtually identical to that obtained when using γ-steering alone. In the case of a severe headwind increase which caused qα-limiting, no adjustment could be made in any case, once limiting was encountered. Apparently, the implemented form of the predictive-adaptive logic and the type of trajectory adjustments which it applied were not able to provide anticipatory adjustments to the trajectory in advance of the onset of qα-limiting. If such adaptation is, in fact, possible, it would probably require a more sophisticated adaptive logic and trajectory adjustment approach than that studied here.

It was found that the predictive-adaptive scheme did not produce any significant modification of the trajectory in the event of an engine failure. The performance loss associated with an engine failure was not reduced by any of the adjustments to the γ-profile which the steering logic tried in its predictive simulations. The investigation employed the failure of an RP engine at 140 seconds. The failure reduced the net thrust to approximately 84% of the nominal until the RP shutdown point (with the remaining engines operating at 105% "emergency" thrust) and caused a large, unacceptable loss of final mass which the predictive-adaptive guidance did not reduce. (Detailed investigation of engine failure and abort alternatives was beyond the scope of this study. The implementation of the vehicle simulation did not provide for alternative orbit or suborbital return modes. The trajectory always attained the target orbit. In cases resulting in "large" loss of final mass, the vehicle would not actually reach the target orbit since it would run out of fuel before the target orbit.)

The case in which predictive-adaptive guidance produced a significant improvement in the achieved final mass was when following a reference trajectory which was substantially off-optimal at the outset. In one illustrative case, the off-optimal trajectory used as the reference reduced the final mass by 64 slugs (2050 lbs) compared to the optimal by being lofted with respect to the optimal one. A predictive-adaptive cycle period of 10 seconds, commencing at 40 seconds and continuing up to 120 seconds was used when following this "high reference" trajectory. (PEG steering was then employed from 120 seconds to orbit.) The predictive-adaptive guidance successfully adjusted the trajectory to increase the final mass achieved on orbit to within 8 slugs (260 lbs) of the optimal trajectory, recovering approximately 88% of the mass which would have been lost.

Similar performance was obtained when following an off-optimal trajectory which was low with respect to the optimal one. In this case the off-optimal "low reference" trajectory used by the guidance reduced the final mass by 70 slugs (2254 lbs) and greatly exceeded the vehicle $Q\alpha$ limit. When this trajectory was followed using the predictive-adaptive guidance the trajectory was adjusted so that the final mass on orbit was only 4 slugs (138 lbs) less than optimal, a recovery of 94%. Also, the maximum $Q\alpha$ attained did not significantly exceed the vehicle limit when using the predictive-adaptive guidance. It was noted, however, that correction of a low off-optimal trajectory required that the predictive-adaptive guidance have enough biasing authority (large enough DELTABIAS and high enough cycle frequency) to accomplish the adjustment early in the flight. If sufficient correction was not made in good time it was found that the vehicle $q\alpha$ limit was reached. Further adjustment then became impossible due to the limiting, resulting in poor performance.

The flight path angle, altitude and velocity time histories of the cases demonstrating performance recovery from both high and low off optimal reference trajectories are shown in Figure 4.11. The velocities in all cases were very similar. The significant differences between the cases can be seen in the altitude and flight path angle plots. In both the high and low off-optimal cases the trajectories clearly can be seen to be brought back towards the optimal one by the predictive adaptive steering. Note that the optimal flight path angle profile gave the smoothest transition to PEG and that the adapted profiles intercepted the optimal one approximately at the start of PEG.
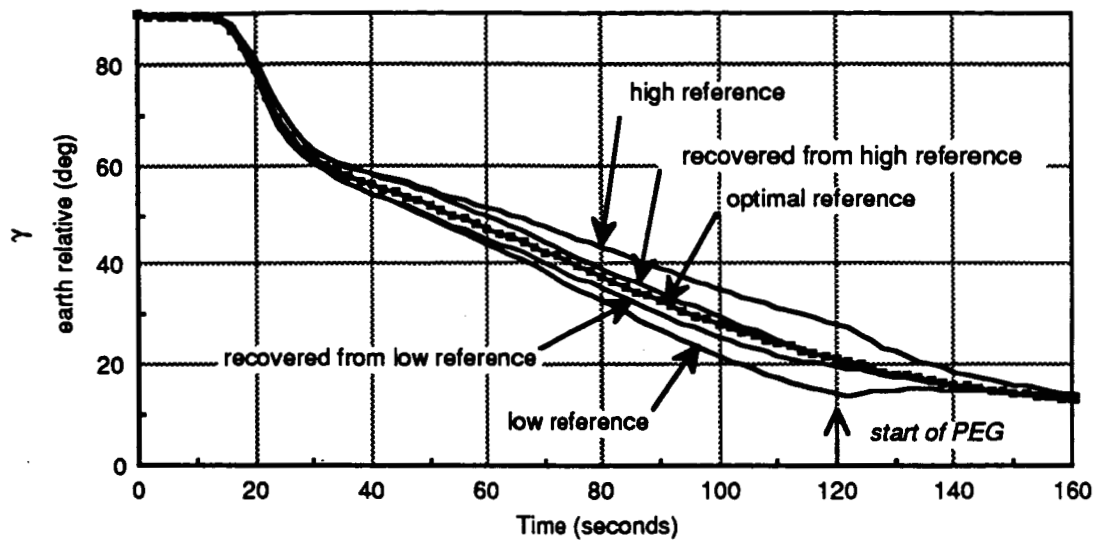
Figure 4.11   Predictive-adaptive adjustment of off-optimal trajectories.

a)   Flight path angle.
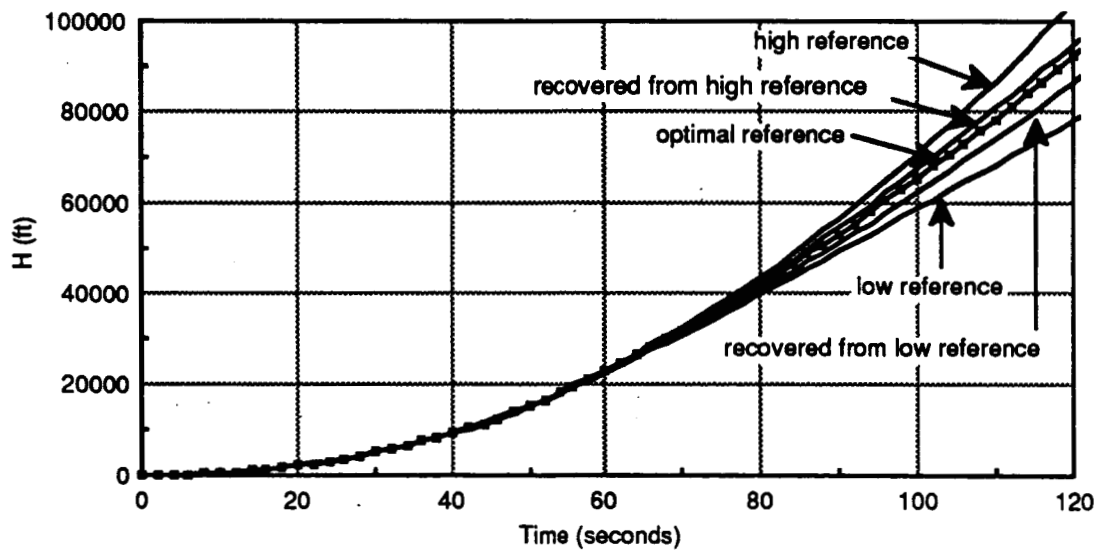
Figure 4.11   Predictive-adaptive adjustment of off-optimal trajectories.

b)   Altitude.
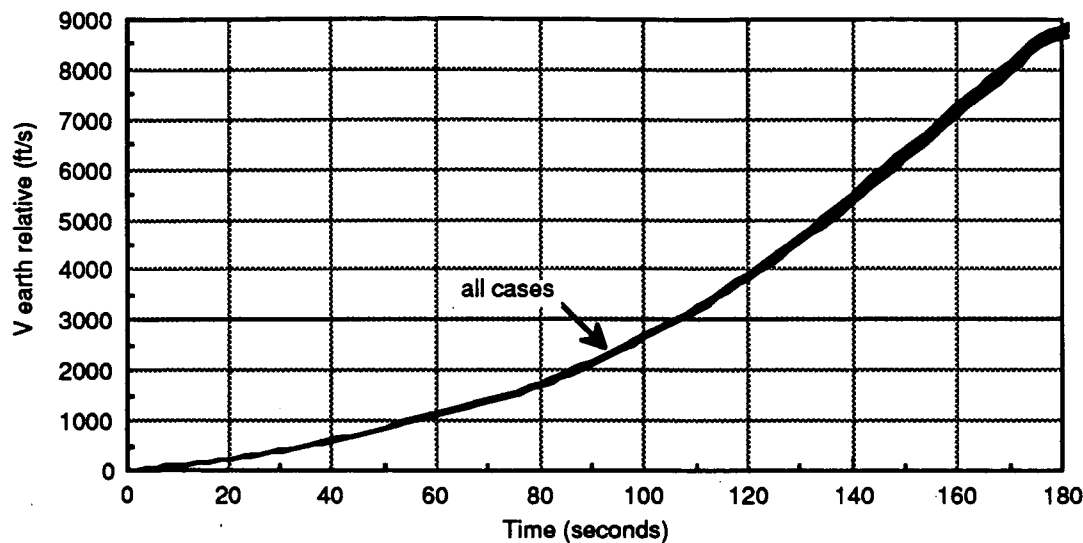
Figure 4.11   Predictive-adaptive adjustment of off-optimal trajectories.

c)   Earth relative velocity.

4.5   Predictive-Adaptive Guidance for Load Reduction

4.5.1   Description

The final mass achieved on orbit was the performance criterion that was used for most of the study. In the trajectory design phase, final mass was maximized subject to the vehicle-imposed limits on the trajectory in order to get the best payload performance. The predictive-adaptive guidance described in the preceding sections sought to maximize the final mass by adjusting the trajectory during flight. This predictive-adaptive guidance for maximum final mass had the objective of improving performance in the presence of dispersions which would otherwise reduce the final mass. However, when dispersions provide a performance *benefit* it may not be necessary to employ the performance gained to improve the final mass beyond that achieved in the nominal, designed trajectory. In such a situation, minimizing the loading experienced by the vehicle might be considered as an alternative performance objective.

The nominal trajectory is presumably designed ahead of time for mission planning and is designed to accommodate some worst-case conditions (a large headwind) while placing the required payload into orbit. If time-of-launch conditions are worse than this worst-case the mission cannot be flown. Normally, the conditions would be more benign than the worst-case. The vehicle would then have some performance margin compared to the nominal mission. Following the designed trajectory would result in extra mass on orbit in the form of fuel left in the tanks. With predictive-adaptive guidance which seeks to maximize mass on orbit the final mass might be increased even further. Having extra fuel might be useful for missions which could make use of it, for example, those involving subsequent on-orbit maneuvering for which it would be a useful reserve. For missions in which such an extra fuel reserve (beyond that scheduled in the nominal mission) would not be particularly beneficial, the performance margin could be used in an alternative way: The trajectory could be modified to reduce the aerodynamic loading experienced by the vehicle during ascent while still accomplishing the required mission. One approach would be to redesign the trajectory immediately prior to launch, making use of the measured wind profile. Another approach would be to employ a predictive-adaptive scheme to adjust the trajectory during flight. (The predictive-adaptive guidance system would also use the wind profile measured prior to launch.) In either case, the mission – attaining orbit using the nominal fuel quantity – would be accomplished while minimizing the wear on the vehicle. This would be particularly desirable for a reusable vehicle such as the Shuttle II.

Employing an in-flight predictive-adaptive scheme to accomplish the load reduction has one significant advantage over a prelaunch redesign of the trajectory. Since the predictive-adaptive scheme can use a reference trajectory which meets the mission objective under worst-case conditions (the mission planning trajectory design), the margin for unfavorable dispersions is retained. A trajectory which is redesigned prior to launch to reduce loads may not be able to achieve the required mission if the wind changes in a drastically unfavorable way following the wind profile measurement upon which the redesign is based. The predictive-adaptive guidance would accommodate such a dispersion by not adjusting the trajectory to reduce loads as much as it would if the conditions remained more favorable.

The concept of predictive-adaptive guidance for load reduction was developed late in the study and only a preliminary scheme was implemented. It employed the same γ-profile biasing approach as used in the mass-maximization predictive-adaptive scheme but the decision criteria used to select the γ-rate biasing were modified. The biasing was selected to reduce the

maximum $q\alpha$ experienced by the vehicle in the portion of the flight remaining until RP shutdown, subject to the requirement that the final mass targeted for the nominal mission would still be achieved. The maximum $q\alpha$ was a good indicator of the peak aerodynamic load experienced by the vehicle.

4.5.2   Implementation

The functional structure of the biasing logic was similar to that described in Section 4.4.2 and illustrated in Figure 4.10. Normally, all three predictive simulations were performed each predictive-adaptive guidance cycle. However, the final decision logic which selected the adjustment to the γ-rate bias was altered to include the criterion of minimizing $q\alpha$. The functional arrangement of the decision logic is shown in Figure 4.12. The primary goal was the achievement of the target final mass. When this goal was satisfied the algorithm made the selection which reduced the maximum $q\alpha$ encountered.

The 3 DOF predictive simulation running with a one second integration timestep was used.

During initial simulation runs made with the load reduction scheme it was found that upon transition to PEG guidance, a very large α was developed. In order to reduce this angle, a limiter was employed which limited α to that value resulting in a $q\alpha$ product no greater than the maximum $q\alpha$ encountered before transfer to PEG.

4.5.3   Performance

A preliminary simulation run employing the predictive-adaptive load reduction scheme showed the decision logic to function correctly. It demonstrated a reduction in the maximum $q\alpha$ while achieving somewhat better than the target final mass. In this case, a no wind optimal trajectory, designed with $q\alpha = 2800$ psf deg, was used as the reference trajectory and the mission was simulated in a tailwind having the magnitude of the Vandenberg #69 profile (see the Appendix). Table 4.1 shows the final mass and maximum $q\alpha$ attained by the reference trajectory, by the trajectory simulated in the tailwind using just the γ-steering, and by the trajectory simulated in the tailwind while using predictive-adaptive load reduction guidance. The tailwind was a beneficial dispersion, increasing the final mass and decreasing the

maximum $q\alpha$ compared to the reference trajectory even when simply using γ-steering. (In general, it was found that tailwinds were favorable, as is discussed in Section 5.2.3.) When the mission was simulated with the predictive-adaptive load reduction and a reduced target mass of 9520 slugs, the maximum $q\alpha$ was further reduced. (A significantly reduced target mass was used to allow for a clear adjustment of the trajectory in this illustrative case.)
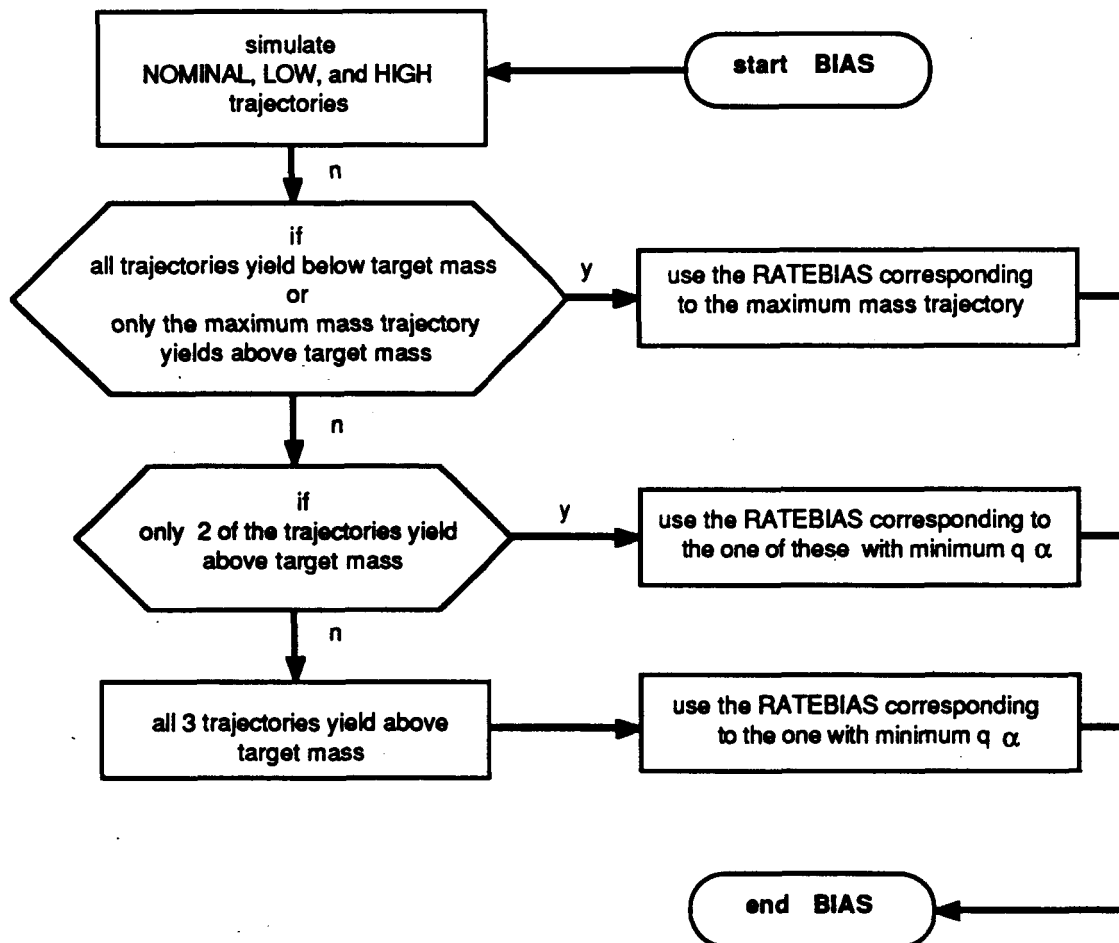
Figure 4.12   Functional arrangement of load reduction biasing logic.

CASE	FINAL MASS (slugs)	$(q\,\alpha)_{max}$ (psf deg)
reference	9545	2800
in tailwind alone	9553	2730
with load reduction	9538	2451

Table 4.1   Effectiveness of predictive-adaptive load reduction.
(Target mass was 9520 slugs.)

The time histories of $q\alpha$, γ and H are given in Figures 4.13, 4.14 and 4.15. The load reduction scheme adjusted the trajectory downwards in terms of altitude by reducing γ with respect to the reference trajectory. (In the case in tailwind alone, the reference trajectory was tracked very closely.) Before the transfer to PEG, the reduction in $q\alpha$ achieved by the guidance scheme is evident. However, following transfer to PEG, $q\alpha$ was driven against the limiter mentioned in Section 4.5.2. In terms of wear on the vehicle, this transient somewhat diminished the benefit of the load reduction gained earlier in the trajectory and was therefore undesirable. The reason for the transient was the fundamental mismatch in the guidance objectives before and after the transfer to PEG. In the phase preceding the transfer, employing the load reduction guidance, the objective was to *degrade* the trajectory final mass performance in such a way so as to minimize $q\alpha$. In this phase, the trajectory was adjusted to be off-optimal. In the subsequent PEG phase, the objective was to follow the mass-optimal trajectory. Thus, in the initial period of PEG guidance, the trajectory, previously adjusted to be off-optimal, was "corrected" back towards the optimal one (the reference trajectory). This is observed in Figure 4.14. Since the trajectory was low after the load reduction guidance phase, the trajectory adjustment occurring during PEG entailed a positive attitude change. This caused the development of a large $q\alpha$ and was consequently limited by the $q\alpha$ limiter. A reduction of this transient in the transfer to PEG will be required in any further development of the predictive-adaptive load reduction scheme. This might be accomplished, for example, by the addition of a transition phase between the load reduction guidance phase and the PEG phase.
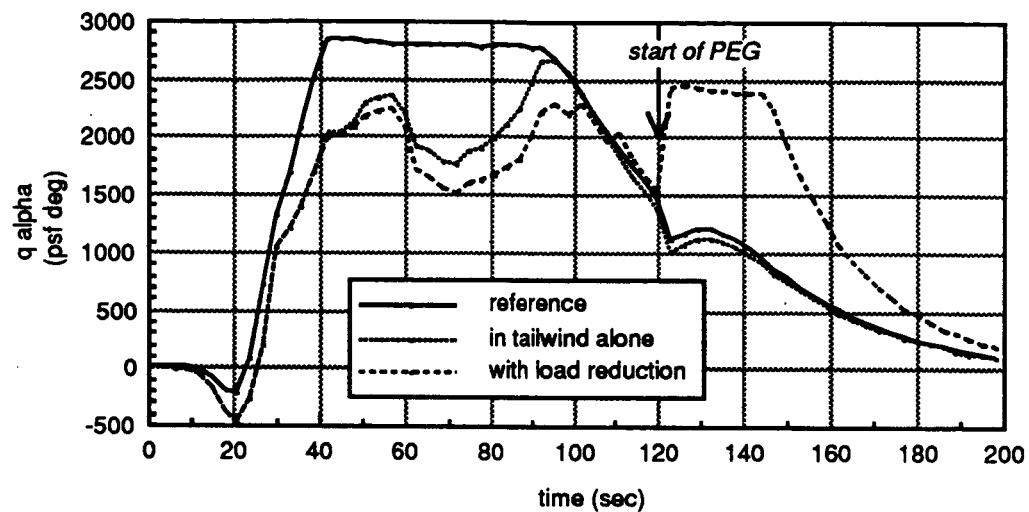
Figure 4.13 Reduction in qα with load reduction predictive-adaptive guidance.
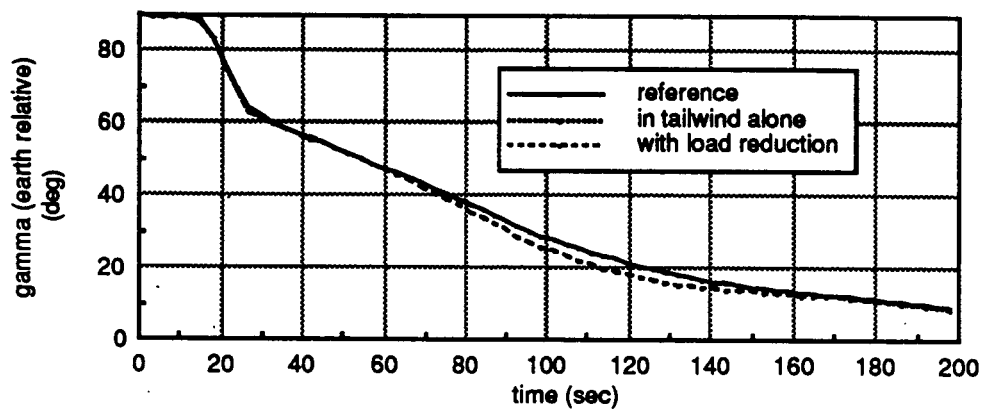
Figure 4.14 Adjustment of γ with load reduction predictive-adaptive guidance.
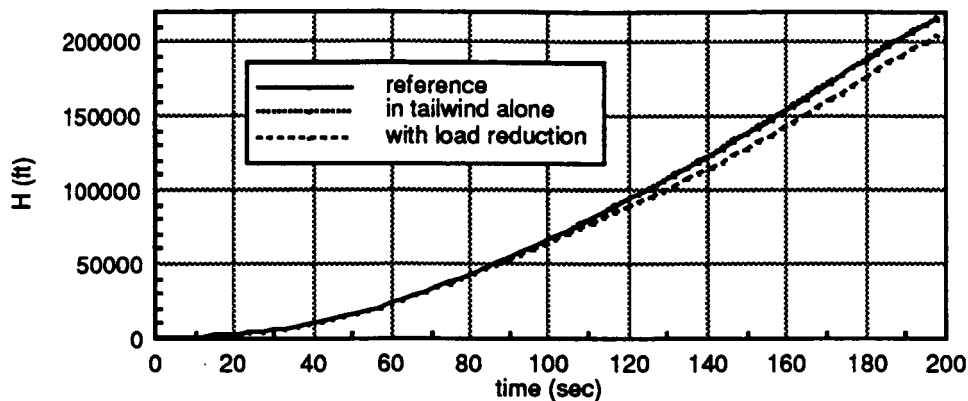
Figure 4.15   Adjustment of H with load reduction predictive-adaptive guidance.

Another case was simulated but it did not demonstrate the significant load reduction achieved in the example described above. In this second case, the target mass was reduced by 50 slugs from the no wind reference trajectory final mass and the trajectory was simulated in nominal (no wind) conditions. There was no beneficial deviation from the nominal case apart from the reduced final mass requirement. A possible limitation on the effectiveness of the predictive-adaptive load reduction guidance in this situation was the nature of the trajectory adjustment employed by the scheme. A trajectory adjustment which is more sophisticated than the monotonic biasing of flight path angle that was used might yield better results. (A similar observation was made in the case of adaptive guidance for maximum final mass, described in Section 4.4.) Thus, in addition to the issue of the transfer to PEG, the nature of the trajectory adjustment applied by the guidance scheme should be re-examined in any future development of the predictive-adaptive load reduction guidance scheme.

The use of an alternative criterion for the load, in place of maximum $q\alpha$, might also be considered. More detailed definition of the structural characteristics of the vehicle would determine what aspect of the loading experienced by the vehicle should be minimized to reduce the net wear on the vehicle during ascent.

The success of the preliminary implementation of the predictive-adaptive load reduction in the case of the tailwind dispersion demonstrated the potential of the approach. It is felt that

64

predictive-adaptive load reduction is an important concept which could be profitably pursued in any subsequent studies of ascent guidance approaches for Shuttle II-type vehicles.

4.6   Powered Explicit Guidance (PEG)

For this study it was assumed that the powered explicit guidance (PEG)[8],[9] scheme would be employed for the final ascent phase, exoatmospheric guidance of the Shuttle II. This scheme has been successfully applied in stage two guidance for the current Shuttle I. PEG is an implementation of linear tangent guidance (LTG). LTG is the classical calculus of variations solution for the achievement of a desired velocity vector change with an optimal thrust vector history. Its assumptions include the absence of aerodynamic forces, hence, it can only be employed when the aerodynamic forces are negligible.

An existing routine implementing PEG was modified and employed in this study to generate the guidance commands during the final ascent phase. Guidance during this final ascent phase was not investigated in any detail. The only issue considered was the determination of when the transfer to PEG should occur. Initially, the RP engines shutdown point was used as the transfer point for reasons of convenience. Subsequent studies indicated, however, that a small performance gain could be realized by starting PEG earlier in the trajectory. For example, in one case it was found that starting PEG at 140 seconds increased the final mass by 5 slugs compared to starting it at RP shutdown, at approximately 180 seconds. In the majority of the simulations run in the latter part of the study, PEG was started at 120 seconds. This corresponded to an altitude of approximately 100,000 ft. At this point, for most cases, the aerodynamic forces were rapidly decreasing and could be neglected for guidance purposes.

The PEG routine was provided with the vehicle state at the start of each PEG cycle. The PEG cycle period was usually four seconds. The routine returned thrust vector direction and rate of rotation information. This was converted into an attitude command which was sent to the FCS every control cycle. The routine also provided an estimate of the final mass at each PEG cycle. It was found that beyond the RP shutdown point this estimate correlated well with the actually achieved final mass in terms of its trends with respect to changes in the trajectory. Thus, it was

[8]   McHenry, R.L., Brand, T.J., Long, A.D., Cockrell, B.F., Thibodeau, J.R..

[9]   Brand, T.J., Brown, D.W., Higgins, J.P., "Space Shuttle G&N Equation Document No.24, revision 2 *Unified Powered Flight Guidance*". C-4108. June, 1974. Charles Stark Draper Laboratory, Inc., Cambridge.

possible to evaluate the impact of trajectory variations on the final mass by monitoring the estimate of final mass provided by the PEG routine around the point of RP shutdown. Use was made of this feature in the predictive guidance simulations, described previously in this chapter, and in the trajectory design procedure, discussed in Chapter 5.

5.   Trajectory Design

5.1   Introduction

A simple technique for the generation of near mass-optimal reference trajectories for use by the steering system was developed as the result of trajectory shaping investigations performed early in the study. The approach that was developed made use of an α-profile shape which was found to be characteristic of an optimal ascent trajectory. For most of the study the trajectory design technique was applied manually to generate reference trajectories for steering purposes. The procedure was eventually automated.

The trajectory design required the iterative adjustment of the launch maneuver. In the early part of the study, when a constant pitchrate launch maneuver was used, the launch maneuver pitchrate was the adjusted variable. Subsequently, when the "smooth" launch maneuver was used, one of the end of launch maneuver state variables, θ or γ, was the adjusted variable. Techniques were developed for designing the "smooth" launch maneuver to produce the desired launch end state.

5.2   The Trajectory Design Approach

5.2.1   Trajectory Shaping Studies

The initial trajectory shaping studies involved investigation of the impact that α and the $q\alpha$ limit had on the shape and final mass performance of the trajectory. These studies were performed by commanding the vehicle to follow a specified α-profile in the vehicle simulation. A no wind environment was used. The launch maneuver was iteratively adjusted in each case until the final mass obtained was maximized. The first type of profile considered was a constant α profile. It was found that following a zero α trajectory yielded poor performance. (Zero α, or "gravity turn" trajectories have been frequently used during the atmospheric boost phase for launch vehicles. Such trajectories result in the minimum normal aerodynamic load.) On the other hand, it was found that following a trajectory with a large, positive constant α yielded good performance. However, these large α trajectories were characterized by a significant period during which α had to be limited to less than the selected constant value to prevent the

vehicle $q\alpha$ limit ($(q\alpha)_{limit}$) from being exceed. During this period of α-limiting, the α commanded to the flight control loop was limited to the value equal to the quotient of the specified $(q\alpha)_{limit}$ and the sensed q. As a consequence of this α-limiting, the trajectories were strongly influenced by the value of the $(q\alpha)_{limit}$.

Based on these initial trajectory shaping results, studies were continued employing a commanded α-profile having the form given in Figure 5.1. Following the launch maneuver the vehicle was commanded to a constant α ($\alpha1$). After a specified value of the $q\alpha$ product, the "design $q\alpha$", was reached the commanded α was continuously adjusted to hold $q\alpha$ at that value. The characteristic shape of the resulting variation of α was called the "$q\alpha$ bucket". Beyond the minimum point of the $q\alpha$ bucket, the commanded α was increased until it attained a second, specified value ($\alpha2$). This value was maintained until the point where steering transferred to PEG. Provisions were included in the simulation to specify more than two segments of different constant α over the ranges outside of the $q\alpha$ bucket. Preliminary trials using two segments of different constant α following the $q\alpha$ bucket did not yield any significant improvements and this feature was not employed subsequently.
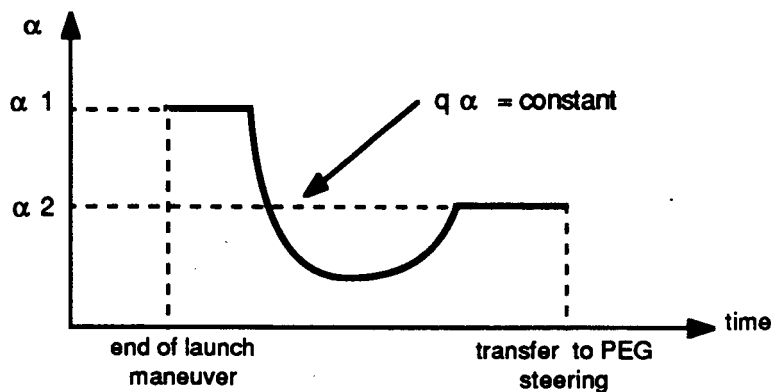
Figure 5.1   Form of the commanded α-profile.

Studies were performed to investigate the impact that the selection of the values, $\alpha1$, $\alpha2$ and the design $q\alpha$, defining the profile, had on the trajectory shape and performance. Comparisons were made to trajectories which were simulated using attitude schedules obtained using the

POST trajectory simulation and optimization package. The POST package was used to numerically optimize the trajectory for best final mass by selecting attitude rates which were held constant over a series of time-based segments of the trajectory. It employed a three degree of freedom simulation which did not include rotational or control dynamics. In terms of the constant attitude rates in the user-selected time segments, POST generated an optimal result which was regarded as the best performance achievable with perfect control assumed.

The variation of final mass with respect to the selection of the $q\alpha$ used in the α-profile is demonstrated by the results given in Table 5.1 and Figure 5.2. It was found that from a performance standpoint it was desirable to have as high a $q\alpha$ as possible. Over the range tested, final mass increased approximately linearly with $q\alpha$. The selection of $\alpha 1$ and $\alpha 2$ was found to have much less of an effect on the final mass. The effects of varying $\alpha 1$ and $\alpha 2$ were illustrated by the results given in Table 5.2. The predicted final mass was only altered at most by 2.1 slugs in that example. It was determined that, in general, $\alpha 1$ should be fairly large and that $\alpha 2$ should be small, approximately half of $\alpha 1$, for good performance.

DESIGN $q\alpha$ (psf deg)	FINAL MASS (slugs)
2000	9542
2200	9549
2400	9550
2600	9554
2800	9558

Table 5.1   Variation of final mass with design $q\alpha$.
(With $\alpha 1 = 10°$, $\alpha 2 = 4°$; final mass predicted by PEG routine at RP shutdown.)

69
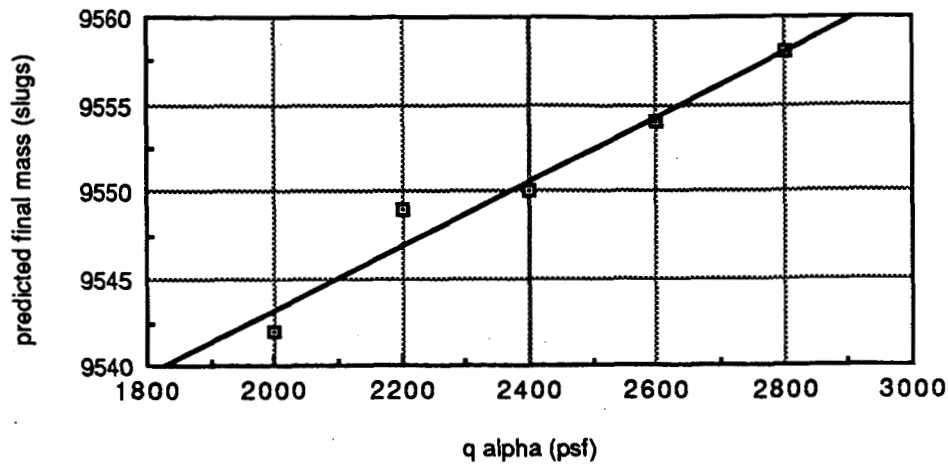
Figure 5.2   Variation of final mass with design qα.

(With α1 = 10°, α2 = 4°; final mass predicted by PEG routine at RP shutdown.)

α1	α2	FINAL MASS (slugs)
8°	4°	9545.8
8°	6°	9546.4
10°	4°	9548.5
10°	6°	9546.9

Table 5.2   Effect of varying α1 and α2 on trajectory design.

(With qα = 2800 psf deg; final mass on orbit.)

When these results were compared to POST-generated reference trajectories it was noted that the α-profile of the form indicated by these results was a fairly close approximation to the α-profile which resulted from the POST trajectories. The trajectory parameters H, V, γ_e, and θ were very closely matched in comparisons between the trajectories shaped with an α-profile of the assumed form and POST trajectories. These variables and the values of α and qα are compared in Figures 5.3a to 5.3f for two α-profile trajectories (Profile #1 and Profile #2) and a

POST-generated reference trajectory. The three trajectories are summarized in Table 5.3. Profile #1 and Profile #2 represent results obtained early in the study at which time the constant pitch rate launch maneuver was used and a moderately low value of $q\alpha$ was assumed for the design. Thus, the final mass performance was somewhat lower in than that achieved in the POST result.

Subsequently, when the "smooth" launch maneuver was employed and a larger design $q\alpha$ was specified, not only were the trajectory shapes similar but the final mass values obtained with the trajectories shaped using the α-profile were close to those yielded by the POST trajectories. For example, under no wind conditions the best achieved final mass was 9558 slugs with an α-profile-shaped trajectory. For the same conditions, the POST-generated trajectory achieved 9559 slugs. (Note that all of these final mass values were those *predicted* at RP engine shutdown by the PEG algorithm. The actually achieved values when trajectories were simulated to orbit were typically on the order of 10 slugs less than this prediction.)

PROFILE	$\alpha 1$	$\alpha 2$	DESIGN $q\alpha$ (psf deg)	FINAL MASS (slugs)
1	6°	4°	2500	9542
2	8°	4°	2500	9547
reference	-	-	-	9559

Table 5.3   Comparison of POST reference trajectory to trajectories shaped by α-profile. (Final mass predicted by PEG routine at RP shutdown.)
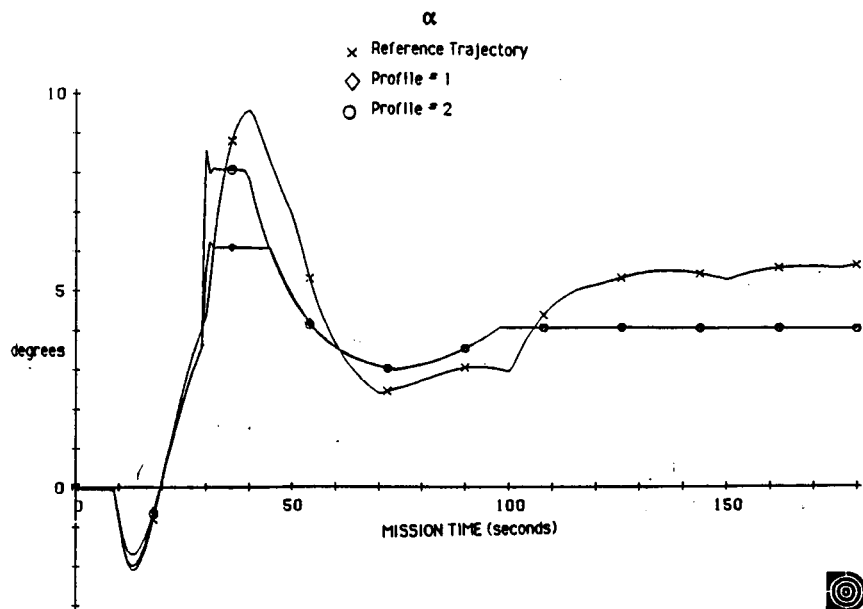
Figure 5.3   Comparison of POST reference trajectory to trajectories shaped by α-profile.

a)   Angle of attack
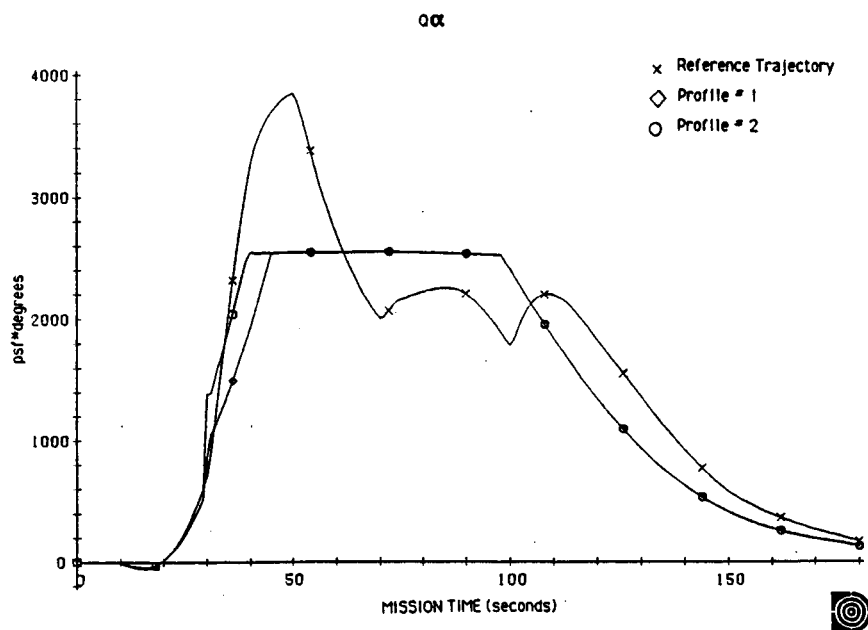
Figure 5.3   Comparison of POST reference trajectory to trajectories shaped by α-profile.

b)   qα product.

72

θ
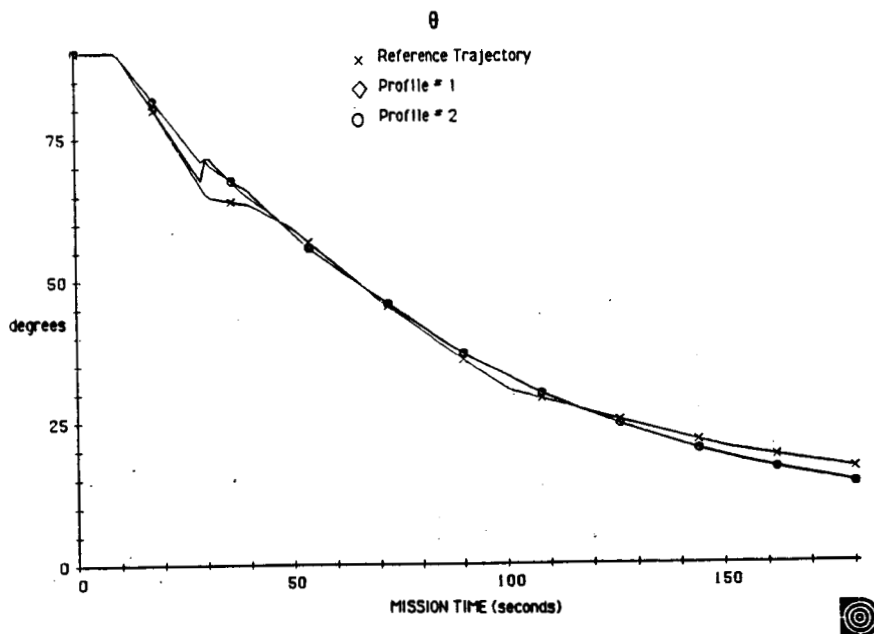
Figure 5.3　Comparison of POST reference trajectory to trajectories shaped by α-profile.

c)　Pitch attitude.
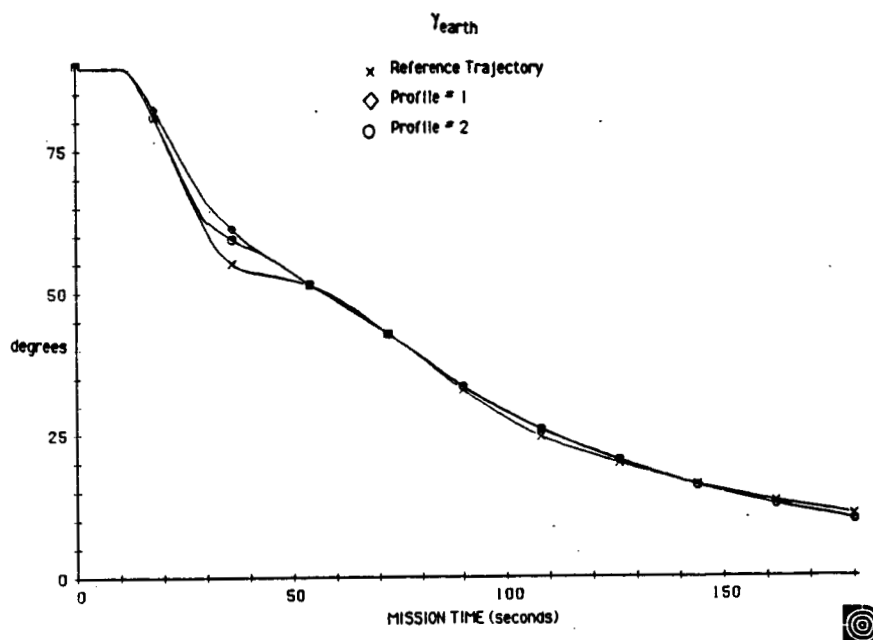
γ_{earth}

Figure 5.3　Comparison of POST reference trajectory to trajectories shaped by α-profile.

d)　Earth-relative flight path angle.
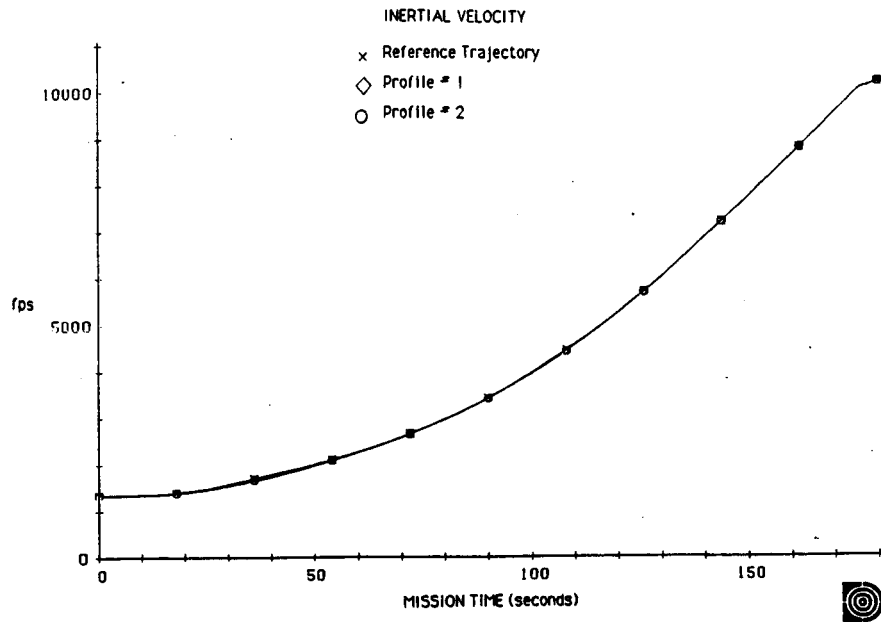
Figure 5.3   Comparison of POST reference trajectory to trajectories shaped by α-profile.

e)   Inertial velocity.
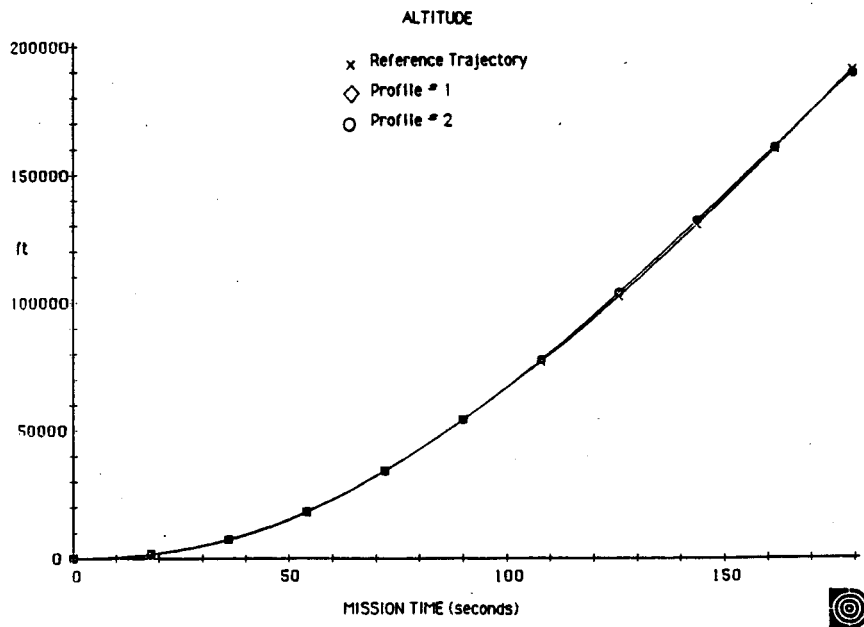
Figure 5.3   Comparison of POST reference trajectory to trajectories shaped by α-profile.

f)   Altitude.

5.2.2   The Trajectory Design Technique

The trajectory design process was used to generate and store γ-profiles which were then followed in simulations of the actual ascent using γ-steering. The same reference trajectory γ-profiles were used when investigating predictive-adaptive guidance techniques since those techniques were based on modifying a reference flight path angle profile. The design process consisted of selecting an α-profile with which to shape the trajectory and then performing iterative simulations of the trajectory with that α-profile, adjusting the launch maneuver until the final mass was maximized. Early in the study when the constant pitchrate launch maneuver was used, the launch maneuver pitchrate was directly adjusted. Subsequently, when the "smooth" launch maneuver was used, the launch end state was used to define the launch maneuver and a launch maneuver design routine was used to determine the launch maneuver parameters (see Section 5.3). When the launch maneuver resulting in the mass-optimal trajectory was found, the γ-profile of that trajectory and the corresponding launch maneuver parameters were stored. The basic form of the trajectory design procedure is illustrated by Figure 5.4.

The design procedure was essentially a maximization of one variable (mass) with respect to one free parameter (one of the end of launch maneuver variables, θ or γ). However, other variables were used as cues to the magnitude and direction of the required adjustment of the free parameter. In particular, the altitude of the RP shutdown point was noted by the user when performing the design. Based on experience, this altitude indicated whether the trajectory was too high or too low with respect to the sought after optimal one.

For trajectory design purposes, the trajectory was simulated only up to the RP engine shutdown. RP engine shutdown was the latest point in the trajectory at which transfer to PEG ever occurred in the study so in all cases a final mass prediction, provided by the PEG algorithm, was available. This predicted value was optimistic, typically on the order of 10 slugs high, compared to that actually achieved when the simulation was continued to orbit. However, in a family of trajectories obtained by varying the end of launch state, the relative magnitudes of predicted final mass and those actually achieved were well correlated. This is illustrated by the results given in Table 5.4. This table shows that the maximum values in the actual final mass and that predicted at RP shutdown were both achieved in the same trajectory, corresponding to the same end of launch flight path angle of 68.08°. Thus, selection of a trajectory based on the predicted final mass at RP shutdown could be used for trajectory

design. (It was found that the trend toward the maximum in predictions provided by PEG at times earlier than RP-shutdown did not always correlate well with the actual final mass. This is also shown in Table 5.4. The trajectory for which maximum final mass was predicted at 140, corresponding to an end of launch flight path angle of 67.98°, was not the same as the trajectory actually achieving the maximum mass on orbit.)
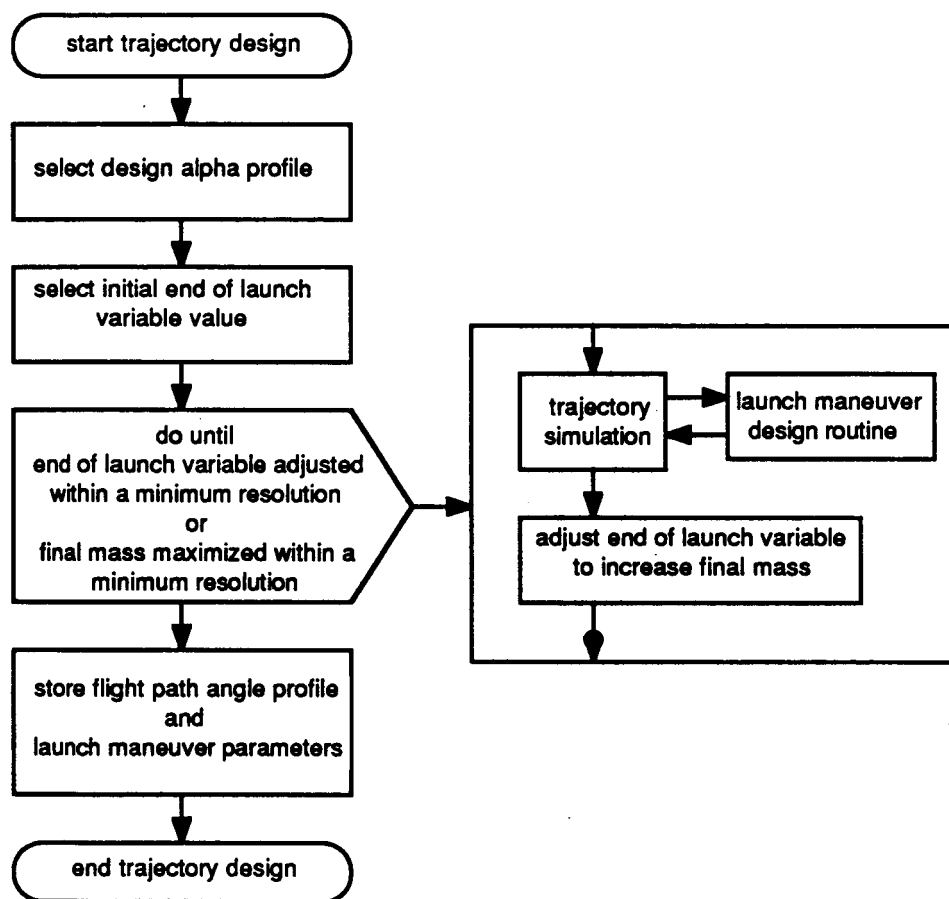
Figure 5.4   Functional sequence in the iterative trajectory design procedure.

Although the trajectory shaping studies from which it was developed had been performed in a no wind environment, this design technique was found to give good results under most wind conditions as well. It was only under some, very severe headwind conditions that the procedure failed to produce a usable trajectory.

The trajectory was found to be sensitive to adjustments in the launch maneuver when following an α-profile. The adjustments in the launch maneuver which were required to locate the mass-optimal trajectory were very small. The trajectory was also very sensitive to wind changes. Any change in wind required a readjustment of the launch maneuver. Due to this sensitivity, commanding the vehicle to follow a reference α-profile was never considered as a candidate in-flight steering technique.

End of Launch Flight Path Angle	Final Mass Predicted by PEG at 140 s (slugs)	Final Mass Predicted by PEG at 180 s * (slugs)	Final Mass at Orbit (slugs)
68.12°	9583.1	9542.2	9539.7
68.10°	9584.7	9548.4	9540.2
68.08° †	9586.5	**9549.0**	**9540.4**
68.06°	9588.1	9548.4	9539.8
68.00°	9590.8	9509.3	9536.4
67.98°	**9591.1**	-	9532.1

Table 5.4   Correlation of predicted and actual final mass for a family of trajectories.
(The end of launch state was defined in terms of flight path angle in these runs.)
* corresponds to the RP engine shutdown point
† maximum final mass trajectory

The process of optimizing the trajectory by adjusting the end of launch attitude (q) for fixed values of α1, α2 and qα is illustrated in Table 5.5 and Figure 5.5. The example shows the optimal trajectory for no wind conditions shaped using a design α-profile defined by α1 = 8°, α2 = 4°, and qα = 2800 psf deg. A trajectory shaped using the same α-profile but which was off-optimal by being too high and one which was off-optimal by being too low are shown for comparison. The sinusoidal launch maneuver with θ, α end condition specification was used (see Section 5.5). Note that the optimized trajectory had an actual final mass of 9545 slugs; the POST generated optimal trajectory for no wind conditions yielded 9559 slugs predicted final mass, corresponding to approximately 9550 slugs at orbit.

CASE	LAUNCH MANEUVER				FINAL MASS (slugs)
	θ	α	Ω_{kick}	t_{kick}	
low	69.25°	5°	-1.2064 °/s	17.2 s	9460
optimal	69.68°	5°	-1.1545 °/s	17.6 s	**9545**
high	70.00°	5°	-1.1363 °/s	17.6 s	9537

Table 5.5   Example trajectory design for no wind conditions.
(Final mass is that actually achieved at orbit.)
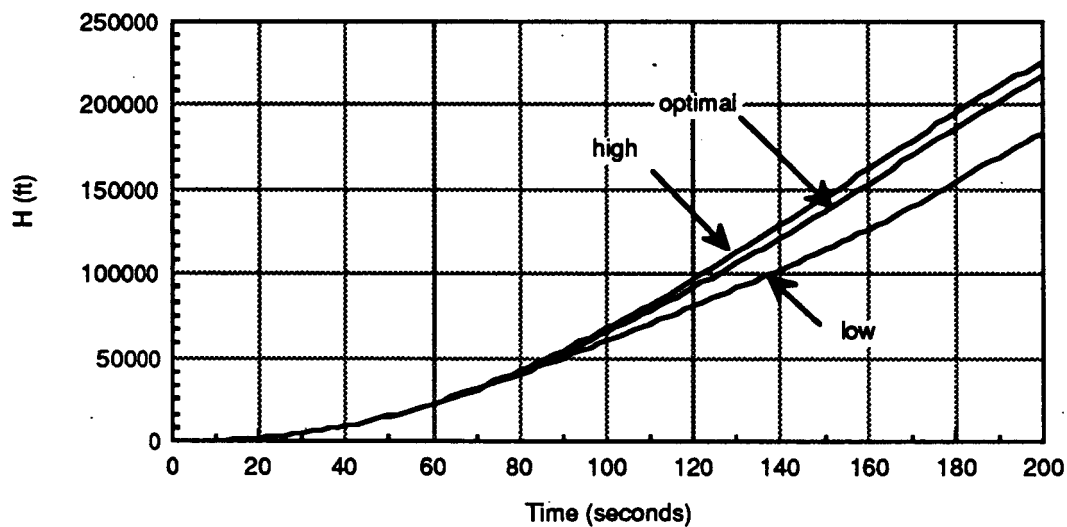
Figure 5.5   Example trajectory design.
a)   Altitude.
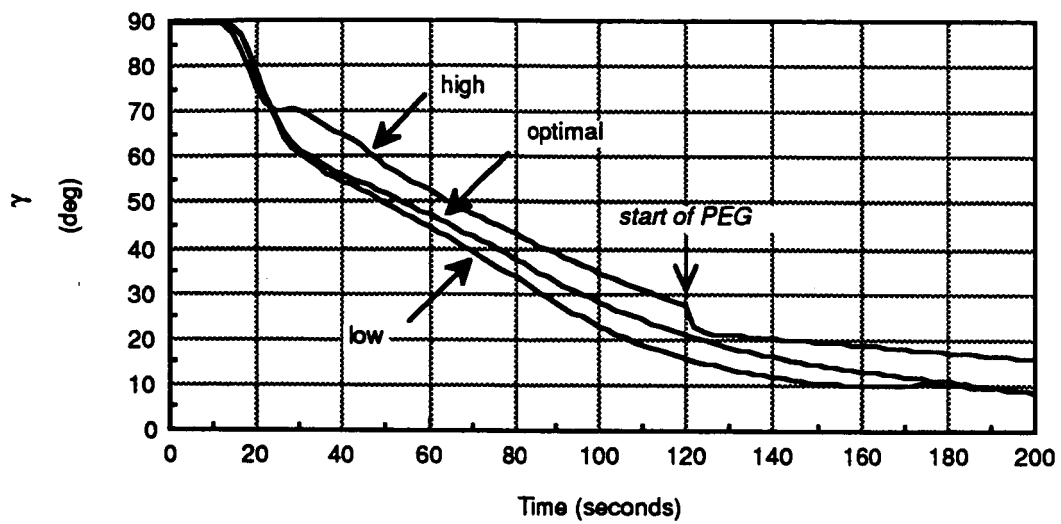
Figure 5.5   Example trajectory design.
b) Earth-relative flight path angle.
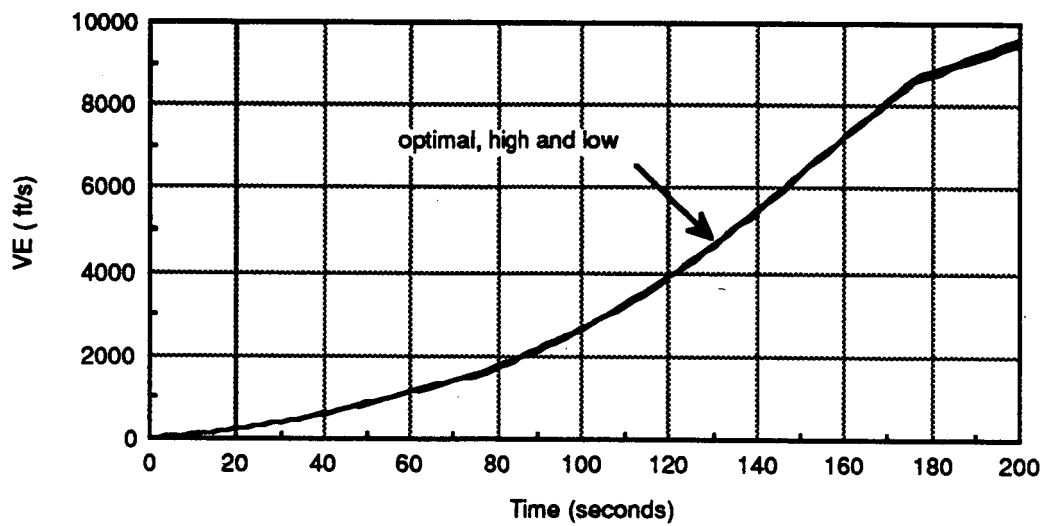
Figure 5.5   Example trajectory design.
c) Earth-relative velocity.

79

5.2.3 Issues in Selection of an α-Profile

Design of trajectories using α-profile shaping required the selection of a fixed α-profile to be used in the design. The most important characteristic of the profile was the design $q\alpha$, which defined the $q\alpha$ bucket in the α-profile. The selection of the design $q\alpha$ was influenced by three considerations. First, the desire for best performance indicated that one should employ a large $q\alpha$, as evidenced by the trajectory shaping results. Second, and counter to this, the desire to minimize the load on the vehicle for structural reasons favored a low design $q\alpha$. Third, the behavior of the steering system used to follow the designed trajectory under nominal and perturbed conditions had to be considered.

For the purposes of trajectory designs performed in this study it was assumed that maximizing performance took precedence over minimizing the load. It was presumed that any $q\alpha$-profile was acceptable as long as it did not significantly exceed the specified maximum value of 3000 psf deg. In an actual vehicle it is expected that the load restrictions would be more stringent and more completely specified. In fact, good definition of those restrictions would be an important aspect of defining the requirements placed on the trajectory design and guidance system.

The use of γ-steering with α-control to follow the trajectory required that the reference trajectory being followed be designed with a design $q\alpha$ less than the vehicle $q\alpha$ limit. If no margin were left between the design $q\alpha$ and the vehicle limit the steering would have no ability to increase the normal force above its nominal value during the period of maximum $q\alpha$. As a result it would be unable to correct for any errors in the trajectory which might have been driving it to the low side (γ decreasing too rapidly). It was found that the steering sometimes commanded α such that the maximum achieved $q\alpha$ was as much as 200 psf deg above the design $q\alpha$ of the trajectory which was being followed, even under nominal conditions. Thus, the largest design $q\alpha$ selected for use in trajectory designs was 2800 psf deg. This left a 200 psf deg margin compared to the vehicle limit.

Simulations were run to investigate how the selection of the design $q\alpha$ affects the performance of the steering in the presence of wind changes. A series of cases were studied in which trajectories were designed under *no wind* conditions with reduced design $q\alpha$ values and then followed under tailwind and headwind conditions using γ-steering. Tailwinds were found not to adversely affect performance. In fact, tailwinds usually increased the on-orbit mass and

reduced the maximum achieved qα. This is demonstrated by the results given in Table 5.6, obtained while following a reference trajectory with a 2800 psf deg design qα.

CASE	FINAL MASS (slugs)	$(q\alpha)_{max}$ (psf deg)
nominal (no wind)	9545	2925
Vandenberg #69 profile tailwind	9553	2730
Vandenberg #70 profile tailwind	9557	2730

Table 5.6   Effect of tailwind on performance when using γ-steering to follow
a trajectory designed for no wind conditions.
(The reference trajectory employed a 2800 psf deg design qα.)

Headwinds, on the other hand, could force the vehicle into the qα-limiting which has been discussed previously in Section 4.3.4. This qα-limiting could drive the vehicle off of its reference trajectory and degrade performance. The magnitude of the headwind increase that would cause qα-limiting was found to depend on the design qα. Table 5.7 summarizes the investigation which was performed. Decreasing the design qα gave the steering a larger margin with which to accommodate headwind increases. Thus, up to a point, it was found to be possible to allow for the eventuality of an unknown headwind increase by using a smaller, more conservative design qα when designing the reference trajectory. Of course, this capability to accommodate a headwind dispersion was accompanied by a performance penalty. For example, in the cases listed in Table 5.7, a headwind increase equivalent to 50% of the Vandenberg wind profile #69 was accommodated by decreasing the design qα to 2400 psf deg. Under nominal (no wind) conditions this carried with it a performance penalty of 6.6 slugs (212 lbs) compared to the case designed with 2800 psf deg. In the face of the headwind increase an additional 3.5 slugs (112 lbs) was lost. This performance loss was small considering the severity of the wind dispersion.

<table>
<tr><td></td><td></td><td colspan="5" align="center">Design qα (psf deg)</td></tr>
</table>

		2000	2200	2400	2600	2800
HEADWIND	100%	9519.3	-	9513.5	-	DIVE
INCREASE	90%	9521.7	9525.7	9523.3	-	-
	80%	-	9527.6	9525.5	-	DIVE
percentage	70%	-	9529.3	9529.4	-	-
of	60%	-	-	9531.4	-	9371.1
Vandenberg	50%	-	-	9533.3	-	-
Wind	40%	-	-	-	9538.2	9537.2
Profile	30%	-	-	-	9539.8	-
# 69	20%	-	-	-	-	9538.2
	10%	-	-	-	-	9538.8
nominal	0%	9530.6	9536.3	9536.8	9540.5	9543.4

Table 5.7   Performance in headwind conditions using γ-steering to follow trajectories designed in no wind with reduced qα. (DIVE indicates vehicle driven completely off of its trajectory.)

In conclusion, the selection of the design qα was driven primarily by the conflicting requirements of final mass performance and the ability to accommodate headwind increases. If a small reduction in final mass was acceptable, the reference trajectory could be designed with a reduced design qα which would give the steering a larger margin with which to successfully fly through a headwind dispersion.

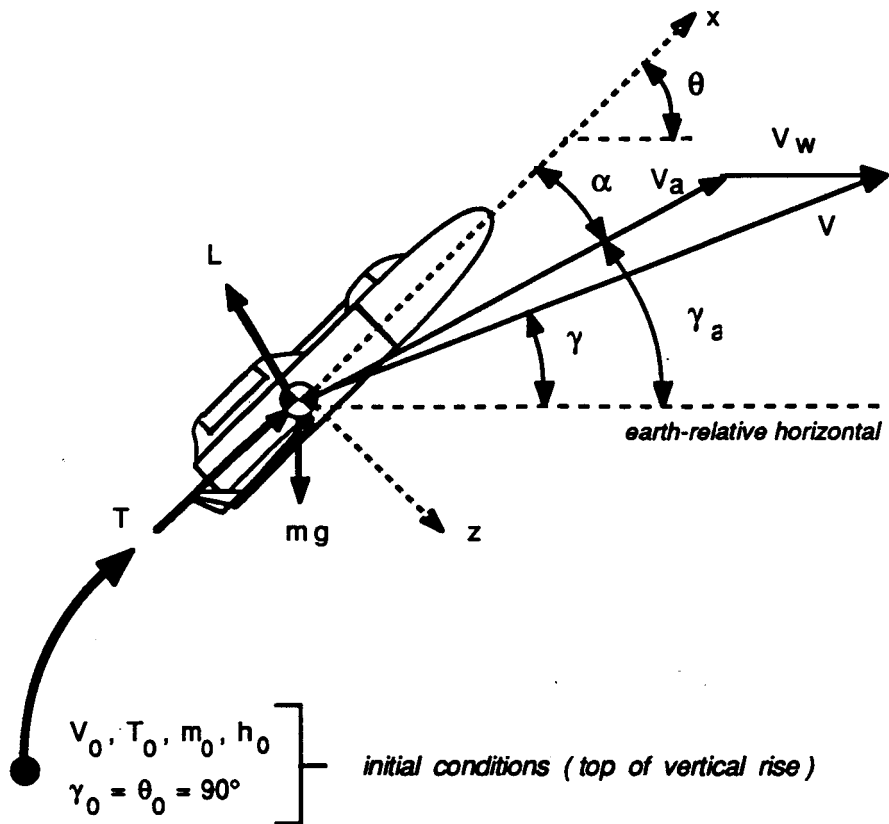## 5.3   Launch Maneuver Design

5.3.1   General Description

When a constant pitchrate launch maneuver was employed early in the study, the user specified the kick pitchrate and kick maneuver duration directly. The trajectory design was accomplished by varying the kick pitchrate while keeping the kick duration at a constant, reasonable value

(typically 20 seconds). With the "smooth" launch maneuver the two parameters, t_{kick} and Ω_{kick}, were used to define the maneuver (see Figure 4.2). These were generated by a launch maneuver design routine during the trajectory design process. The launch maneuver design routine determined the launch maneuver parameters which would give the desired end of launch state, described either in terms of γ and α or in terms of θ and α. The launch maneuver end state was specified by the user when performing a manual trajectory design or by the trajectory design algorithm during an automated trajectory design. The trajectory design process iteratively adjusted γ or θ to achieve maximum final mass. When the actual flight trajectory was simulated, the launch maneuver parameters corresponding to the reference trajectory to be used by the guidance system were provided to the guidance system.

Two versions of the launch maneuver design algorithm were developed. The first of these employed γ and α to describe the launch end state. These variables were chosen because they corresponded to the steering and control variables used by the guidance system following the launch maneuver. The objective was to achieve a smooth transition from the launch maneuver into the subsequent guidance mode. This algorithm is described in Section 5.3.2. In the second version of the launch maneuver design algorithm, θ and α were used to describe the launch end state. The second algorithm was developed when the first one proved to lack the accuracy required for trajectory design purposes. This algorithm is described in Section 5.3.3.

Both versions of the launch design algorithm employed a numerical minimization of the error in one of the launch end state variables (γ or α). The minimization used one of the launch maneuver parameters, t_{kick}, as the free variable. The other launch maneuver parameter, Ω_{kick}, was analytically related to t_{kick} based on the launch end state. The procedure adjusted the parameter, t_{kick}, to minimize the error in the selected end state variable. The error was determined by performing an idealized simulation of the launch maneuver each iterative cycle with the trial value of t_{kick} and the corresponding Ω_{kick}. In the first implementation of the launch maneuver design algorithm an ad hoc technique was used to perform the minimization. It was eventually replaced by a simple and more elegant bisection search using the "golden ratio" bisection factor[10]. The launch design algorithm searched between specified maximum and minimum values of t_{kick} for the value which minimized the error in the specified end of launch state variable. The desired value of the other end of launch state variable was achieved approximately by its inclusion in the analytical relationship between t_{kick} and Ω_{kick}.

[10] Press, W.H., Flannery, B.P, Teukolsky, S.A., Vetterling, W.T., Numerical Recipes. 1986. Cambridge: Cambridge University Press. (pp 274).

$$\frac{dm}{dt} = \text{constant}$$

$$\frac{dT}{dt} = \text{constant}$$

$$\frac{d\theta}{dt} = \Omega_{kick}\left(1 - \cos\left(\frac{2\pi}{t_{kick}}t\right)\right)$$

$$\frac{dV}{dt} = \frac{T}{m}\cos(\theta - \gamma) - g\sin(\gamma)$$

$$\frac{d\gamma}{dt} = \frac{T}{m}\sin(\theta - \gamma) - \frac{g}{V}\cos(\gamma) + \left(\frac{S\rho Cl_\alpha V}{2m}\right)\alpha$$

$$\frac{dh}{dt} = V\sin(\gamma)$$

Figure 5.6   Model used for launch maneuver simulation.

84

The launch simulation used by the launch maneuver design algorithm employed a simple two degree of freedom pitch plane model which is summarized in Figure 5.6. In this model it was assumed that thrust and mass varied at constant rates. Values for these rates were determined by obtaining average thrust and mass rates from the time histories observed in a series of typical launch maneuvers flown in the full vehicle simulation. The thrust vector deflection was assumed to be zero and gravity (g) was constant. The vehicle was assume to rotate at the rate specified by the launch maneuver pitchrate profile (see Figure 4.2). Initially, the aerodynamic force was neglected. The lift component of the aerodynamic force was subsequently included to improve accuracy but it had only a small impact on the performance. It was assumed that lift was expressed as:

$$L = Sq \, Cl_\alpha \, \alpha$$

where Cl_α was a constant. The launch simulation employed a fourth order Runge-Kutta integration with a 0.1 second integration time step.

The launch simulation made use of the design wind profile to obtain the wind velocity at each integration step. The wind velocity was used to calculate the air-relative velocity for the evaluation of α. (For simplicity, the earth-relative velocity, not the air-relative velocity, was used to determine q for the calculation of lift since the error which this entailed had only minor effect on the overall algorithm performance.)

The implementation and performance of the two launch maneuver design algorithms are discussed below.

5.3.2 γ, α End Condition Launch Maneuver Design

The implementation of the launch maneuver design algorithm in which the launch end state was specified in terms of γ and α was as follows. The error between the the achieved and the desired end of launch γ was minimized by the design procedure. The desired end of launch α was included in the analytical relationship between t_{kick} and Ω_{kick}. The relationship between t_{kick} and Ω_{kick} was obtained by predicting the final θ required, given the specified final γ and α. The launch parameters were dependent on the final θ since, with the sinusoidal pitchrate variation, the total attitude change ($\Delta\theta = \theta_{final} - \theta_0$) was simply equal to the product $t_{kick} \cdot \Omega_{kick}$. The determination of final θ involved the prediction of the end of launch state

85

for each t_{kick} tried by the algorithm before the corresponding simulation was performed. Figure 5.7 illustrates the functional sequence in this iterative launch maneuver design procedure.
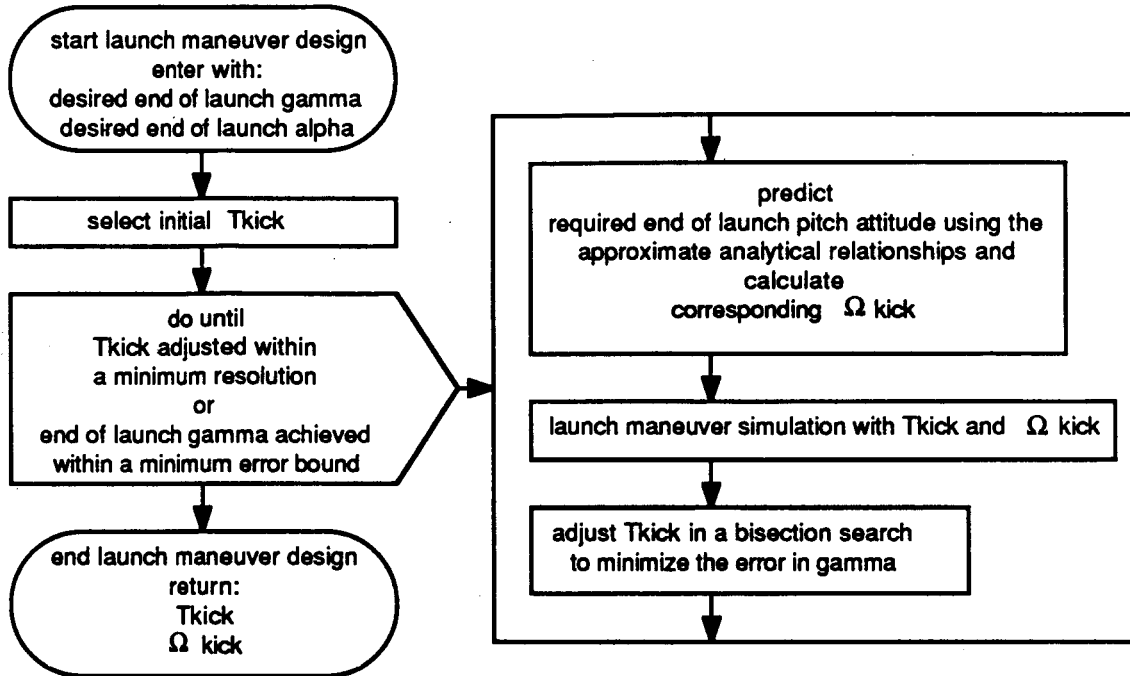
Figure 5.7   Functional sequence in the iterative launch maneuver design procedure for end state specified by γ and α.

The prediction of the final state was made using a series of approximations. An average, constant acceleration (a) due to thrust was determined by

$$a = 0.5 \left(\frac{T_0}{m_0} + \frac{T_0 + \dot{T}\, t_{kick}}{m_0 + \dot{m}\, t_{kick}} \right)$$

(5.1)

The variation of γ during the maneuver was approximated as a linear function

$$\gamma(t) = \left(\frac{\gamma_{final} - \frac{\pi}{2}}{t_{kick}} \right) t + \frac{\pi}{2}$$

(5.2)

86

With these two approximations the velocity equation (for dV/dt) was integrated to give the predicted final velocity:

$$V_{final} = V_0 + \left(a - g \left(\frac{\sin\left(\gamma_{final} - \frac{\pi}{2}\right)}{\gamma_{final} - \frac{\pi}{2}} \right) \right) t_{kick} \qquad (5.3)$$

and altitude equation (for dh/dt) was integrated to yield the predicted final altitude:

$$h_{final} = \left(\frac{t_{kick}}{\gamma_f - \frac{\pi}{2}} \right)^2 \left\{ a \left[\sin(\gamma_f) + \left(\frac{\pi}{2} - \gamma_f \right) \cos(\gamma_f) - 1 \right] - \frac{g}{2} \cos^2(\gamma_f) \right\} - \left(\frac{V_0 \, t_{kick}}{\gamma_f - \frac{\pi}{2}} \right) \cos(\gamma_f) + h_0 \qquad (5.4)$$

In the implementation, the launch design algorithm selected a trial value of t_{kick} each iteration while searching for the one which minimized the γ_{final} (γ_f) error. The end of launch velocity and altitude were predicted using Equations (5.3) and (5.4) with the desired γ_f and this trial value of t_{kick}. Given the predicted altitude and the design wind profile, the wind velocity at the end of the launch (V_{wf}) was found. Then, with V_{wf}, V_f, and γ_{final}, the values of V_a and γ_a were determined and, using the desired final α (α_f), θ_{final} was found (see Figure 5.6 for the relationships of V, V_w, V_a, α, θ, γ, and γ_a). Finally, the value of Ω_{kick} was calculated and the launch maneuver simulation was run with this value and the selected t_{kick}.

It was found that the predicted V_f and h_{final} were within approximately 2% and 3%, respectively, of the values attained in the full vehicle simulation in typical runs. This was quite good, considering the approximations made in the predictions. The θ_{final} was accurately achieved in the full vehicle simulation since it depended only on the specified launch maneuver attitude schedule which the flight control system followed with negligible error.

The search algorithm in the launch design procedure was able to find the t_{kick} value which minimized the error in γ_f in the launch maneuver design simulation to within approximately ±0.05°, the specified error bound. It was noted that there were upper and lower limits on the α_f which could be achieved. These limits depended in part on the wind conditions and in part on the particular form of the θ-profile employed in the maneuver. In headwinds they were higher (typically in the range 2° to 6°) while with tailwinds they were lower (typically 0° to 4°).

Unfortunately, despite its general success, this launch design approach proved to be insufficiently accurate for use in the trajectory design process. When compared to the full vehicle simulation, the γ_f achieved in the launch simulation differed approximately 1% to 2% from that actually attained "in flight" using the full vehicle simulation. There was usually an error of approximately 0.7° in the γ_f attained "in flight" compared to the desired value after a launch maneuver employing parameters determined using the γ_f, α_f launch design algorithm. Since the trajectory design procedure required γ_f adjustments on the order of 0.1° to precisely locate the optimal trajectory, the accuracy achieved by this launch design approach was not sufficient.

It is possible that the launch simulation accuracy could be improved so that this launch design technique could be successfully employed.

5.3.3 θ,α End Condition Launch Maneuver Design

In order to achieve the accuracy required for the trajectory design process it was decided to use θ and α as the specified end of launch states. In this implementation, θ_{final} was directly specified by the user or by the algorithm performing the trajectory design rather than being approximated from other variables. It was employed as the launch maneuver state variable which was adjusted in the trajectory design process and was always accurately achieved in the full vehicle simulation. The error in α_f was the quantity minimized by the launch maneuver design algorithm, using t_{kick} as the adjusted variable.

This approach was much simpler than the one described in section 5.3.2. No predictions of the end of launch state were required. The minimization algorithm selected t_{kick} and Ω_{kick} was then directly found from the specified θ_f and t_{kick}. The launch simulation was run and the achieved α_f was compared to the desired one to give the error value which was returned to the minimization algorithm. The functional sequence of the launch maneuver design procedure is illustrated by Figure 5.8.

The launch design algorithm adjusted t_{kick} until the achieved α_f error was less than 0.05° or the value of t_{kick} yielding the minimum error had been located within 0.1 second. The values of t_{kick} which were used were always rounded to the nearest 0.1 second to ensure accuracy with the 0.1 second integration time step used in both the launch and full vehicle simulations.
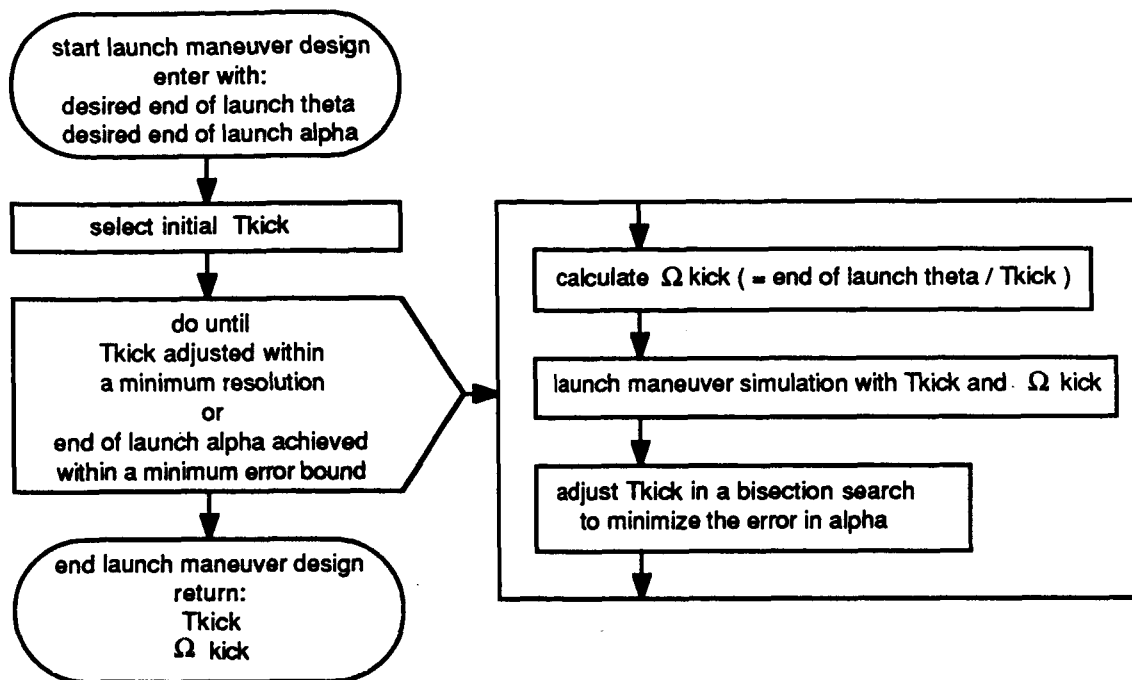
Figure 5.8   Functional sequence in the iterative launch maneuver design procedure for end
state specified by θ and α.

This launch design approach was found to be satisfactory for use in combination with the trajectory design process.

The design of a launch maneuver employing θ,α end condition specification but a different pitchrate profile was briefly investigated. In this version of the launch maneuver, the pitchrate profile was composed of a sinusoidal rise followed by a period of constant pitchrate and then a sinusoidal decay back to zero. The duration of the period of constant pitchrate was the variable which the search algorithm adjusted to minimize the error in α_f. The overall duration of the launch maneuver was held constant. Holding the launch maneuver duration constant was considered desirable since it was approximately equivalent to holding the end of launch velocity constant. This approach did not prove successful. It was found that the variation in the end of launch conditions resulting from changes in the constant pitchrate period length was too small to be useful. That parameter had insufficient authority to be used as the controlling variable. It was decided to continue using the variable duration launch maneuver employing a sinusoidal pitchrate profile.

89

5.4   Automated Trajectory Design

A program was developed to automate the trajectory design procedure which had been performed by manual iteration for most of the study. The objective of the trajectory designer routine was to generate and store the reference γ-profile of a final mass optimal trajectory which could be followed in flight using the γ-steering. The launch maneuver parameters were also obtained from the trajectory design process. The design trajectory was shaped by a user-selected α-profile and the design was accomplished by finding the launch maneuver which then resulted in maximum mass being achieved on orbit.

The procedure used in the automated trajectory designer was a maximization in one parameter, similar to the minimization algorithm employed in the launch maneuver design routine. The independent variable used in the maximization was the end of launch attitude (θ_f) and the maximized quantity was the final mass. The end of launch angle of attack (α_f) was normally selected to be a fraction (typically 95%) of the α which would be commanded in the trajectory shaping steering which followed the launch maneuver or was set equal to a constant value (5° was found to give good results in many cases). It was intended initially to use a parabolic interpolation search technique but, for simplicity, the first implementation of the trajectory designer routine used a bisection search technique of the same form as that utilized by the launch maneuver design algorithm. The algorithm searched for the end of launch θ which resulted in the maximum final mass. The final mass value was predicted by the PEG algorithm at the end of a simulation of the trajectory from launch to RP engine shutdown. A version of the 3 DOF predictive simulation, modified to include the vertical rise and the launch maneuver, was used. This simulation included all of the load, acceleration and q-limiting features applied to the full vehicle so that the designed trajectories met the vehicle and crew constraints. An integration time step of 0.1 second was employed in the trajectory design simulations.

The trajectory designer routine was found to function well, generating trajectories which were very similar to those obtained by manual design. The automated trajectory designer, using the simple search technique, required approximately 50% more iterations to locate the best trajectory than a typical manual design operation but since it ran as one batch job it took less total CPU time and, of course, required much less operator involvement. A more sophisticated maximization routine, such as the parabolic technique initially considered, would reduce the number of iterations required.

6. Summary, Conclusions and Recommendations

6.1 Overview

The ascent guidance study included the following efforts:

- development of an extensive simulation capability for launch vehicles
- study of a robust closed-loop steering technique for the endoatmospheric phase of the ascent trajectory (γ-steering with α-control)
- investigation of a predictive-adaptive steering scheme for maximization of final mass for use in conjunction with γ-steering
- preliminary investigation of predictive-adaptive steering for load reduction for use in conjunction with γ-steering
- development of a dynamic pressure control concept using engine throttling
- study of trajectory shaping leading to a simple design approach employed in the study to generate reference trajectories for use by the steering system
- development of a launch maneuver concept and design technique.

The conclusions and recommendations resulting from these efforts are presented below.

6.2 Simulation Capability

The modular ascent vehicle simulation which was developed for use in the ascent guidance study provides a useful tool for further investigations. The vehicle properties and the guidance, steering and control routines may be easily changed or expanded for investigation of vehicles other than the SSTO Shuttle II model used in the current study.

6.3 γ-Steering with α-Control

The γ-steering with α-control steering technique developed in the study was demonstrated to be robust in the presence of most wind dispersions and trajectory dispersions such as off-nominal launch. Only very severe headwind increases (compared to the nominal design environment) were found to compromise performance. The ability of the γ-steering approach to accommodate dispersions is a valuable contribution towards autonomous guidance. When

91

used in conjunction with a prelaunch trajectory design system or an inflight predictive-adaptive guidance system it provides the capability to accurately follow the designed or adapted γ-profile. In this study the vehicle was a winged launcher but in previous studies[11] the same general approach was demonstrated to be effective in conventional boost vehicles. Thus, γ-steering with α-control is applicable to a wide range of launch vehicles.

6.4   Predictive-Adaptive Guidance for Maximum Final Mass

The predictive-adaptive scheme to maximize the final mass was intended to enable the vehicle to recover from dispersions that would otherwise lead to sub-optimal performance. Such a capability would enable increased vehicle autonomy. The scheme which was implemented proved to be beneficial only in the case in which the reference γ-profile was off-optimal. In this situation it proved very effective in recovering performance – a final mass recovery up to 94% was demonstrated – which was otherwise lost compared to the optimal case. However, it is unlikely that an off-optimal reference trajectory would be used in practice so this result was of limited significance. The predictive-adaptive scheme did not alter performance in the presence of a wind dispersion if the original reference trajectory being followed had been optimal in the design environment. It also provided no significant adjustment to the trajectory in the event of an engine failure.

The lack of adjustment under conditions of wind variation indicated that the γ-profile designed in the nominal wind environment remained near optimal in the perturbed conditions. This led to conclusion that the wind was not a primary influence on the shape of the optimal trajectory. The wind and wind dispersions imposed a constraint on the trajectory only when they limited the ability of the steering to follow the designed trajectory. Limiting was found to occur when severe headwind increases drove the vehicle into its $q\alpha$ limit. The inference can thus be made that exact knowledge of the wind is not necessarily required when designing the trajectory as long as the vehicle and the steering technique which is used in flight can accommodate the range of winds which may actually be encountered. However, it was demonstrated that the degree of wind variation which can be accomodated when using γ-steering must be traded off against performance. Thus, reducing the range of dispersion which must be allowed for in the trajectory design by having good wind information when performing the design is beneficial.

---

[11]   Bonnice.

92

The predictive-adaptive scheme which was implemented may also have been limited in its effectiveness due to the monotonic nature of the adjustment which it applied to the trajectory. It simply adjusted the γ-profile which was followed by applying a monotonically changing γ-bias (generated with a γ-rate bias selected and adjusted by the adaptive logic) over the whole remaining period of γ-steering. In the case of an off-optimal reference γ-profile this was very effective in correcting the trajectory by adjusting the γ-profile towards the optimal one. In other cases such an adjustment was found to yield no benefit.

Perhaps a more sophisticated γ-profile adjustment approach would enable better performance. However, increasing the complexity of the adjustment applied to the trajectory would rapidly raise the level of sophistication required in the adaptive logic which selects the adjustments. The end of the spectrum in this respect would be predictive-adaptive guidance using a numerical optimization employing the full, constrained ascent trajectory equations of motion. Such an approach is normally considered to be undesirable due to its heavy computational requirements. It might be most beneficial in future studies of predictive-adaptive techniques to consider alternative approaches for adjusting the γ-profile. The objective would be a technique which is more flexible than the one investigated in this study but which does not require solution of the full trajectory optimization problem.

The selection of the magnitude of the adjustment which is applied to the γ-profile is one aspect of the trajectory adjustment approach which could be improved without changing the fundamental approach used in the guidance scheme which was implemented. In the current scheme, the algorithm only determines the direction of the adjustment. The magnitude of the adjustment is fixed. A slightly more sophisticated algorithm, perhaps employing more predictive simulations each adaptive cycle, could also determine the magnitude of the adjustment which gives the desired change. This might yield a faster adaptive response and therefore improve performance.

6.5   Predictive-Adaptive Guidance for Load Reduction

The predictive-adaptive guidance to minimize loads was only studied in a preliminary form. The objective was to achieve a reduction in the loading experienced by the vehicle when excess performance capability, beyond that required to fly the mission, was available. A significant reduction in loading was demonstrated in one case. However, an undesirable transient was

encountered when the guidance switched to PEG. This transient diminished the benefit of the load reduction achieved earlier in the trajectory. Future development of this guidance approach will have to reduce this transient, perhaps by using a transition phase between the load reduction guidance and PEG phases.

Other issues which should be addressed in future development of predictive-adaptive load reduction include the choice of load criterion and the nature of the trajectory adjustment applied by the guidance algorithm. Maximum $q\alpha$, used in the study as the load criterion, may not be the best choice. More detailed definition of the structural characteristics of the vehicle would determine what aspect of the loading experienced by the vehicle should be minimized to reduce the net wear on the vehicle during ascent. As was concluded in the case of predictive-adaptive steering to maximize final mass, the simple trajectory adjustment which was employed by the adaptive algorithm may have limited the effectiveness of the system. A more flexible γ-profile adjustment approach may enable better performance. An improvement of the current scheme which would determine the magnitude as well as the direction of the trajectory adjustment might give a significant improvement in performance, for example.

The concept of adjusting the trajectory to reduce loads by flying a less efficient profile, making use of excess vehicle performance, is felt to be potentially valuable. Accomplishing a mission while minimizing wear on the vehicle would be particularly advantageous in a reusable system such as Shuttle II.

6.6   Dynamic Pressure Control using Throttling

The control of dynamic pressure using engine throttling was demonstrated to be very effective. During the period of maximum q, the thrust level was controlled to prevent the specified vehicle q-limit from being exceeded. The control approach which was implemented was based on the relationship which was derived between thrust and the time rate of change of q (Equation (3.8)). The thrust level was calculated to achieve the q-rate commanded by the q-control loop compensation. In the study it was assumed that the achieved thrust was equal to this commanded level, which may not be the case in a real system. Future studies might consider alternative implementations of the q-control concept which would be more applicable to a real system. For example, an outer control loop employing q as the feedback variable could be used in conjunction with an inner loop utilizing acceleration as the feedback variable

by directly applying the q-rate to acceleration relationship, Equation (3.6). Such an approach would allow the 3 g acceleration limit to be met by applying a limiter directly in the inner loop. The inner loop would also indirectly accommodate thrust errors.

6.7   Trajectory Design

The α-profile shaping trajectory design technique which was developed as the result of the early trajectory shaping studies proved to give quite good results for such a simple approach. The "optimal" trajectories which were generated with it were comparable in shape and in performance to trajectories optimized using the sophisticated POST program. The final mass performance of trajectories obtained using POST was only slightly better than that yielded by using the α-profile shaping design technique. The design technique was well suited to the generation of the reference trajectory γ-profiles used in the study since it could be performed manually in a reasonable amount of time and was easy to implement in an automated form. However, its application required some operator experience and "feel" for the trajectory behavior, even when using the automated form, and it was found to encounter difficulties in some cases under severe wind conditions. Additionally, the performance achieved with it may not be as close to that obtained with POST, for example, when the vehicle constraints (such as qα) are more extensively specified and possibly variable with flight condition. Thus, while it is a useful tool for study of ascent guidance, the technique is not felt to be well suited to an operational system, particularly if a large degree of autonomy from operator involvement is desired. In an operational system a more general method employing a full numerical optimization, such as POST or an equivalent program, would be used for the prelaunch trajectory design since the required computational capacity would undoubtably exist.

6.8   Launch Maneuver Development

The launch maneuver form was developed to provide a smooth transition from the initial vertical attitude the vehicle had after clearing the launch pad to the state at which it was desired to commence the ascent steering. The development of the launch maneuver and the related design technique was found to be of importance due the impact which the launch maneuver had on the subsequent trajectory in the trajectory shaping studies. The initial implementation of the maneuver employed α and γ to specify the desired end of launch state in order to correspond to

95

the control and steering variables (α and γ, respectively) subsequently used during ascent. Unfortunately, the launch maneuver designer routine proved to be insufficiently accurate with these variables. The successful implementation of the launch maneuver designer routine employed θ and α to specify the end of launch state. Future study could include consideration of alternative launch maneuver forms and improvements to the designer routine.

C-2

Appendix: Ascent Vehicle Simulation

A.1   General Description

An extensive simulation capability was developed for use in the ascent guidance study. The simulation was constructed in a modular form to allow easy modification and addition of elements. The main vehicle simulation included full six degree of freedom (6 DOF) motion while two smaller derivatives of the main simulation employed three degree of freedom (3 DOF) models. The elements composing the vehicle simulation suite and its structure are outlined in Section A.3.

The reference frames assumed by the simulation are described in Section A.2. The simulation used a simple and intuitive Euler angle set to describe the vehicle attitude. As a consequence, in its present form, the simulation is not suited for full orbital simulations due to the occurrence of singularities in the angle set. However, it is quite well suited to its intended task of ascent trajectory simulation.

The simulation was written in the MAC programming language developed and used at CSDL. This language includes the algebraic manipulation of vectors and matrices and provides a fourth order Runge-Kutta integration facility making it well suited to dynamic simulation tasks. The fourth order Runge-Kutta integration was used in all of the simulation elements which required integration of dynamical expressions.

A.2   Definition of Reference Frames

Three reference frames were used in the simulation:

1) Earth-centered inertial axes   - a nonrotating axes set fixed to the center of the earth, with positive z ($\underline{Z}$) directed north, positive x ($\underline{X}$) initially aligned with zero longitude at time zero and y ($\underline{Y}$) completing the right-handed set.

2) Local geographic coordinates - a north (<u>NORTH</u>), east (<u>EAST</u>), down (<u>UZG</u>) directed axes set, fixed to the vehicle CG, which assumed a spherical earth for the definition of its relationship to the inertial axes. This was the frame in which all earth relative angles and the wind direction were defined.

3) Body-fixed axes - the axes set fixed to the vehicle CG with the x direction (<u>UBX</u>) towards the nose of the vehicle, the y direction (<u>UBY</u>) out the right wing and the z direction (<u>UBZ</u>) completing the right-hand set.

The attitude of the body-fixed axes in relation to the inertial axes was described by an Euler angle set, (Ψ, Θ, Φ), representing an azimuth, elevation and roll transformation from the inertial axes to the body axes.

The relationships of the axes systems are shown in the relative orientation which existed at time zero, at the start of the launch, in Figure A.1. The vehicle was vertical on the launch pad with its underside facing down range. The initial Euler angle set was

$$(\Psi, \Theta, \Phi)_{initial} = (longitude_{launch}, - lattitude_{launch}, - azimuth_{launch}).$$

(Note that the azimuth$_{launch}$ was defined in the north-east plane and corresponded to the roll transformation mentioned above, not the azimuth transformation.) At this initial condition the vehicle had an inertial velocity and angular rate relative to the earth-centered inertial axes due to the earth's rotation (ω_{earth}).

The general relationship of the vehicle body axes to the local geographic axes is illustrated by Figure A.2. In the ascent guidance study only the pitch attitude (θ) was of interest. The bank angle was normally close to zero and the heading was determined by the initial launch azimuth.
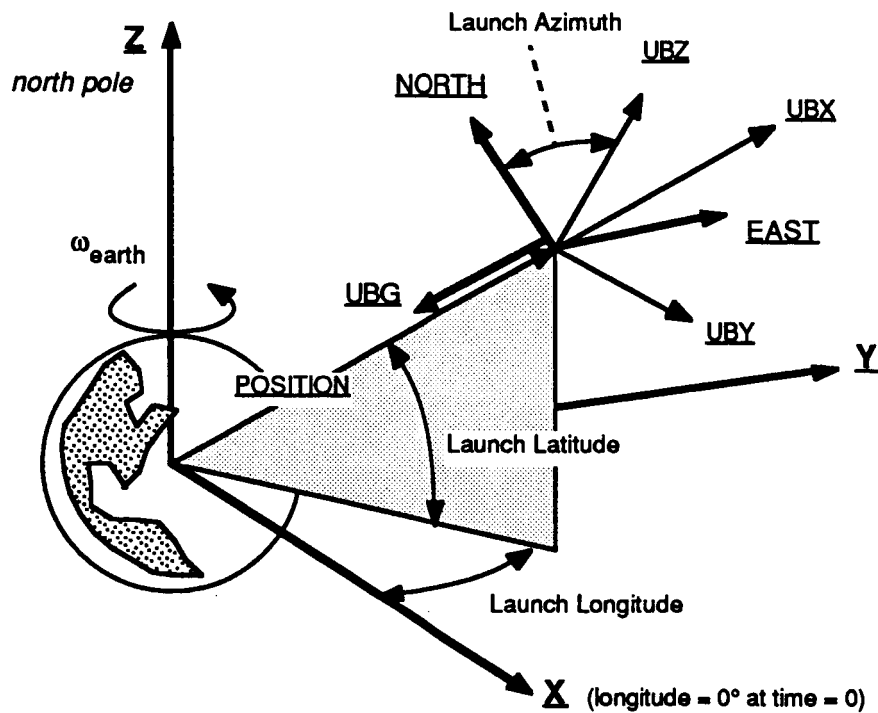
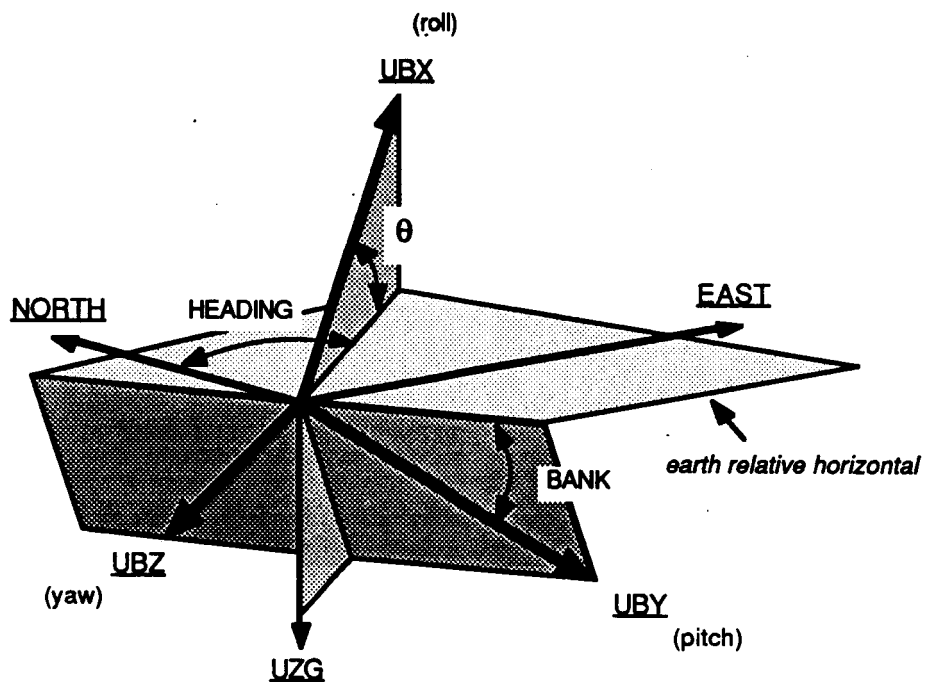Figure A.1   Reference frame relationships at time zero.

Figure A.2   Relationship of the vehicle body axes to the local geographic axes.

The position, velocity, acceleration and force vectors were defined in the inertial frame and the corresponding equations of motion were integrated in the inertial frame. The moments acting on the vehicle were defined relative to the body-fixed axes. In general, the resulting roll, pitch and yaw rates in the body-fixed frame (P, Q, R) were transformed into rates in the Euler angle set with the transformation[12]

$$\dot{\Theta} = Q \cos(\Phi) - R \sin(\Phi)$$

$$\dot{\Phi} = P + Q \sin(\Phi) \tan(\Theta) + R \cos(\Phi) \tan(\Theta)$$

$$\dot{\Psi} = Q \sin(\Psi) \sec(\Theta) + R \cos(\Phi) \sec(\Theta)$$

and these were then integrated to give the attitude. (In the study, roll and yaw rates were negligibly small. They resulted only from the motion which the vehicle had on the pad due to the earth rotation, there being no roll or yaw torques represented in the simulation.) The unit vectors defining the body-fixed frame were calculated from the (Ψ, Θ, Φ) set with

$$\underline{UBX} = \begin{bmatrix} \cos(\Psi) \cos(\Theta) \\ \sin(\Psi) \cos(\Theta) \\ -\sin(\Theta) \end{bmatrix}$$

$$\underline{UBY} = \begin{bmatrix} \cos(\Psi) \sin(\Theta) \sin(\Phi) - \sin(\Psi) \cos(\Phi) \\ \sin(\Psi) \sin(\Theta) \sin(\Phi) + \cos(\Psi) \cos(\Phi) \\ \cos(\Theta) \sin(\Phi) \end{bmatrix}$$

$$\underline{UBZ} = \underline{UBX} \times \underline{UBY} .$$

[12] Etkin, B. _Dynamics of Flight - Stability and Control_. 2nd Edition. 1982. New York: John Wiley & Sons, Inc. (p 91).

A.3   Simulation Structure and Elements

### A.3.1   Structure of the Vehicle Simulation

The overall structure of the vehicle simulation is illustrated in Figure A.3. The master element was the main program which contained the vehicle equations of motion and the calls to the subroutines within the main simulation integration loop (the MAC language resident fourth-order Runge Kutta integration was used). The main program also handled the simulation control and all normal input/output for the simulation.

The first level of subroutines included the sensor, flight control and guidance subroutines. For the ascent guidance study, in which no sensor deterministic error or noise was assumed, the sensor subroutine simply assigned the "true" state information to the "measured" variables which the flight control and guidance systems used. The flight control subroutine contained the flight control algorithms which were selected according to flags set by the user and by the guidance system. The guidance subroutine contained the throttling routine and the guidance algorithms.

In the guidance subroutine the guidance algorithms were selected according to the current ascent phase and by user-specified flags. The predictive-adaptive guidance algorithm employed calls to the predictive simulation subroutine. The predictive simulation was identical in structure to the main program but used a simplified three degree of freedom model, as discussed previously. The guidance algorithms required by the predictive simulation were included directly in the predictive simulation subroutine. The PEG guidance employed during the final ascent phase was implemented with a preexisting PEG routine accessed through interface elements.

The second-level subroutines included the vehicle-dependent and environmental subroutines which are outlined in the sequel, and the PEG subroutines. These common subroutines were employed by all three simulations used in the study.

Figure A.3 Hierarchical relationship of the program elements in the vehicle simulation.
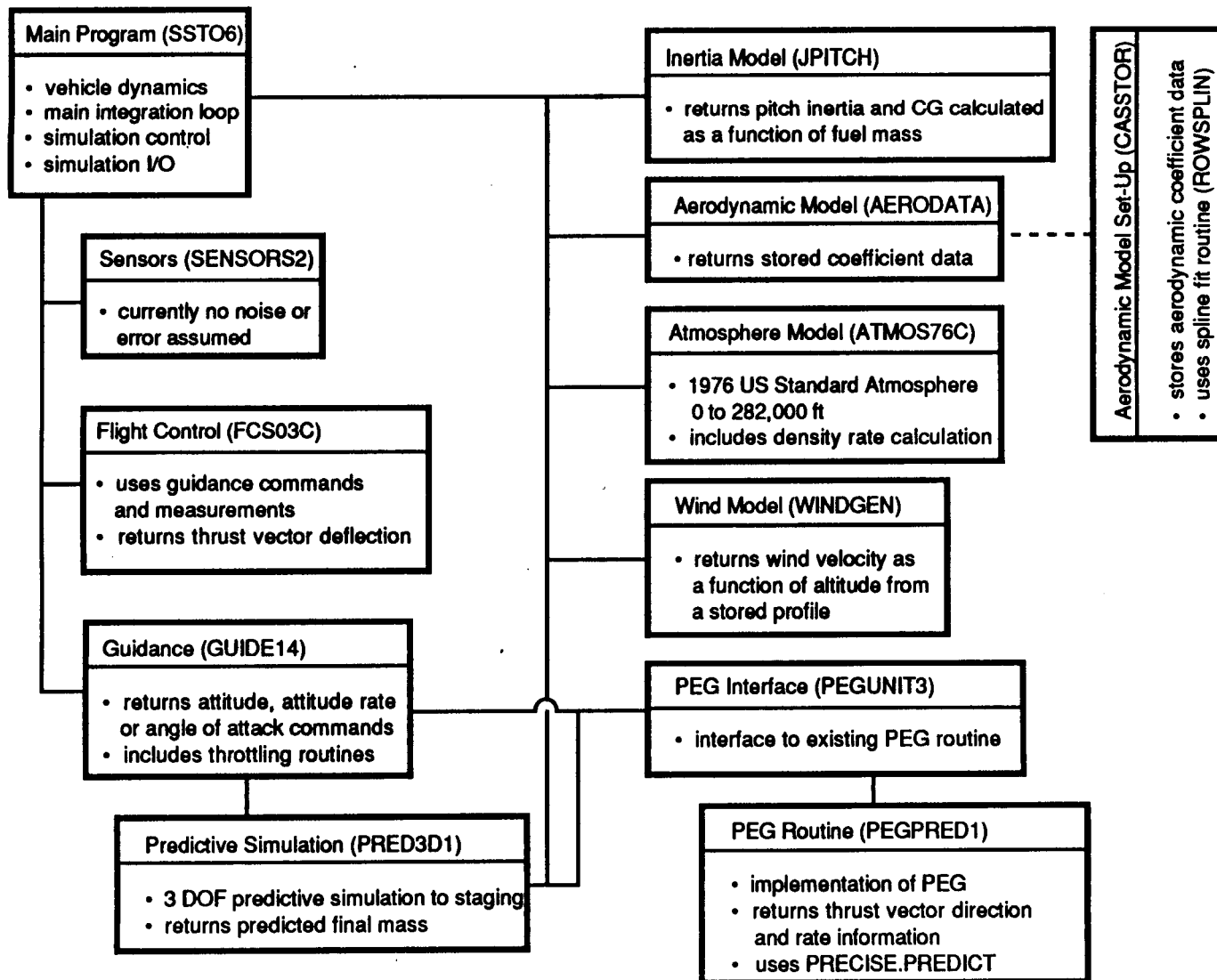
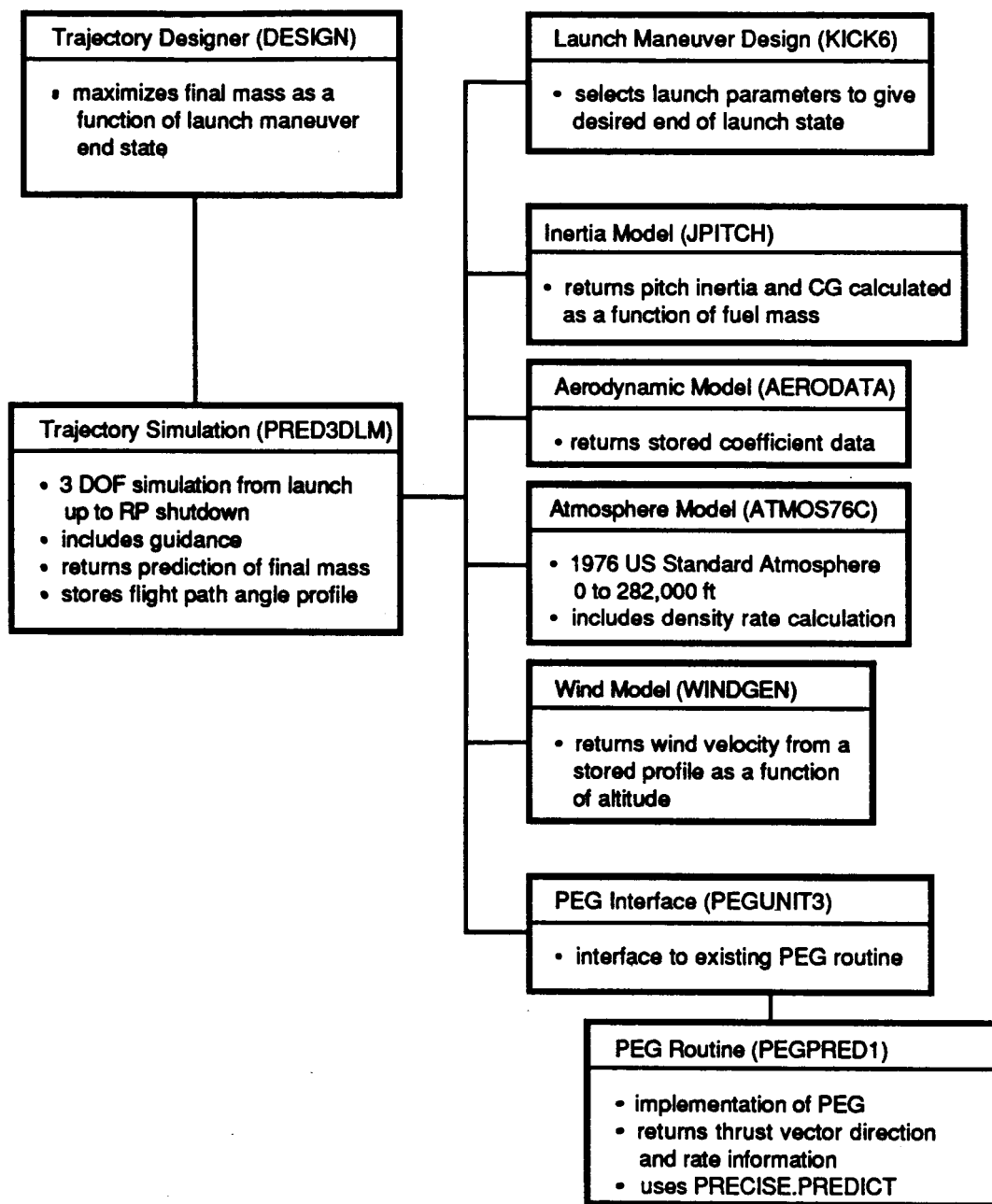## A.3.2 Structure of the Trajectory Design Program

Figure A.4 Hierarchical relationship of the program elements in the automated trajectory design.

The structure of the trajectory design program is shown in Figure A.4. The master element was the trajectory designer routine which included the design algorithm discussed in Section 5.4. The trajectory designer routine called a three DOF trajectory simulation which was an adapted version of the predictive simulation used by the predictive-adaptive guidance. The trajectory design simulation used the same second-level subroutines as did the other simulations. It also employed the launch maneuver designer routine. The launch maneuver designer routine, which itself contained an idealized simulation of the launch maneuver, was called to determine the launch maneuver parameters yielding the end of launch conditions which the trajectory designer specified at each trajectory design iteration. It was called by the trajectory simulation when the top of the vertical rise was reached.

When the trajectory design was performed manually the launch maneuver designer routine was also employed. However, the trial simulations of the trajectory were made using the full, six DOF vehicle simulation. As in the automated trajectory design, the launch maneuver design routine was called by the guidance system at the start of the launch maneuver to determine the launch parameters yielding the end of launch conditions which the user specified.

A.3.3   Environmental Elements

The simulation employed an oblate earth, "J2", gravity model. The equations for this model were implemented in a subsection of the main simulation program.

There were two subroutines which provided the atmospheric environment model. One was the atmosphere model, a direct implementation of the equations describing the pressure, density and speed of sound given in the 1976 US Standard Atmosphere[13]. The other environmental element was the wind model. The atmosphere model equations were valid up to 282,000 ft. Beyond this altitude the aerodynamic forces were neglected. An extension to the atmosphere model also provided the density time rate of change corresponding to the current vehicle altitude rate. This density rate was required for the throttling algorithm. The wind model used a piece-wise linear wind profile which was stored as wind speed and azimuth break points with respect to altitude. Wind speed and azimuth were interpolated between the breakpoints. Multiple wind profiles were stored in the wind model and could be selected by the user. A magnitude scaling factor could be applied to the wind speed profile. Different profiles could be

---

[13] U.S. Standard Atmosphere, 1976. NOAA, NASA, USAF. (pp 1 - 20).

specified for the main simulation and the predictive simulation in order to investigate the effects of dispersions in the wind actually encountered during ascent from the prelaunch measured and stored profile.

The wind profiles which were used in the ascent guidance study were based on actual wind profiles measured with the Jimsphere radar-tracked balloon system in use at KSC and Vandenberg AFB. A large collection of data was provided in graphical format by NASA Langley Research Center documenting pairs of profile measurements in which the measurement of the profiles in each pair was separated by three and a half hours. Examples which appeared to be worst cases in terms of overall magnitude and variation over the three and a half hour interval were selected for use in the simulations. The magnitude variations between pairs of profiles were of special interest since they gave an indication of how large the differences might be between the prelaunch measured wind, available to the trajectory design and guidance systems, and that actually encountered during ascent. The wind speed profiles of these cases were approximated with linear segments. The azimuth information was not used since the sidewind component had no effect on the vehicle in this study. The wind profiles were assumed to lie in a plane and to be either a headwind (from due east) or a tailwind (from due west). (The vehicle launch used throughout the study was eastward from KSC.) The azimuths of the documented profiles frequently differed considerably from east or west. The assumption of the profile either being a headwind or tailwind therefore tended to increase the effective magnitude of the wind profile. This was in keeping with the objective of the wind model, which was to provide a reasonably severe environmental stress on the guidance and control system. The model was a pessimistic one based on actual "worst case" data.

The worst case pair of all the Jimsphere measurements considered in this study was a pair made at Vandenberg AFB, designated "Vandenberg #69" and "Vandenberg #70". These profiles, illustrated in Figure A.5, were the most frequently used ones during the study. All of the cases reported in this thesis employed them. Figure A.6 shows the linearized profiles derived from these profiles which were actually used in the wind model program.
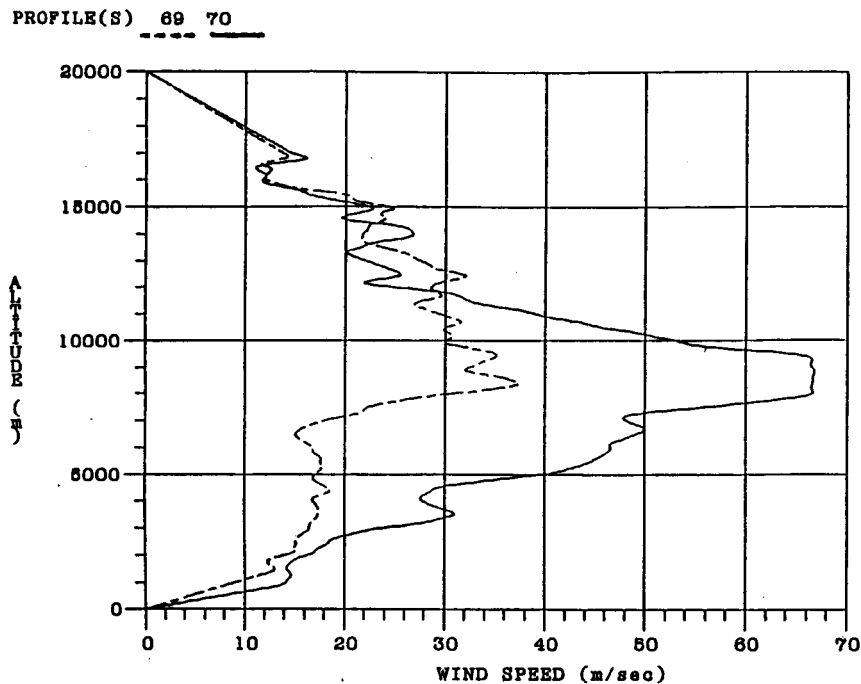
Figure A.5   Representative original Jimsphere measurement of wind velocity data.
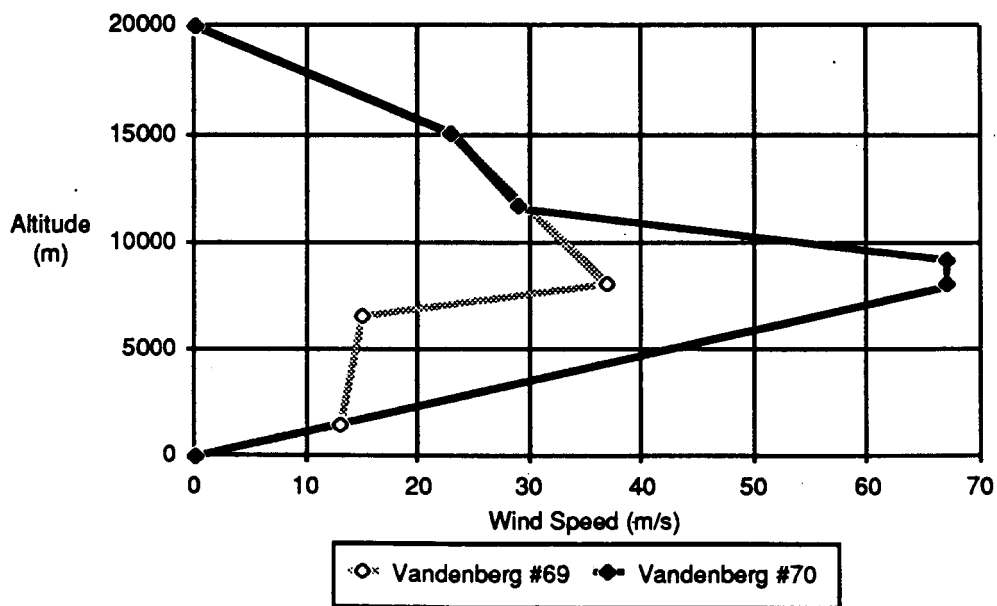(The two profiles were separated by 3.5 hours.)

Figure A.6   Simplified wind profiles based on those in Figure A.5.

A.3.4   Vehicle Elements

The vehicle-dependent elements were the inertia model and the aerodynamic model. In the study, the inertia model contained the simple pitch inertia model outlined in Section 2.2.2 which provided the pitch inertia and center of gravity location. The aerodynamic model employed a hybrid interpolation scheme to calculated the vehicle aerodynamic coefficients from stored data. In this scheme a cubic spline was fitted to the aerodynamic coefficients with respect to angle of attack (α) and the data was linearly interpolated with respect to Mach number (M). This was done since α varied more rapidly than M in flight and a smooth parameter variation was desirable with respect to α. To obtain an aerodynamic coefficient at a given flight condition the coefficient splines at the Mach numbers bracketing the current M were each evaluated at the current α and the results were then interpolated to give the value at the current M. The aerodynamic model set-up routine was employed before running the simulation to process the aerodynamic coefficients, which were provided tabulated with respect to α and M, and to store the data in the form of spline coefficients, also with respect to α and M. (Once stored, this data was available to all subsequent simulations so this data processing was only performed preceding the first time the simulation was run with a particular set of aerodynamic coefficients.)

Summary of References

1. Condon, J., "Autonomous Ascent", Mission Planning and Analysis Division presentation, NASA Johnson Spaceflight Center, Autonomous Ascent - Quarterly Meeting, May 27, 1987.

2. Talay, T.A., "Shuttle II." SAE Paper 871335, Aerospace Vehicle Conference, Washington, D.C., June 8–10, 1987.

3. Talay, T.A., "Shuttle II - A Progress Report." Space Systems Division, NASA Langley Research Center, May 6, 1986.

4. Bauer, G.L., Cornick, D.E. , Harper, A.R., Peterson, F.M., Stevenson, R., "Program to Optimize Simulated Trajectories (POST)." Vol. II, *Utilization Manual*, NASA CR-132690, April 1975.

5. McHenry, R.L., Brand, T.J., Long, A.D., Cockrell, B.F., Thibodeau, J.R., "Space Shuttle Ascent Guidance, Navigation and Control". *The Journal of the Astronautical Sciences*, Vol. XXVII, No. 1, pp 1-38, January-March, 1979.

6. Schleich, W.T., "The Space Shuttle Ascent Guidance and Control". AIAA Guidance and Control Conference, August 9-11, 1982. San Diego, California. AIAA 82-1497.

7. Bonnice, W.F., "Steering of a Boost Vehicle to a Desired Flight Path Angle Trajectory using Angle of Attack Control". 1983. Massachusetts Institute of Technology Masters of Science Thesis, published as CSDL Report T-802. Charles Stark Draper Laboratory, Inc., Cambridge.

8. Brand, T.J., Brown, D.W., Higgins, J.P., "Space Shuttle G&N Equation Document No.24, revision 2 *Unified Powered Flight Guidance*". C-4108. June, 1974. Charles Stark Draper Laboratory, Inc., Cambridge.

9. Press, W.H., Flannery, B.P, Teukolsky, S.A., Vetterling, W.T., Numerical Recipes. 1986. Cambridge: Cambridge University Press.

10. Etkin, B., Dynamics of Flight - Stability and Control. 2nd Edition. 1982. New York: John Wiley & Sons, Inc.

11. U.S. Standard Atmosphere, 1976. NOAA, NASA, USAF.